VIBRATIONAL PROPERTIES OF DISORDERED BINARY ALLOYS

By

RAVI PRATAP SINGH

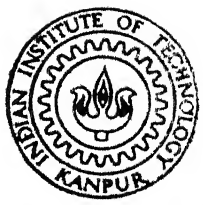

DEPARTMENT OF PHYSICS

INDIAN INSTITUTE OF TECHNOLOGY KANPUR

NOVEMBER, 1982

VIBRATIONAL PROPERTIES OF DISORDERED BINARY ALLOYS

A Thesis Submitted
In Partial Fulfilment of the Requirements
for the Degree of
DOCTOR OF PHILOSOPHY

By
RAVI PRATAP SINGH

to the
DEPARTMENT OF PHYSICS
INDIAN INSTITUTE OF TECHNOLOGY KANPUR
NOVEMBER, 1982

PHY - 1982 - D - SIN - VIB

अम्मा व दद्दा को

CERTIFICATE

This is to certify that the work in this thesis entitled: "VIBRATIONAL PROPERTIES OF DISORDERED BINARY ALLOYS" has been carried out by RAVI PRATAP SINGH under my supervision. No part of this work has been submitted elsewhere for a degree.

Abhijit Mookerjee
Assistant Professor
Department of Physics
Indian Institute of Technology
Kanpur, India

November, 1982

ACKNOWLEDGEMENTS

The able guidance, constant help and wise counsel of Dr. Abhijit Mookerjee is gratefully acknowledged. His patient care made it possible for me to carry out and complete this investigation. At times I could afford to falter for I knew that he was around to help me and he did it. It is embarrasingly impossible to list out what all I got from him. Working with him has been an unforgettable experience of life.

My sincere thanks are due to Dr. M. Yussouff for many helpful discussions at various stages of this work. His constant encouragement and appreciation about the progress of my work helped me in achieving the goal without hurdles. I wish to thank Dr. M.J. Kelly of University of Cambridge for helpful discussions and Dr. R. Haydock of University of Cambridge for providing the useful programmes. I am thankful to Professor D.C. Khan for taking interest in the progress of my research work.

I thank my friend Mr. Pankaj Joshi for his critical comments from time to time.

I must thank my friends Dr. A.K. Nigam, J.K. Sharma, V.K. Srivastava, Vasundhra Choudhry and Messrs A.K. Upadhyaya, Arun Agrawal, B.P. Singh, D.S. Misra, V.D. Chafekar and many others who helped me in more than one ways during the course of this work.

It is a pleasure to thank Dr. M. Misra for his timely help in many ways at the time of completion of this thesis.

My thanks are also due to the Director (Personnel), Oil and Natural Gas Commission, Mr. M.M. Goswami (Supdg. Geophysicist(s)) and Mr. M.B. Singh, Sr. Geophysicist(s), ONGC, Nazira for providing me leave for completing this work.

I am grateful to Council of Scientific and Industrial Research, New Delhi for financial support in the form of Junior Research Fellowship for 2 years during this research work.

I thank Mr. R.N. Srivastava for neat typing, Mr. J.S. Sharma for tracing the figures and Mr. H.K. Panda and Mr. L.S. Rathore for cyclostyling this thesis.

I take this opportunity to pay homage to my dear friend late C.P.K. Reddy whose untimely death has created a void in my life.

My warmest thanks go to my dear friend Gyanesh and to my younger brother Rajive whose company made a homely atmosphere for me during my stay at IIT Kanpur.

In the end, I would like to appreciate the importance of computer DEC-10 of IIT Kanpur without which it was quite difficult to achieve my goal.

(Ravi Pratap Singh

CONTENTS

LIST OF TABLES

LIST OF FIGURES

SYNOPSIS

When atoms of different masses (site energies) and difference interatomic force constants (overlap-integrals) alloy substitutionally in a crystal, there are, in general three types of changes in the system — Hamiltonian — diagonal ϕ_{ii}, off-diagonal ϕ_{ij} (where j is some neighbouring site of i) and environmental ϕ_{jk}. Unlike electronic systems, such types of disorder are coupled in a vibrational system by the general translational and/or rotational symmetry of the system (Chapter I), rendering its study extremely cumbersome.

The first successful theoretical study of substitutionally disordered vibrational system was due to Taylor (1967) known as mass-defect coherent potential approximation (MCPA or 1CPA). The MCPA is a self-consistent single-site approximation for alloys with diagonal disorder. The need to go beyond MCPA has been felt for a long time. Several suggestions have been put forward about the ways of generalizing the MCPA and ways of incorporating off-diagonal disorder, environmental disorder and short range-order (SRO) (Briefly reviewed in Chapter II of the thesis). Calculations based on these suggestions suffer from two main drawbacks. Firstly, for any exactly solvable realistic model, in which all types of disorder are coupled, the corresponding algebraic equations become tediously unwieldy, particularly on a three-dimensional lattice. Secondly, any tractable or further simplified approximation always leads to the unphysical averaged Green's function in the strong scattering regime. The essential Herglotz property of the Green's function is violated.

The "augmented space" of Mookerjee (1973) preserves the correct Herglotz property of Green's function. This formalism is discussed in detail in Chapter II. The present work which is based on "augmented space" offers an unambiguous, tractable, self-consistent cluster generalization (CCPA) of MCPA, which retains the Herglotz property at all frequencies for all ranges of disorder. The general formalism of the CCPA is also discussed in Chapter II. A graphical method coupled with the recursion technique of Haydock (1972) enables us to work on a realistic three-dimensional lattice.

The most important contribution of this work is the generation of a self-consistent self-energy. This produces the vibrational properties (viz. dispersion curves, density of states, neutron scattering cross-section, etc.) more accurately than that produced by MCPA. The results of self-consistent cluster calculations for the density of states for linear chain are reported in Chapter II. The band edges are much better reproduced, as well as the structure near the band edges, especially in those cases where there is an impurity band with considerable structure.

In Chapter III our cluster - CPA formalism is applied for the calculation of vibrational properties of random transition metal alloys e.g. $Ni_{1-c}Pt_c$, $Ni_{1-c}Pd_c$, $Ni_{1-c}Cr_c$ $(0 < c < 1)$ where effects of off-diagonal disorder and clusters are expected to be important. These alloys form a continuous series of FCC solid solutions and their experimental results are available to compare with the theoretical ones. Bosi et al. (1980; 1978) have applied MCPA to these alloys. They have treated the diagonal disorder in MCPA but off-diagonal disorder in virtual crystal approximation

(VCA). This is not a consistent procedure. The fit with experiment is not satisfactory and clustering has been forwarded as being responsible. We have taken off-diagonal disorder into account and the cluster coherent potential medium is made self-consistent. Our results are closer to experimental results. The trend of changes due to clusters is in the right direction.

Last but not the least is the work related with the screening density around an impurity of unit charge given in the Appendix (R.P. Singh and M. Youssouff, Phys. Stat. Sol. (b) 101, K93 (1980)).

In the concluding Chapter IV, the possible extension and future usefulness of the cluster CPA have been discussed.

Chapter I

Introduction

1.1 Lattice Dynamics of Disordered Systems:

The study of matter with random composition has for many years received much less attention from physicists than better definable crystalline materials. Nevertheless, some important results on average permittivity of a heterogeneous medium were obtained very early in certain disordered systems (Rayleigh, 1892). Apparently the first work devoted to a calculation of the frequency spectrum of a disordered three-dimensional crystal was that of Lifshitz and Stepnova (1956). These authors obtained the leading terms in the expansion of the spectrum in powers of the concentration of the minority species and determined the shift of the maximum frequency of the unperturbed crystal due to the introduction of a finite concentration of impurities. Their results were not applied to the numerical calculation of the spectrum of any crystal model.

An essentially analogous method for expanding the spectrum in powers of the impurity concentration, based on the use of Green's function was proposed for the linear chains by Davies and Langer (1963). This method was subsequently generalized to the three-dimensional disordered crystals and the calculations were made self-consistent by Taylor (1967) ensuring that his approximations to the frequency spectrum should be independent of which type of atom is regarded as host and which is regarded as the impurity. One of the consequences of ensuring that this symmetry is present in the theory is that the impurity bands which

are predicted do not overlap the maximum frequency of the monoatomic light-atom lattice. Within this formalism - widely known as Mass-defect Coherent Potential Approximation (MCPA) - however, the randomness in the force constants could not be taken into account. Moreover being a one-site approximation, effects of random clustering also could not be taken into account.

Despite these approximations, the MCPA theory has been useful in explaining the experimental results of the alloys with small mass-disorder such as Nb-Mo, Cu-Zn, Cu-Ni (Grunewald, 1980). In case of large mass-disordered alloys such as Pd-Pt, Nb-Ta, Ge-Si etc., the large resonances and localized modes observed experimentally were found in general to be in fair agreement with MCPA provided that the disorder was essentially in the masses only and not in the bonding (Bosi et al, 1978). The agreement was unsatisfactory for the alloys such as Cr-W, Cu-Au, Ni-Pd, Ni-Pt. The experiments have shown both resonant and localized modes. For resonant modes it was found that the frequency shifts were branch dependent for Cr-W and Cu-Au, contrary to the expectation of MCPA theory (Cunningham et al, 1970; Svensson and Kamitakahara, 1971). It was found that the zero frequency shift is at higher energy than the resonance in Cr-W and Cu-Au alloys. For Ni-Pd the phonon width dependence on frequency is different for various branches and in disagreement with MCPA calculations (Kamitakahara and Brockhouse, 1974). In the case of Ni-Pt, the energy splitting of the phonon dispersion curves at the resonance mode frequency has a branch dependence in contrast to the MCPA prediction. Moreover, the experimental phonon density of states deviates from the MCPA calculations for the samples with

concentration C $\geq$ 0.30 and the difference is most conspicuous for the maximum phonon frequency which decreases faster with increasing Pt concentration than the theory predicts (Tsunoda et al, 1979).

Such deviations urge the need of incorporating other disorders viz. off-diagonal and environmental, which are coupled in the case of phonons, by the general translational and rotational symmetry of the system. In the following work we shall concentrate on substitutionally disordered binary alloys with off-diagonal disorder. In view of this, we have first reviewed the requirements of detailed study of disordered alloys in this chapter. In Chapter II, we review the earlier methods (i.e. MCPA, etc.) with their drawbacks and discuss possible lines of generalisation with the self consistent cluster coherent potential approximation (CCPA) based on "augmented space" of Mookerjee (1973). This formalism (CCPA) has been applied to transition metal alloys e.g. $Ni_{1-c}Pt_c$, $Ni_{1-c}Cr_c$ and $Ni_{1-c}Pd_c$ which fall in the category of substitutionally disordered alloys in which the effects of off-diagonal disorder and clustering are expected to be important (Chapter III). In the concluding Chapter IV, we have discussed the main achievements of CCPA formalism in the study of vibrational properties and its various possible applications to similar problems.

1.2 The Harmonic Model

In the harmonic approximation, the Hamiltonian for the vibrational motion of an ordered crystal is

$$H^{o} = \sum_{l\alpha} \frac{p_{\alpha}^{2}(l)}{2M_{\alpha}^{o}} + \sum_{\substack{l,\alpha \\ l',\alpha'}} u_{\alpha}(l).\phi^{o}_{\alpha\alpha'}(l,l').u_{\alpha'}(l') \qquad (1.1)$$

with the force constant matrix ϕ^{o} being translationally invariant. Here $u_\alpha(l)$ and $p_\alpha(l)$ are the Cartesian coordinates of the displacement and momentum operators, respectively, of an atom in the unit cell at R(l), coordinate, where M^{o}_α is the mass of that atom. We take the same form for the alloy i.e.

$$H^{A} = \sum_{l\alpha} \frac{p^2_\alpha(l)}{2M_\alpha(l)} + \sum_{\substack{l\alpha \\ l'\alpha'}} u_\alpha(l).\phi_{\alpha\alpha'}(l,l').u_{\alpha'}(l') \qquad (1.2)$$

Note that the mass now depends upon l and that ϕ is not translationally invariant. The Heisenberg equations of motion for these operators are

$$ih \frac{\partial}{\partial t} u_\alpha(l) = \left[u_\alpha(l,t), H\right] = M^{-1}_\alpha(l)\, p_\alpha(l,t) \qquad (1.3a)$$

$$ih \frac{\partial}{\partial t} p_\alpha(l) = \left[p_\alpha(l,t), H\right] = - \sum \phi_{\alpha\alpha'}(l,l')u_{\alpha'}(l',t) \qquad (1.3b)$$

So that

$$M_\alpha(l) \frac{\partial^2}{\partial t^2} u_\alpha(t) = - \sum_{l'\alpha'} \phi_{\alpha\alpha'}(l,l')\, u_{\alpha'}(l',t) \qquad (1.4)$$

When Fourier transformed to frequency w, this expression becomes

$$\sum_{\alpha' l'} \left[M_\alpha(l)\, \delta_{\alpha\alpha'}\, \delta(l,l')\, w^2 - \phi_{\alpha\alpha'}(l,l')\right] u_{\alpha'}(l') = 0 \qquad (1.5)$$

In the perfect crystal, the characteristic frequencies and normal modes may be readily obtained because of the translational symmetry (Maradudin et al, 1971). But in the disordered crystal the translational symmetry is lost. Nevertheless, the equation of motion (1.5) in the disordered crystal can conveniently be expressed in terms of that for the perfect crystal where it becomes

$$\sum_{\alpha' l'} \left[M_\alpha^\circ w^2 \delta_{\alpha\alpha'} \delta_{ll'} - \phi^\circ_{\alpha\alpha'}(l,l') - V_{\alpha\alpha'}(l,l') \right] u_{\alpha'}(l) = 0 \qquad (1.6)$$

where

$$V_{\alpha\alpha'}(l,l') = M_\alpha^\circ w^2 \varepsilon_\alpha(l) \delta_{\alpha\alpha'} \delta_{ll'} + \Delta \phi_{\alpha\alpha'}(l,l') \qquad (1.7)$$

with

$$M_\alpha(l) = M_\alpha^\circ - \Delta M_\alpha(l) = M_\alpha^\circ (1 - \varepsilon_\alpha(l)) \qquad (1.8a)$$

and

$$\phi_{\alpha\alpha'}(l,l') = \phi^\circ_{\alpha\alpha'}(l,l') + \Delta \phi_{\alpha\alpha'}(l,l') \qquad (1.8b)$$

This problem is formally identical to the problem of non-interacting electrons, in disordered crystals (Elliott et al, 1974). Within the harmonic approximation, the knowledge of frequency and spatial extent of each normal mode is necessary, which could be obtained for the translationally invariant crystal by the use of symmetry transformation. In an imperfect crystal this procedure is no longer of use and other means of attack on the equation of motion (1.5) are required. It is a fact that the experiments on disordered crystals (viz. neutron scattering, optical absorption, etc.) simply measure a correlation or response function rather than the properties of particular modes (Van Hove, 1954). A well defined formalism which leads immediately to these quantities without the necessity to solve for the normal modes is that of thermodynamic Green's functions which we use and discuss below.

1.3 Lattice Green's Functions

The required function of the lattice dynamics is almost always the displacement-displacement correlation function

$$S_{\alpha\alpha'}(l,l';w) = \left(\frac{1}{2\pi}\right) \int_{-\infty}^{\infty} \langle u_\alpha(l,t) \cdot u_{\alpha'}(l',0)\rangle_T \, e^{iwt} \, dw \qquad (1.9)$$

where $\langle \ldots \rangle_T$ denotes a thermal average.

Such correlation functions are readily calculated via Green's functions (Fetter and Walecka, 1971). We choose to use Green's functions given by

$$G_{\alpha\alpha'}(l,l';w) = \left(\frac{1}{\hbar}\right) \int_{-\infty}^{\infty} \langle\langle u_\alpha(l,t);\, u_{\alpha'}(l',0)\rangle\rangle \, e^{iwt} \, dt \qquad (1.10a)$$

where

$$\langle\langle A(t);\, B \rangle\rangle = \mp i\, \theta\,(\pm t) \langle [A(t),\, B]\rangle_T \qquad (1.10b)$$

is a double time Green's function (Zubarev, 1960). The upper and lower signs give respectively, the retarded and advanced Green's functions with $\theta(t)$ being the usual Heaviside unit step function.

These Green's functions are related to the correlation function (1.9) via the "spectral representation"

$$G_{\alpha\alpha'}(l,l';Z) = \left(\frac{1}{\hbar}\right) \int_{-\infty}^{\infty} \frac{(1 - e^{-\beta w})\, S_{\alpha\alpha'}(l,l';w)}{Z - w + i\varepsilon} \, dw \qquad (1.11)$$

where $\beta = \hbar/k_B T$. A more explicit relation between these functions is obtained from the discontinuity of the Green's function across the real axis i.e.

$$\underline{G}(w + io^+) - \underline{G}(w - io^+) = 2i \, \mathrm{Im}\, \underline{G}(w)$$

$$= \left(\frac{2\pi i}{\hbar}\right)(1 - e^{-\beta w})\, \underline{S}(w) \qquad (1.12)$$

From the analytic form (1.11) it is clear that $\underline{G}(w)$ is analytic in the upper (lower) half complex Z plane and thus the

real and imaginary parts of $\underline{G}(w)$ are related by Kramers-Kronig relations

$$\text{Re } \underline{G}(w) = \left(\frac{1}{\pi}\right) P \int_{-\infty}^{\infty} \frac{\text{Im } G(w')}{w - w'} dw' \tag{1.13a}$$

and

$$\text{Im } G(w) = \left(-\frac{1}{\pi}\right) P \int_{-\infty}^{\infty} \frac{\text{Re } G(w')}{w - w'} dw' \tag{1.13b}$$

where $P \int$ is the principal part of the integral. Since displacement operator $u_\alpha(l;t)$ is even under time reversal, we find

$$G(-w + i\delta) = G^*(w + i\delta) \tag{1.14}$$

So that the Hilbert transform (1.12) may be folded into integrals over only the positive frequencies

$$\text{Re } G(w) = \left(\frac{2}{\pi}\right) P \int_{0}^{\infty} \frac{w' \text{ Im } G(w')}{w^2 - w'^2} dw' \tag{1.15a}$$

and

$$\text{Im } G(w) = \left(-\frac{2w}{\pi}\right) \int_{0}^{\infty} \frac{\text{Re } G(w')}{w^2 - w'^2} dw' \tag{1.15b}$$

The major experimental quantities (viz. phonon dispersion curves, density of states, etc.) can be determined if the Green's functions can be found from the equation of motion which we discuss next.

1.3.1 Equation of motion of the Green's function

Differentiating the formal Green's function (1.10) with respect to time gives the equation of motion

$$i\hbar \left(\frac{\partial}{\partial t}\right) \langle\langle u_\alpha(l;t),\ u_{\alpha'}(l';0)\rangle\rangle$$

$$= 2\pi\delta(t) \langle [u_\alpha(l),\ u_{\alpha'}(l')]\rangle$$

$$+ \langle\langle [u_\alpha(l;t),\ H];\ u_{\alpha'}(l';0)\rangle\rangle$$

$$= 0 + i\hbar \langle\langle p_\alpha(l,t)/M_\alpha(l);\ u_{\alpha'}(l',0)\rangle\rangle \qquad (1.16)$$

This contains a different Green's function, so proceeding to the next equation

$$i\hbar \left(\frac{\partial}{\partial t}\right) \langle\langle p_\alpha(l,t)/M_\alpha(l);\ u_{\alpha'}(l';0)\rangle\rangle$$

$$= 2\pi\delta(t) \langle [p_\alpha(l)/M_\alpha(l);\ u_{\alpha'}(l')]\rangle$$

$$+ \langle\langle [p_\alpha(l;t)/M_\alpha(l),\ H];\ u_{\alpha'}(l';0)\rangle\rangle$$

$$= -\frac{2\pi i\hbar}{M_\alpha(l)}\,\delta(t)\,\delta_{\alpha\alpha'}\,\delta_{ll'}$$

$$-\frac{i\hbar}{M_\alpha(l)} \sum_{\alpha'' l''} \Phi_{\alpha\alpha''}(l,l'') \cdot \langle\langle u_{\alpha''}(l'',t);\ u_{\alpha'}(l';0)\rangle\rangle \qquad (1.17)$$

Defining

$$G_{\alpha\alpha'}(l,l';t) = \langle\langle u_\alpha(l;t),\ u_{\alpha'}(l';0)\rangle\rangle \qquad (1.18)$$

We find

$$M_\alpha(l) \frac{\partial^2}{\partial t^2} G_{\alpha\alpha'}(l,l';t)$$

$$= -2\pi\delta(t)\,\delta_{ll'}\,\delta_{\alpha\alpha'} - \sum_{\alpha'' l''} \Phi_{\alpha\alpha''}(l,l'')\, G_{\alpha''\alpha'}(l'',l';t) \qquad (1.19)$$

The Fourier transform to frequency gives

$$M_\alpha(l)\, w^2\, G_{\alpha\alpha'}(l,l';w) = \delta_{\alpha\alpha'}\,\delta(l,l') + \sum_{\alpha''l''} \Phi_{\alpha\alpha''}(l,l'') \cdot G_{\alpha''\alpha'}(l'',l';w) \qquad (1.20)$$

Written in the full matrix notation

$$\underline{M}\, w^2\, \underline{G}(w) = \underline{1} + \underline{\Phi}\, \underline{G}(w)$$

or

$$\underline{G}(w) = \left[\underline{M}\, w^2 - \underline{\Phi}\right]^{-1} \qquad (1.21)$$

The Green's function for a perfect crystal described by the Hamiltonian H^o (1.1) satisfies a similar equation

$$\underline{G}^o(w) = \left[\underline{M}^o\, w^2 - \underline{\Phi}^o\right]^{-1} \qquad (1.22)$$

Hence on introducing the perturbation matrix

$$\underline{V}(w) = (\underline{M}^o - \underline{M})\, w^2 + \left[\underline{\Phi} - \underline{\Phi}^o\right] \qquad (1.23)$$

We can obtain the basic Dyson equation relating $\underline{G}(w)$ and $\underline{G}^o(w)$,

$$\underline{G}(w) = \underline{G}^o(w) + \underline{G}^o(w)\, \underline{V}(w)\, \underline{G}(w) \qquad (1.24)$$

Solution to this equation will be described in Chapter II. However it is clear that a detailed knowledge of $\underline{G}^o(w)$ is required and we, hence, direct our attention to this problem. We first discuss lattice symmetries and their utility in evaluating $G^o(w)$ and $G(w)$ as well.

1.4 Lattice Symmetries

Symmetry operations, S, consist of a special translation and/or rotation $S(\underline{T},r)$, which leave not only the potential but also the lattice itself invariant:

$$S\,\underline{R}^{\underline{m}} = \underline{T} + r\,\underline{R}^{\underline{m}} = \underline{R}^{\underline{m}_s} \qquad (1.25)$$

where m, m_s are lattice site indices.

i.e. with $\underline{R}^{\underline{m}}$, $\underline{R}^{\underline{m}_s}$ also covers all lattice sites. These symmetries are very important; they allow one to reduce the number of independent force constants and to obtain the eigenvectors of the coupling matrix. Therefore we discuss them in detail for three-dimensional (3-D) Bravais Lattices. Here the translation-rotational invariance

$$\begin{aligned}\phi(\ \cdots\ \underline{X}^{\underline{m}} + \underline{S}^{\underline{m}} + \cdots\ ) &= \phi(\ \cdots\ I + r\,\underline{X}^{\underline{m}} + r\,\underline{S}^{\underline{m}}\ ) \\ &= \phi(\ \cdots\ \underline{X}^{\underline{m}_s} + r\,\underline{S}^{\underline{m}} \cdots\ ) \qquad (1.26)\end{aligned}$$

means that the expansion of internal potential U about $\underline{X}^{\underline{m}}$ with displacement $\underline{S}^{\underline{m}}$ is identical to the expansion about $\underline{X}^{\underline{m}_s}$ with displacements $r\,\underline{S}^{\underline{m}}$,

$$\begin{aligned}2U &= (\underline{S}^{\underline{m}},\ \phi^{\underline{m}\underline{n}}\ \underline{S}^{\underline{n}}) = (r\,\underline{S}^{\underline{m}},\ \phi^{\underline{m}_s\underline{n}_s}\ r\,\underline{S}^{\underline{n}}) \\ &= (\underline{S}^{\underline{m}},\ r^{-1}\ \phi^{\underline{m}_s\underline{n}_s}\ r\,\underline{S}^{\underline{n}}) \qquad (1.27)\end{aligned}$$

which leads to

$$\begin{aligned}\phi^{\underline{m}\underline{n}} &= r^{-1}\ \phi^{\underline{m}_s\underline{n}_s}\ r\ ; \\ \phi^{\underline{m}\underline{n}}_{ik} &= r_{i'i}\ \phi^{\underline{m}_s\underline{n}_s}_{i'k'}\ r_{k'k} \qquad (1.28)\end{aligned}$$

Translational symmetry, $\underline{m} = \underline{m} + \underline{h}$, $r = 1$ means

$$\phi^{\underline{m}\underline{n}} = \phi^{\underline{m} + \underline{h},\ \underline{n} + \underline{h}} = \phi^{(\underline{m} - \underline{n})} \qquad (1.29a)$$

Inversion about a lattice point, $r = -1$, $\underline{m}_s = -\,m$, is also a symmetry operation for every Bravais lattice,

$$\phi^{\underline{mn}} = \phi^{\pm(\underline{m}-\underline{n})} = \phi^{\underline{nm}} ;$$

$$\phi^{\underline{mn}}_{ik} = \phi^{\underline{mn}}_{ki} \quad . \tag{1.29b}$$

Besides inversion the point symmetries contain rotations about lattice points which depend on the type of lattice. Let us discuss (1.28)

$$\phi^{(\underline{h})} = r^{-1}\, \phi^{(\underline{h}_s)}\, r \; ; \quad r\, \underline{R}^{\underline{h}} = r\underline{R}^{\underline{h}_s} \tag{1.30}$$

or in another notation#,

$$\phi(\underline{R}^{\underline{h}}) = r^{-1}\, \phi(\underline{R}^{\underline{h}})\, r \tag{1.30a}$$

If we consider rotations only which leave $\underline{R}^{\underline{h}}$ invariant for any value of $\underline{R}^{\underline{h}}$, then

$$\phi(\underline{R}^{\underline{h}}) = r^{-1}\, \phi(\underline{R}^{\underline{h}})\, r$$

or (1.30b)

$$\phi^{(\underline{h})} = r^{-1}\, \phi^{(\underline{h})}\, r$$

restricts the form of $\phi^{(\underline{h})}$ to make it compatible with the particular point symmetry. After having found a compatible $\phi^{(\underline{h})}$, one can find the coupling matrix for equivalent $\underline{h}'_s$ from (1.30).

Here we discuss only structures of highest symmetry. Figure (1.1a) shows the linear lattice, with the obvious point symmetries unity and inversion, corresponding to $\tilde{x} = (r\ X) = \pm X$. The symmetries of the plane square, lattice, Figure 1.1b, consist of all rotations which leave the elementary square (the Wigner-Seitz-Cell) invariant. These are 8 operations($\pm$ X, $\pm$ Z), ($\pm$ Z, $\pm$ X). The highest symmetry in three-dimensional lattices is cubic. It contains all 48 rotations (Figures 1.1c-e) about

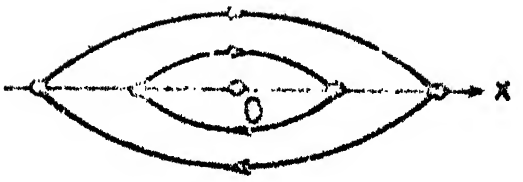

FIG. 1-1c

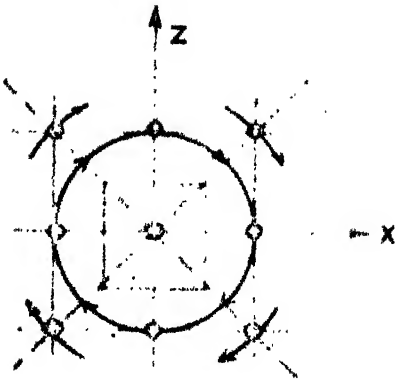

FIG. 1-1b

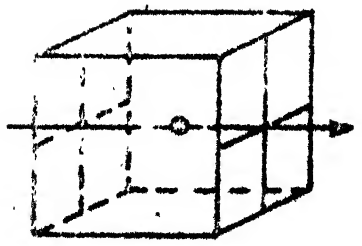

axis: [100]
angle: π/2

FIG. 1-1c

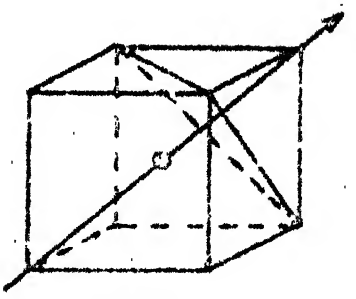

[111]
2π/3

FIG. 1-1d

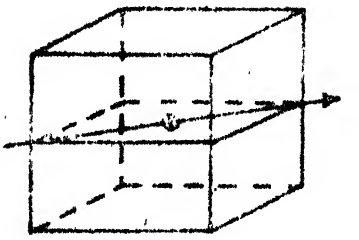

[110]
π

FIG. 1-1e

the center of a cube which transforms that cube into itself: ($\pm$ X, $\pm$ Y, $\pm$ Z) and permutations of X, Y, Z.

1.4.1 Reduction of the force constant Matrix for Cubic Symmetry

Let us first discuss $\phi^{(o)} = \phi(o)$ which, obviously, is invariant against all 48 operations: the off-diagonal elements must vanish, the diagonal elements are equal and $\phi^{(o)}$ is scalar.

$$\phi_{ik}^{(o)} = f\,\delta_{ik}, \quad \text{1 independent parameter f} \tag{1.31}$$

If $\underline{R}^h \parallel [100]$ the rotations (X, $\pm$ Y, $\pm$ Z) and (X, $\pm$ Z, $\pm$ Y) do not change $\underline{R}^h$. The coupling must have the form

$$\phi(\underline{R}^h \parallel [100]) = \phi^{100} = -\begin{bmatrix} f_l & 0 & 0 \\ 0 & f_t & 0 \\ 0 & 0 & f_t \end{bmatrix}, \tag{1.32}$$

2 independent parameters

It can be represented by a longitudinal (spiral) spring f_l and an isotropic transverse (leaf) spring f_t, Figures (1.2a-c),

$$-\phi^{100} = f_l P_l^{[100]} + f_t (1 - P_l^{[100]})$$

$$= f_l P_l^{[100]} + f_t P_t^{[100]} \tag{1.33a}$$

with the longitudinal projector in direction $\underline{R}^h$,

$$P_l^{100} = |\underline{\hat{R}}^h\rangle\langle\underline{\hat{R}}^h| = \begin{bmatrix} 1 & 0 & 0 \\ 0 & 0 & 0 \\ 0 & 0 & 0 \end{bmatrix} \tag{1.33b}$$

By the rotation (- Y, X, Z), where $[100] \rightarrow [010]$, one obtains from (1.30a)

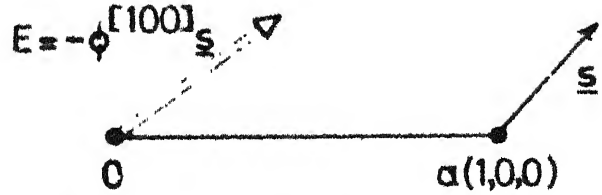

a) Force $\underline{F}$ on atom 0 due to an arbitrary displacement $\underline{s}$ of an atom at $\underline{R}^h \parallel [110]$, here $\underline{R}^h = (1, 0, 0)$.

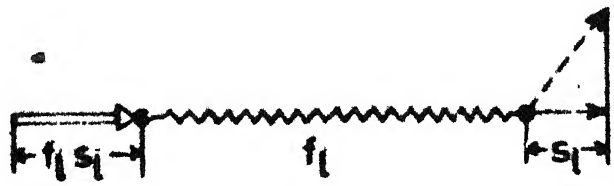

b) The longitudinal component of $\underline{s}$, s_l leads to a force $f_l s_l$ in [100]-direction, which can be represented by a longitudinal (spiral) spring f_l.

c) The transversal component of $\underline{s}$, s_t, leads to a force $f_t s_t$ perpendicular to the [100]-direction, which can be represented by an isotropic transversal (leaf) spring f_t.

FIG.1-2 Coupling in [100] direction

$$-\phi^{[010]} = \begin{bmatrix} f_t & 0 & 0 \\ 0 & f_l & 0 \\ 0 & 0 & f_t \end{bmatrix} = f_l P_l^{[010]} + f_t P_t^{[010]} ;$$

$$P_l^{[010]} = \begin{bmatrix} 0 & 0 & 0 \\ 0 & 1 & 0 \\ 0 & 0 & 0 \end{bmatrix}$$

this shows how to extend (1.33a) to other <100> couplings.

If $\underline{R}^{h} \,||\, [111]$ all permutations of (X, Y, Z) leave $\underline{R}^{h}$ unchanged and $\phi^{(\underline{h})}$ has a representation equivalent to that of (1.30a)

$$-\phi^{[111]} = f_l P_l^{[111]} + f_t(1 - P_l^{[111]}) , \quad P_l^{[111]} = \frac{1}{3} \begin{bmatrix} 1 & 1 & 1 \\ 1 & 1 & 1 \\ 1 & 1 & 1 \end{bmatrix} , \tag{1.34}$$

There are then 2 independent parameters, although the form of $\phi^{(\underline{h})}$ is changed (Figures 1.3a-d).

If $\underline{R}^{h} \,||\, [110]$ all operations (X, Y, $\pm$Z), (Y, X, $\pm$Z) are admitted. The coupling is represented by

$$-\phi^{[110]} = f_l P_l^{[110]} + f_{t'} P_{t'}^{[110]} + f_t P_t^{[110]} , \tag{1.35}$$

3 independent parameters

i.e. a longitudinal spring and two different transversal springs; P_t projects onto a cubic edge

$$P_l^{[110]} = \frac{1}{2} \begin{bmatrix} 1 & 1 & 0 \\ 1 & 1 & 0 \\ 0 & 0 & 0 \end{bmatrix} , \quad P_t^{[110]} = \begin{bmatrix} 0 & 0 & 0 \\ 0 & 0 & 0 \\ 0 & 0 & 1 \end{bmatrix} = P_l^{[001]} ,$$

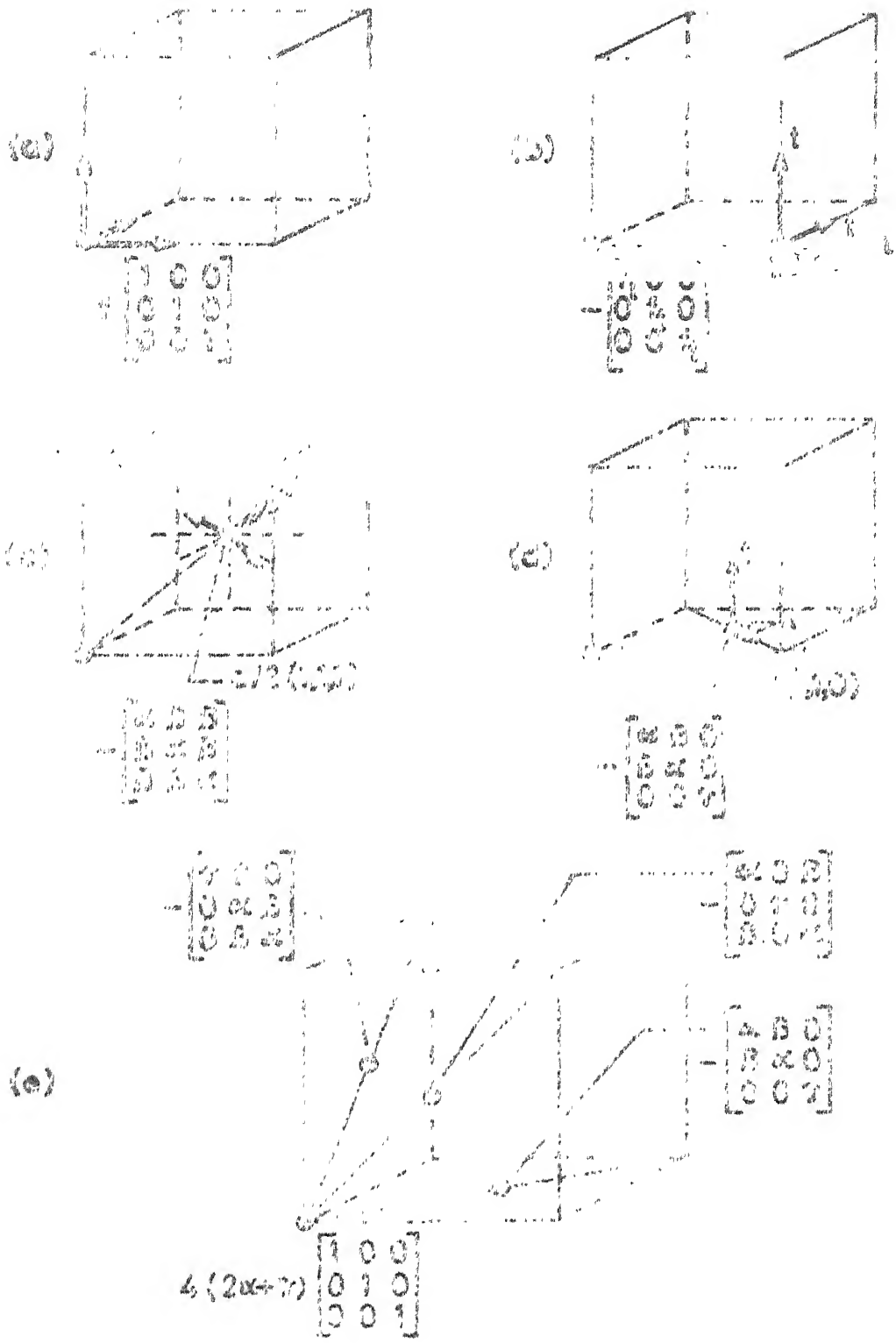

FIG. 13

$$P_{t'}^{[110]} = \frac{1}{2}\begin{bmatrix} 1 & \bar{1} & 0 \\ \bar{1} & 1 & 0 \\ 0 & 0 & 0 \end{bmatrix} = P_l^{[1\bar{1}0]} \qquad (1.35a)$$

The coupling is still longitudinal and transversal in character, but the transversal behaviour is no longer isotropic (Figures 1.3a-d).

Now we are in position to construct a force constant model for cubic lattices. Because of translational invariance

$$\sum_{\underline{h}} \phi^{(\underline{h})} = 0 \quad \Longrightarrow \quad \phi^{(o)} = - \sum_{\underline{h}\neq o} \phi^{(\underline{h})} \qquad (1.36)$$

In cubic crystals, where $\phi^{(o)}$ is scalar,

$$\phi_{ik}^{(o)} = \delta_{ik} \frac{tr\{\phi^{(o)}\}}{3} = - \frac{\delta_{ik}}{3} \sum_{\underline{h}\neq o} tr\{\phi^{(\underline{h})}\}$$

$$= f^{(o)} \delta_{ik} \qquad (1.36a)$$

A very crude model, where only $\phi^{(o)}$ enters, is the Einstein model in which each atom moves independently with the rigid environmental coupling. A first neighbour model in cubic Bravais crystals contains then only the parameters of 1st neighbour coupling (2 for SC <100> and BCC <111> : f_l, f_t; 3 for FCC <110> : $f_l, f_{t'}, f_t$) while $\phi^{(o)}$ is given by (1.36):

For SC:

$$\phi^{[100]} = - \begin{bmatrix} \alpha & 0 & 0 \\ 0 & \beta & 0 \\ 0 & 0 & \beta \end{bmatrix} ; \quad f_l = \alpha , \quad f_t = \beta$$

and

$$f^{(o)} = -\frac{6}{3} X \sum_{\underline{h}\neq o} tr(\phi^{(\underline{h})})$$

$$= 2(f_l + 2f_t) \qquad (1.37a)$$

For BCC:

$$\phi^{[111]} = -\begin{bmatrix} \alpha & \beta & \beta \\ \beta & \alpha & \beta \\ \beta & \beta & \alpha \end{bmatrix} \quad ; \quad f_l = \alpha + 2\beta \,, \quad f_t = \alpha - \beta$$

and

$$f^{(o)} = \frac{8}{3}(f_l + 2f_t) \qquad (1.37b)$$

For FCC:

$$\phi^{[110]} = -\begin{bmatrix} \alpha & \beta & 0 \\ \beta & \alpha & 0 \\ 0 & 0 & \gamma \end{bmatrix} \quad ; \quad f_l = \alpha+\beta \,, \; f_{t'} = \alpha - \beta \,, \; f_t = \gamma$$

and

$$f^{(o)} = 4(f_l + f_{t'} + f_t) \qquad (1.37c)$$

Figure (1.3e) illustrates the 1st neighbour model for the FCC lattice.

Now we discuss the translational-rotational invariance

$$\sum_{\underline{h}} \phi^{(\underline{h})} = 0 \qquad \text{and} \qquad \sum_{\underline{h}} \underline{X}^{(\underline{h})} \cdot \phi^{(\underline{h})} = 0 \qquad (1.38)$$

Validity in substitutionally disordered lattices. For simplicity, we consider a substitutional defect, as shown in Figure (1.4a), which disturbs the translational symmetry of the lattice. Now $\sum_{\underline{h}} \phi^{(\underline{h})} \neq 0$. Moreover, the transversal springs between two atoms, in general, do not really represent an interaction between those

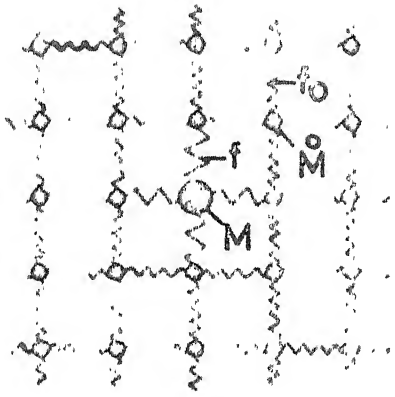

(a)

A substitutional defect representation.

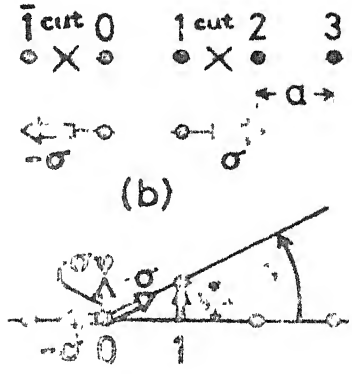

(c)

[illegible] spring f_1 under tension σ. (a) Cutting a spring requires forces $\pm\sigma$ in order to maintain equilibrium (b) for a transversal displacement, φ a, of atom 1 the net force on atom 0 is $\sigma\varphi$; this can be represented by a transversal spring, $f_t = \sigma\varphi/\varphi a = \sigma/a$.

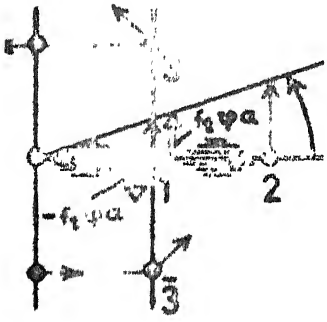

(d)

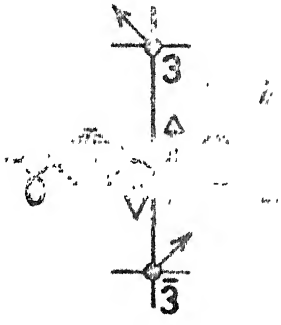

(e)

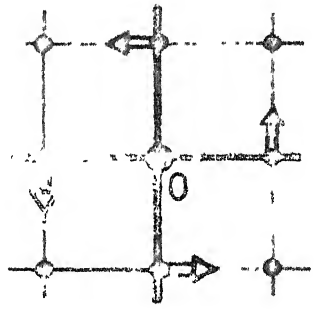

(f)

Violation of rotational invariance for a substitutionally defect model (SC structure with lattice distance a). (d) Displacement pattern for rotation by an angle φ about atom 0. The forces on 1 by the spring (0-1) $-f_t\varphi a$ and the spring (1-2), $f_t\varphi a$ cancel. The same holds for the forces from 3 and $\bar{3}$. e) A defect with a different spring f_{t_1} is substituted at 0. The forces on one due to 0 and 2 are not balanced. f) Force pattern around defect due to rotation; the resulting torque is $-4(f_{t_1} - f_t)\varphi a^2$.

FIG.1-4

two atoms alone but rather many body interactions. This is more easily seen for a longitudinal spring f_l under tension σ which produces a transversal spring $f_t = \sigma/a$ (Figure 1.4b). The tension is carried by the environment. The consequence is that the modified transverse springs violate rotational invariance in the lattice as shown in Figure (1.4c) for a SC structure, i.e. total torque is non-zero. This simple example demonstrates that the springs - transverse and longitudinal, have to be properly treated if one wishes to study the substitutionally disordered lattices with force-constant disorder (Chapters II and III).

So far we have discussed the highest symmetry directions in real space which fix the eigenvectors and the degeneracy of the eigenvalues for the coupling. The same considerations apply to $\tilde{\Phi}(\underline{k})$ in K-space if $\underline{k}$ is parallel to a high symmetry direction. Now we make use of these symmetries in defining Green's functions and dispersion curves.

1.5 Green's Function and Dispersion Curves

The translational symmetry shows further that if $e(\underline{n})$ is eigen vector of $\Phi_{ik}^{\underline{mn}}$, so is

$$T(\underline{h})\{\underline{e}(\underline{n})\} = \underline{e}(\underline{n} + \underline{h}) \qquad (1.39$$

with the same eigenvalue, which means that by shifting a displacement pattern its property of being an eigenvector of $\Phi(\underline{h})$ remains unchanged. This allows us to find immediately harmonic solutions of the equations of motion by employing displacements which are eigenvectors of $\underline{T}(\underline{h})$, namely,

$$\underline{e}(\underline{n}) = A\, e^{i\underline{k}.\underline{R}^n}$$

$$T(\underline{h})\{\underline{e}(\underline{n})\} = \underline{e}(\underline{n} + \underline{h}) = e^{i\underline{k}.\underline{R}^h}\, \underline{e}(\underline{n}) \qquad (1.4$$

with an eigenvalue $\exp(i\underline{k}.\underline{R}^{h})$ and with a yet unspecified "polarized" vector $\underline{A}$. Thus

$$\underline{\underline{\Phi}}^{mn} \underline{A}\, e^{i\underline{k}.\underline{R}^{n}} = \sum_{h} \underline{\underline{\Phi}}^{(\underline{h})} e^{-i\underline{k}.\underline{R}^{(\underline{h})}} \underline{A}\, e^{i\underline{k}.\underline{R}^{(\underline{m})}}$$

$$= \tilde{\underline{\underline{\Phi}}}(\underline{k})\, \underline{A}\, e^{i\underline{k}.\underline{R}^{(\underline{m})}} \qquad (1.41)$$

where

$$\tilde{\underline{\underline{\Phi}}}(\underline{k}) = \sum_{h} \underline{\underline{\Phi}}^{(\underline{h})} e^{-i\underline{k}.\underline{R}^{(\underline{h})}} \qquad (1.41a)$$

has the properties

$$\tilde{\underline{\underline{\Phi}}}(\underline{k}) = \tilde{\underline{\underline{\Phi}}}(-\underline{k}) = \tilde{\underline{\underline{\Phi}}}^{*}(\underline{k})$$

Therefore the eigenvectors of $\underline{\underline{\Phi}}$ are determined by the eigenvectors $\underline{e}(\underline{k}, \sigma)$, $\sigma = 1, 2, 3$ of the 3×3 symmetrical matrix $\underline{\underline{\Phi}}(\underline{k})$ $\left[M\,\omega^{2}(\underline{k}) = \tilde{\underline{\underline{\Phi}}}(\underline{k})\right]$,

$$\underline{\underline{\Phi}}(\underline{k})\, \underline{e}(\underline{k}, \sigma) = \tilde{\underline{\underline{\Phi}}}(\underline{k}, \sigma)\, \underline{e}(\underline{k}, \sigma),$$

with

$$(\underline{e}(\underline{k}, \sigma), \underline{e}(\underline{k}', \sigma')) = \delta_{\sigma\sigma'}\, \delta(\underline{k} - \underline{k}') \qquad (1.42a)$$

Finally,

$$\underline{\underline{\Phi}} \,|\, \underline{k}\sigma \rangle = \tilde{\underline{\underline{\Phi}}}(\underline{k}\sigma)\,|\underline{k}\sigma\rangle, \quad \langle a_{i}^{m}|\underline{k}\sigma\rangle = e_{i}(\underline{k}\sigma)\, \frac{e^{i\underline{k}.\underline{R}^{m}}}{\sqrt{V_{0}}} \qquad (1.42b)$$

All quantities are periodic in the reciprocal lattice i.e. $\underline{k}$ can be restricted to the Brillouin Zone, $\underline{k}$ in V_{B}. Thus

$$\underline{\underline{\Phi}}^{(\underline{h})} = \int_{V_{B}} \frac{d\underline{k}}{V_{B}}\, \tilde{\underline{\underline{\Phi}}}(\underline{k})\, e^{i\underline{k}.\underline{R}^{(\underline{h})}} \qquad (1.43$$

Since $G^{(\underline{h})}(w)$ and $\tilde{G}(\underline{k}, w)$ also have same symmetries like $\underline{\underline{\Phi}}^{(\underline{h})}$ and $\tilde{\underline{\underline{\Phi}}}(\underline{k})$ respectively, we can define,

$$G^{(\underline{h})}(w) = \int_{V_B} \frac{d\underline{k}}{V_B} \cdot G(\underline{k}, w)\, e^{i\underline{k}.\underline{R}^{(\underline{h})}} \qquad (1.44a)$$

with

$$\tilde{G}_{ij}(\underline{k}, w) = \sum_{\sigma} \frac{e_i(\underline{k}\,\sigma)\, e_j(\underline{k}\,\sigma)}{\tilde{\Phi}(\underline{k}\,\sigma) - M(w + i\eta)^2} \qquad (1.44b)$$

Here $\Phi(\underline{k}\,\sigma)$ are the eigenvalues of $\tilde{\Phi}(\underline{k})$

$$\tilde{\Phi}(\underline{k}\,\sigma) = M\,\Omega^2(\underline{k}\,\sigma) = (\underline{e}(\underline{k}\,\sigma), \tilde{\Phi}(\underline{k})\, \underline{e}(\underline{k}\,\sigma))$$

which represent twice the potential energy per atom for a wave $\underline{S}^m = \underline{e}(\underline{k}\,\sigma) \exp(i\underline{k}.\underline{R}^m)$. For cubic crystals we use the results discussed in Section 1.4.1 where the eigenvectors of $\Phi(\underline{R}^h)$ were derived for $\underline{R}^h$ parallel to the main symmetry directions. The eigenvectors of $\Phi(\underline{R}^h)$ illustrated in Figures (1.3a-d) can be viewed as polarizations for the corresponding three $\underline{k}$-directions. Dynamical stability requires $\tilde{\Phi}(\underline{k}) > 0$ except for translations, $k = 0$, $\tilde{\Phi} = 0$. The eigenvectors $|\underline{k}\,\sigma>$ form a complete basis for displacements with $(\underline{S}, \underline{S}) < \infty$; the eigenvalues themselves cannot be normalized, but their displacements remain atleast bounded at infinity. This does not hold for rotations. Consequently, rotations are not even admitted as proper displacement fields (Leibfried and Breuer, 1978).

To avoid the difficulties connected with the normalization of eigenvectors and the invariance inconsistency, we reverse the procedure to get the dispersion curves in disordered lattices (Chapter III). If $G(w)$ is known, we can get immediately $G(\underline{k}, w)$. The imaginary part of $G(\underline{k}, w)$ directly gives information about the eigenvalues. In a periodic system it is a delta function at eigenvalues, while a disordered lattice broadens the peaks making

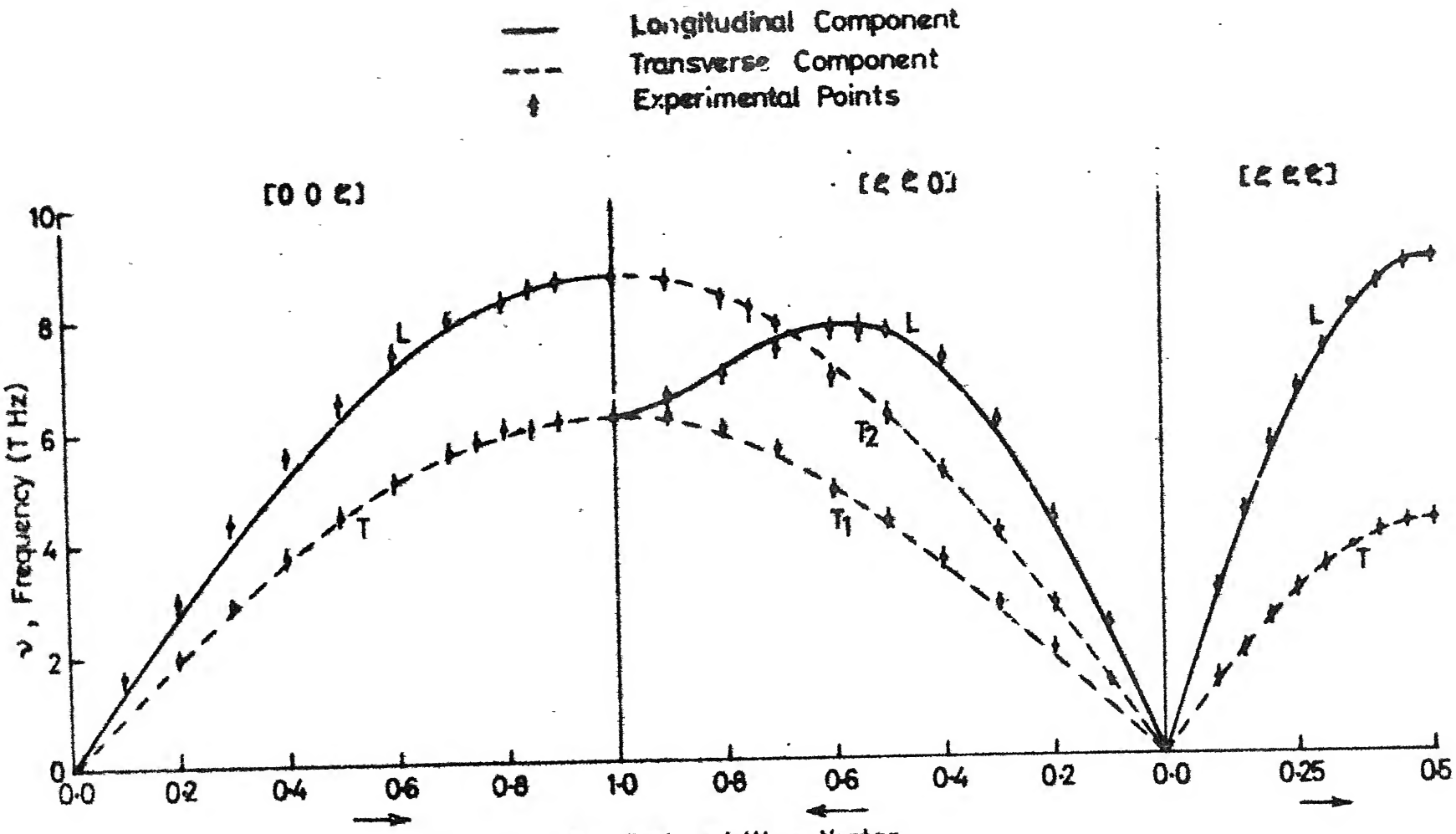

FIG.1-5 Dispersion Curves for Nickel

the phonon life time finite. For periodic systems we still use force constants model for evaluating the dispersion curves which is discussed below.

1.5.1 Born-von Karman Models in Cubic Lattices

Because a theory of the potential and of the force parameters is rather complicated and it is difficult to obtain results from first principles, one often uses models with fitting parameters to represent the dispersion curves. The number of parameter should be small. In metals, as a rule, the electrons screen the interaction between ions such that one expects interaction only between near neighbours. Consequently one can use near neighbour force constants as fitting parameters. This is called Born-von Karman model. If $\Omega(\underline{k})$ is smooth, only near neighbours contribute, whereas structure indicates contributions from more distant neighbours. Here we restrict ourselves to short range interactions and for demonstration we choose the FCC lattice with 1st neighbou interaction only, Figure 1.5, for which,

$$\tilde{\phi}_{11}(\underline{k}) = -2 \sum_{\underline{h}} \phi_{11}^{(\underline{h})} \frac{\sin^2(\underline{k}.\underline{R}^{\underline{h}})}{2}$$

$$= 4\gamma \left(\sin^2 \frac{k_2 + k_3}{4} a + \sin^2 \frac{k_2 - k_3}{4} a\right)$$

$$+ 4\alpha \left(\sin^2 \frac{k_1 + k_2}{4} a + \sin^2 \frac{k_1 - k_2}{4} a + \sin^2 \frac{k_1 + k_3}{4}\right.$$

$$\left. + \sin^2 \frac{k_1 - k_3}{4} a\right)$$

$$4\alpha = 2(f_1 + f_{t'}), \quad 4\gamma = 4f_t \qquad (1.4$$

$$\tilde{\phi}_{12}(\underline{k}) = 4\beta \left(\sin^2 \frac{k_1+k_2}{4} a - \sin^2 \frac{k_1-k_2}{4} a\right), \; 4\beta = 2(f_1-f_{t'}),$$

Comparison is made with experimental points for Ni. How much the deviations affect the study of disordered lattices will be treated in detail in Chapter III.

This model is rather abstract, in the sense that one does not see the cause of the interaction. In particular, for transversal springs, the origin is not clear and one cannot remove them without violating rotational invariance. Consequently, the use of such model for disordered lattice calculations is rather restricted. One can however, explore other couplings which are based on more physical models and which, then must obey rotational invariance. But we will not enter into a discussion of sophisticated models which are out of scope of our work.

We have so far discussed Green's functions and their relations with dispersion curves. But there are also other experimental quantities viz. density of states, neutron scattering cross section, etc. which are related to Green's functions and are the check for the study of ordered and disordered lattices. So we discuss them for the sake of completeness.

1.6 Experimental Quantities

1.6.1 Density of states

The vibrational (phonon) density of states $\rho(w)$ is related to the "mass weighted" displacement-displacement Green's function $G(w)$ (Eq. 1.21),

$$\rho(w) = -\frac{2w}{\pi\, dn}\, \mathrm{Tr}\, \left(\mathrm{Im}_{\delta \to 0^+}\, \underline{M}\, \underline{G}(w + i\delta)\right) \qquad (1.46)$$

where $\underline{M}$ is the mass matrix, n is the number of atoms per unit cell, d is the dimensionality of the system. For the periodic

lattices, we can make use of Eqs. (1.44) to rewrite the density of states in terms of $\Omega(\underline{k}\,\sigma)$,

$$\rho(w) = \frac{2\,Mw}{dn} \sum_{\underline{k}\sigma} \delta(w^2 - \Omega^2(\underline{k}\,\sigma)) \qquad (1.46a)$$

This expression holds good if one gets the normal modes easily (Maradudin et al, 1971). But in disordered lattices, the transformations like (1.42) seem to be quite difficult because of lack of translational invariance. So we avoid "k-space" idea in our work wherever it is possible. Instead, we choose the real space technique - 'Recursion' method for evaluating $\underline{G}(w)$ and developing our formalism for the study of disordered alloys (Chapter II). The recursion method is explained in Appendix A.

1.6.2 Inelastic Neutron Scattering

Inelastic neutron scattering cross-section consists of a coherent and an incoherent part (Elliott and Leath, 1975; Sjolander, 1964). The coherent part is related to a weighted average over the displacement correlation function, specifically

$$\frac{d^2\sigma^c}{d\Omega\,dw} = \frac{h}{\pi}\frac{K'}{K} \sum_{\substack{\alpha\alpha' \\ AA'}} B_\alpha^A B_{\alpha'}^{A'} q_\alpha q_{\alpha'} \operatorname{Im} \langle G_{\alpha\alpha'}^{AA'}(q, w)\rangle \; n(w) \qquad (1.47)$$

where

$$B_\alpha(l) = b_\alpha^c(l) \exp\{-\tfrac{1}{2}\langle[\underline{q} \cdot \underline{u}_\alpha(l)]^2\rangle\}$$

$$n(w) = \frac{1}{(\exp(\hbar w/K_B T) - 1)}$$

Here A defines the atomic species at site . The incoherent scattering

$$\frac{d^2\sigma^i}{d\Omega dw} = \frac{h}{\pi}\frac{K'}{K}\sum_{\alpha A} \rho_\alpha^A q_\alpha^2 \, \mathrm{Im} \langle G_{\alpha\alpha}^{AA}(0, 0; w)\rangle n(w) \qquad (1.48)$$

is related to a weighted average of the single site Green's function and hence to the density of states.

These weighted Green's functions are related to unweighted Green's functions. For single site approximation the expressions developed by Elliott and Leath (1975) are frequently used. But we follow a entirely different approach. After obtaining configurationally averaged Green's functions (discussed in Chapter II), we make use of 'Recursion' method (Appendix A) for getting weighted Green's functions. Here we carry out the similar recursion procedure as in the ordered lattice with new self-energies except at those sites where we wish to evaluate the weighted Green's function.

However, the coherent cross-section allows a direct measurement of $\langle G(k, w)\rangle$ and gives the most detailed experimental information about phonons in mixed crystals. The imaginary part of $\langle G(k,w)\rangle$, the spectral function, is proportional to line-shapes and their widths are finite. These are the quantities which are frequently measured and hence we discuss them in Chapter III.

Chapter II

The Coherent Potential Approximations

2.1 Introduction

In this chapter we shall review briefly the existing methods for the solution of Eq. (1.24) alongwith our method. Though attractive at first, some approaches become intractable for the phonon study, while others involving simplifying assumptions either become far removed from reality or loose features essential for physical relevance. In the study of phonons in disordered solids all the disorders - diagonal, off-diagonal and environmental - are coupled. Our aim, therefore, is to examine these methods with their shortcomings and discuss the basic ideas behind the different approaches, so as to expose avenues of generalisation including all effects which yield physically valid results in the real alloys.

2.2 Virtual Crystal Approximation (VCA)

In the virtual crystal limit when the scattering by the disorder is very weak i.e. the mass changes and force constant changes are small, a perturbation expansion in powers of V as defined in (1.24) is valid. The expansion is

$$\langle \underline{G}(l,l') \rangle = \underline{G}^{o}(l,l') + \sum_{mm'} \underline{G}^{o}(l,m) \langle \underline{V}(m,m') \rangle \underline{G}^{o}(m',l') + \sum_{\substack{mm' \\ nn'}} \underline{G}^{o}(l,m) \langle \underline{V}(m,m') \underline{G}^{o}(m',n) \underline{V}(n,n') \rangle \underline{G}^{o}(n',l') \qquad (2.1$$

In the VCA, it is assumed that all the $\underline{V}(m,m')$ are very small so that the higher order products of $\underline{V}$'s need only be treated approximately. Thus all such average products of $\underline{V}$'s are decoupled (a random phase approximation) into products of average

$$\langle \underline{V}(1,1')\, V(2,2') \ldots V(n,n') \rangle$$

$$\simeq \langle V(1,1') \rangle \langle V(2,2') \rangle \ldots \langle V(n,n') \rangle \qquad (2.2)$$

This gives

$$\langle \underline{G}(w) \rangle = \underline{G}^{o}(w) \left[\underline{I} - \langle \underline{V} \rangle \underline{G}^{o}(w)\right]^{-1} \qquad (2.3a)$$

$$= \left[\langle \underline{M} \rangle w^2 - \langle \underline{\phi} \rangle\right]^{-1} \qquad (2.3b)$$

so that the Green's function is approximated by one for a perfect crystal with the atomic masses equal to the mean mass of the disordered crystal and with force constants equal to the mean force constant of the disordered crystal. Thus, the frequency spectrum of the disordered crystal is rigidly shifted to that of a virtual crystal without broadening the states. The phonon dispersion curves in the VCA limit simply shift linearly with concentration. Here phonon K-modes have an infinite life time.

2.3 The Average T-matrix Approximation (ATA)

Rearrange equation (2.1) in such a way that all terms involving repeated scattering by the same impurity are collected together,

$$\langle \underline{G}(1,1') \rangle = \underline{G}^{o}(1,1') + \sum_{m} \underline{G}^{o}(1,m) \langle \underline{t}(m,m') \rangle \underline{G}^{o}(m',1')$$

$$+ \sum_{m,n}{}' \underline{G}^{o}(1,m) \langle t(m,m')\, \underline{G}^{o}(m',n)\, \underline{t}(n,n') \rangle \underline{G}^{o}(n',1') \qquad (2.4)$$

where $\underline{t}(m,m') = t^m$ is given by

$$\underline{t} = \underline{V}\,(\underline{I} - \underline{G}^{o}\,\underline{V})^{-1} \tag{2.5}$$

In matrix form

$$\langle \underline{G} \rangle = \underline{G}^{o} + \underline{G}^{o} \langle \underline{t} \rangle \underline{G}^{o} + \underline{G}^{o} \langle \underline{t}\, \underline{G}^{o'}\, \underline{t} \rangle \underline{G}^{o} + \ldots \tag{2.6}$$

where

$$\underline{G}^{o'}(n,m) = \underline{G}^{o}(n,m) - \underline{G}\,(m',m)\,\delta_{nm'} \tag{2.7}$$

The average t-matrix approximation (ATA) is to decouple the average of the product of t's according to

$$\langle \underline{t}(1)\, \underline{t}(2) \ldots \underline{t}(n) \rangle = \langle \underline{t}(1) \rangle \langle \underline{t}(2) \rangle \ldots \langle \underline{t}(n) \rangle \tag{2.8}$$

which is somewhat better approximation than the VCA (2.2), because adjacent sites are restricted by $\underline{G}^{o'}$ from coinciding (Elliott and Taylor, 1967). Then,

$$\langle \underline{G} \rangle = \underline{G}^{o} + \underline{G}^{o} \left[\langle \underline{t} \rangle (\underline{I} - \underline{G}^{o} \langle \underline{t} \rangle)^{-1} \right] \underline{G}^{o} \tag{2.9}$$

or $\underline{\Sigma}$ as defined in Dyson's equation

$\langle \underline{G} \rangle = \underline{G}^{o} + \underline{G}^{o}\ \underline{\Sigma}\ \langle \underline{G} \rangle$ is given by

$$\underline{\Sigma} = \langle \underline{t} \rangle / \left[\underline{I} + \langle \underline{t} \rangle \underline{G}^{o} \right] \tag{2.10}$$

For mass disorder $\underline{V}$ is diagonal, in the site representation and

$$V_{\alpha\alpha'}(l,l') = \Delta M_{\alpha}\, w^2\ \delta_{\alpha\alpha'}\ \delta(l,l') \tag{2.11}$$

and so is $\underline{t}$. Then

$$\langle t_{\alpha\alpha} \rangle = \frac{C\ \Delta M_{\alpha}\, w^2}{\left[1 - \Delta M_{\alpha}\, w^2\ G^{o}_{\alpha\alpha}(o)\right]} \tag{2.12}$$

and

$$\Sigma_{\alpha\alpha}(w) = \frac{C \Delta M_\alpha w^2}{\left[1 - (1 - c) \Delta M_\alpha w^2 G^o_{\alpha\alpha}(o)\right]} . \qquad (2.13)$$

This single site self energy is site diagonal and is equivalent to an effective mass (complex and frequency dependent) on the disordered site. A weak point of this approximation is its general failure to locate the band edges. To shift the band edges from those of the unperturbed lattice one must treat the scattering in a self consistent field.

2.4 Single Site Mass Coherent Potential Approximation (1CPA or MCPA)

It is a statistically averaged theory which specifies an average Green's function for the equation (1.24) (Taylor, 1967; Soven, 1967). This average-medium Green's function $\underline{g}$ is fixed by the requirements (i) that the effective-medium quasi-particles scatter from each atomic site the minimum amount, that is, the single-site effective medium transition matrix, when averaged over all possible alloy configuration is zero (it is not practical to require that the multisite T-matrix vanishes), and (ii) that its self-energy $\underline{\Sigma}$ assumesthe mathematically simple form

$$\underline{\Sigma} = \sum_n |n\rangle \underline{\sigma}(w) \langle n| \equiv \sum_n \sigma_n(w) \qquad (2.14$$

thereby giving a single frequency dependent life-time and level shift to all the quasinormal modes of the statistically averaged alloy. Requirement (ii) gives the simple result for the effecti medium Green's function

$$\underline{g}(w^o) = \underline{G}^o(w^2 - m_B^{-1} \sigma(w)) \qquad (2.1$$

where $\underline{G}^{o}(w^2)$ is the perfect lattice Green's function for a lattice with all masses equal to m_B. In the MCPA, the choice of reference lattice is irrelevant, because the self-consistent MCPA Green's function is invariant under a change of reference lattice (Elliott et al, 1974). Rewrite the equation (1.24)

$$\underline{G} = \underline{G}^{o} + \underline{G}^{o}\ \underline{V}\ \underline{G} \tag{2.16}$$

where we have

$$\underline{V} = (\underline{\emptyset} - \underline{\emptyset}_o) - (\underline{M} - \underline{M}_o)\ w^2 \tag{2.16a}$$

For the mass-disorder only, $\underline{V}$ is always diagonal and is non-zero only at impurity atom sites:

$$\underline{V} = \sum_n \underline{v}_n \tag{2.17a}$$

with

$$\underline{v}_n = |\ n > (m_B - m_n)\ w^2\ < n\ | \tag{2.17b}$$

The effective medium Green's function is defined as the configuration average of the alloy Green's function $\underline{G}$,

$$\underline{g} = \langle\langle\ \underline{G}\ \rangle\rangle \tag{2.18}$$

where double brackets denote an ensemble average over alloy configurations. In the MCPA the statistically averaged Green's function is assumed to satisfy

$$\underline{g} = \underline{G}^{o} + \underline{G}^{o}\ \underline{\Sigma}\ \underline{g} \tag{2.19}$$

which results in the simple expression Eq. (2.15) where $\underline{\Sigma}$ is the (as yet unknown) self-energy. Eliminating $\underline{G}^{o}$ from Eqs. (2.16) and (2.19), we obtain,

$$\underline{G} = \underline{g} + \underline{g}\,(\underline{V} - \underline{\Sigma})\,\underline{G}$$

$$= \underline{g} + \sum_n (v_n - \sigma_n)\,\underline{G} \qquad (2.20)$$

The single-site effective medium transition matrix is

$$\tau_n = \frac{(v_n - \sigma_n)}{[1 - g(v_n - \sigma_n)]} \qquad (2.21)$$

In the ICPA (MCPA), the configuration-average of τ_n must vanish, thus we have

$$\langle\langle \tau_n \rangle\rangle = 0$$

$$= |n\rangle\langle n| \left(\frac{(1-c)(-\sigma)}{1 + \sigma\langle n|g|n\rangle} + \frac{c\,[(m_B - m_A)w^2 - \sigma]}{1 - \langle n|g|n\rangle\,[(m_B - m_A)w^2 - \sigma]}\right) \qquad (2.22a)$$

which results in the equation for $\sigma(w)$,

$$\sigma(w) = \frac{c(m_B - m_A)w^2}{1 - \langle n|\, G^o(w^2 - m_B^{-1}\,\sigma(w))\,|n\rangle\,[(m_B - m_A)w^2 - \sigma(w)]} \qquad (2.22b)$$

When combined with the known expression for G^o, Eq. (2.22b) can be solved for the self-consistent self-energy $\sigma(w)$. The self-energy is diagonal and branch independent. The MCPA phonon density of states takes the form.

$$\rho(w) = \left(\frac{2w}{N\pi}\right) \mathrm{Im}\,(\mathrm{Tr} \langle\langle \underline{M}\,\underline{G} \rangle\rangle)$$

$$= \left(\frac{2w}{\pi}\right) \mathrm{Im}(m_B(1 - \tilde{\sigma})\langle n|\,\underline{G}^o(w^2(1 - \tilde{\sigma}))\,|n\rangle) \qquad (2.23a)$$

with

$$\sigma(w) = m_B\, w^2\, \tilde{\sigma}(w) \qquad (2.23b)$$

2.4.1 Failures of MCPA

The MCPA provides a reasonably good description of an alloy over a wide range of parameters. It works well when mass difference of two components of a binary alloy is small and becomes inadequate when $\delta = \frac{|\Delta M| w^2}{|Z \phi_{BB}|}$ is large. (Here Z is the number of nearest neighbours).

Since MCPA is a single site approximation it cannot take correctly into account the effects due to two or more sites. Firstly, it cannot correctly account for the randomness in the force constant matrices involving two or more sites. In binary alloys the shape of the vibrational density of states function as well as the spectrum width depend on relative values of various interactions between neighbouring atoms. These numbers can be very different for the two constituents of an alloy even though their atomic force constants are similar. Secondly, short range order due to chemical clustering cannot be taken into account. Finally, the effect of statistical clustering which is particularly important in the impurity bands is totally absent. The local modes show some fine structures (Payton and Visscher, 1967; Dean, 1972; Alben et al, 1975) which are lost in MCPA. The MCPA fails to give correct bandwidths even in the absence of off-diagonal disorder. In fact, MCPA (1CPA) was not designed to reproduce the spectrum, but was constructed to properly mimic in long wavelength properties of the lattice vibrations in the alloy.

The experiments on the vibrational properties of Ni-Pd, Ni-Cr, Ni-Pt alloys indicate that local environment strongly affects the density of states, dispersion curves, and width functions (Kamitakaha and Brockhouse, 1974; Bosi et al, 1978; 1980;

Tsunoda, 1979). In fact MCPA ignores all environmental effects. The failure of ICPA (MCPA) for large $\underline{V}$ (defined in (1.24) can be understood from the fact that for large $\underline{V}$ the excitation mean free path is small and in order to obtain a good estimate of the configurationally averaged Green's function we must consider scattering due to pairs, triplets etc. in a self-consistent manner.

2.5 Generalisation of CPA

From time to time suggestions have been put forward about ways of generalising the CPA to take into account the effect of clusters, off-diagonal disorder and SRO, for the multisite scattering, neglected in ordinary CPA (Mookerjee, 1979; Srivastava and Joshi, 1973). In principle, these generalisations should produce accurate alloy theories, provided a sufficient number of sites are included in the determination of a self-consistent self-energy $\underline{\Sigma}(\underline{k}, w)$.

In the multisite scattering approach the system is partitioned into clusters, each containing n-sites (Tsukada, 1972) and clusters are labelled as $c_1, c_2, \ldots c_j \ldots$ just as individual sites are labelled as $R_1, R_2, \ldots R_j \ldots$ Parallel to single site transition matrix (2.21)

$$\underline{\tau}_j = (\underline{v}_j - \underline{\Sigma}_j)(\underline{I} - \underline{G}_j (\underline{v}_j - \underline{\Sigma}_j))^{-1} \qquad (2.24)$$

where $\underline{G}_j$ is an (n x n) matrix. The CCPA equation then reads

$$\langle \underline{\tau}_j \rangle = 0 \qquad (2.25)$$

The self-consistency condition (2.25) may be written in terms of the matrix elements of the configurationally averaged Green's function, if we observe that the Green's function for the

system with the averaged medium everywhere except the cluster (or cell) j, can be written as:

$$\underline{G}_j = \langle \underline{G} \rangle + \langle \underline{G} \rangle \tau_j \langle \underline{G} \rangle \qquad (2.26)$$

Then,

$$\langle \underline{G}_j \rangle = \langle \underline{G} \rangle \qquad (2.26a)$$

which is similar to MCPA condition.

This equation when applied to simple model of random binary alloy on a linear chain, with diagonal-disorder only, yields satisfactory results. The band edges are produced more accurately than in MCPA. Ducastelle has shown that for CCPA with cluster-diagonal self-energy, the approximate Green's function retains the Herglotz property of the exact Green's function which is a very favourable point for the generalisation in this form. But when we apply CCPA equations to realistic situations the calculations become infeasible (Tsukada, 1972). For this reason several other simplifications have been suggested e.g. central site approximation, boundary site approximation etc. (Kumar and Joshi, 1975).

So far we have discussed the situations where only diagonal-disorder was present. Several attempts have been made to include randomness in the hopping integrals especially for electronic studies (Kumar et al, 1975). Here it is assumed that the diagonal term of the Hamiltonian can have either of two values m_B or m_A and hopping integrals may have values $\emptyset_{AA}$, $\emptyset_{AB}$ or $\emptyset_{BB}$ depending on the configuration of the nearest neighbour pairs.

2.6 Cluster Embedding

In addition to various approaches for cluster generalisations discussed in the previous section, people have tried to embed large size clusters in some non-self-consistent effective medium e.g. immersion of a large size cluster in MCPA or VCA medium (Diehl and Leath, 1979a; Myles and Dow, 1979; Choudhry, 1981). Here once the effective medium (MCPA or VCA) is obtained, we get the effective Green's function $\underline{g}(w)$. Embedded in the effective medium is a cluster of N_c atoms giving the Green's function for the alloy with this specific configuration of atoms in the cluster $\underline{G}(w)$. We then define the scattering potential $V^*(w)$ which vanishes outside the cluster. The alloy Green's function $\underline{G}$ can be written as

$$\underline{G} = \underline{g} + \underline{g}\,\underline{V}^*\,\underline{G} \qquad (2.27)$$

which need only be solved for atoms within the cluster ($\underline{G} = \underline{g}$ outside). This gives

$$\underline{G} = (\underline{I} - \underline{g}\,\underline{V}^*)^{-1}\,\underline{g} \qquad (2.28)$$

By choosing cluster of larger sizes, details of environment implanted can be gradually increased. For each possible configuration over a cluster, one can determine the density of states at the central site and also the configurationally averaged Green's function. Particular features in the density of states curve can be attributed to specific clusters.

But this kind of cluster embedding often gives rise to two kinds of difficulties: (1) the band width remains incorrect and (2) because the density of states per mode still integrates

to unity, this has the effect of distorting the structure specially near the band edges to preserve normalization. Thus spurious structure may be obtained where there should be none.

From the discussion of the previous few sections, it is obvious that none of the proposed cluster generalisations are satisfactory. We, therefore, turn to an altogether different viewpoint of configuration-averaging, namely the "augmented space" (Mookerjee, 1973; Mookerjee and Bishop, 1974; Haydock and Mookerjee, 1974; Mookerjee, 1975a; 1975b; Kaplan and Gray, 1976-77; Kaplan et al, 1980; Kumar et al, 1982). Basing ourselves on this formalism, we shall develop an unambiguous, tractable generalisation of ICPA (MCPA) which retains the Herglotz property at all frequencies for all ranges of disorder. Off-diagonal disorder and short range order shall also be incorporated.

Recently in a series of papers (Kaplan and Gray, 1976; 1977; Diehl and Leath, 1979a; 1979b) the authors have examined "augmented space" and have generated self-consistent results, with off-diagonal disorder on linear chains in particular (Kaplan et al, 1980). Parallel to their algebraic equations is the graphical method (Mookerjee and Bishop, 1974) that has been adapted in our work. The graphical method has the added advantage that it is ideally suited in conjunction with the "Recursion" technique (Appendix A) of Haydock et al. (1972, 1975) for the application to realistic models on three-dimensional lattices. The equivalent algebraic equations soon become tediously unwieldy, as soon as the cluster size increases, particularly on three-dimensional lattices.

2.7 'Augmented Space' Formalism

The Green's function (1.21) or (1.24) for the disordered binary alloy's Hamiltonian (1-2) is averaged in the earlier Sections (Sections 2.1 to 2.6) where basic principle is same: The dynamical behaviour of the system is described by a Hamiltonian suitably set up, whereas the statistical behaviour is, as it were, imposed from the outside by allowing the potentials involved in the Hamiltonian to vary randomly according to some prescription. The Hamiltonian, in itself, does not describe the full behaviour of the system completely and has to be augmented with the distribution of the set of random potentials (the configuration). In the 'augmented space' formalism, the excitations in a random array of disordered potentials are considered to be in periodic potentials along with a "field" which describes the disorder (Mookerjee, 1979). An analogy is the case of electrons in the presence of an electromagnetic field. The Hamiltonian, expanded to include the disorder field, completely describes the disordered system. It is not necessary to put in the statistical description by hand. Since the statistical description is incorporated within the Hamiltonian, the configuration averaging is not a further extra process as in the earlier mentioned approaches.

First we shall give a version of the 'augmented space' formalism (ASF) of Mookerjee for the disordered vibrational system case that we are interested in. We start with the assumption that the lattice sites are randomly occupied by the atoms of type A and B in a binary system. The Hamiltonian involves a random occupation variable N_i, defined to take the value 0 or 1

corresponding to the occupation of site i by A or B type of atom. A set of values taken up by the random occupation variables $\{N_i\}$ is called a configuration. Suppose there is no correlation between these random variables so that we can define their distribution function in the form

$$P(\{N_i\}) = \prod_i p_i(N_i) \tag{2.29}$$

where $p_i(N_i)$ is the probability density of the individual variables. This assumption ignores short range order due to chemical cluster effect. The more general case of dependent variables have been considered by Kaplan and Gray (1981).

Haydock (1972) noted the fact that the probability density $p_i(N_i)$ satisfies the properties

$$p_i(N_i) \geq 0 \quad \text{and} \quad \int_{-\infty}^{\infty} p_i(N_i)\, dN_i = 1$$

These properties are specific to the imaginary part of a Herglotz function e.g. the resolvent of a self-adjoint operator in a certain Hilbert space. Taking clue from this Mookerjee (1973) suggested that a Hilbert space $\mathcal{H}_i$ and a basis $\{|f_n^i\rangle\}$ may be introduced such that $p_i(N_i)$ corresponds to the imaginary part of the resolvent of a suitably chosen operator $\underline{M}_i$ in $\mathcal{H}_i$. If $|f_o^i\rangle$ is a specifically chosen member of the orthonormal basis $\{|f_n^i\rangle\}$ in $\mathcal{H}_i$ then

$$p_i(N_i) = -\frac{1}{\pi} \langle f_o^i | (Z\,\underline{I} - \underline{M}_i)^{-1} | f_o^i \rangle \tag{2.30}$$

where $Z \to N_i + i\,0^+$

For a given p(Z), one can construct a suitable operator $\underline{M}$ provided p(Z) can be expanded in a convergent continued frac-

$$\cfrac{\cdot \quad 1}{z - a_1 - \cfrac{b_1^2}{z - a_2 - \cfrac{b_2^2}{z - a_3 - \cfrac{b_3^2}{\cdot \cdot \cdot}}}}$$

The operator $\underline{M}$ will then be a tridiagonal matrix with a_1, a_2, a_3 ... etc. along the diagonal and b_1, b_2, ... b_3 ... etc. along the off-diagonal positions.

$$\begin{bmatrix} a_1 & b_1 & 0 & 0 & 0 & . \\ b_1 & a_2 & b_2 & 0 & 0 & . \\ 0 & b_2 & a_3 & b_3 & 0 & . \\ . & . & . & . & . & . \\ . & . & . & . & . & . \end{bmatrix}$$

in some basis $\{|f_n>\}$. For a convergent continued fraction expansion, we have to restrict ourselves to probability functions with moments finite to all orders. This conforms to physical requirement. Most of the physically valid probability distributions are of this kind, the exception only being the Lorentzian. This is the inverse of the procedure involved for determining matrix elements of Green's operator from the recursion method (Haydock, 1972).

For a binary alloy A_cB_{1-c} with diagonal disorder only $\{m_i\}$ forms a set of random variables described by

$$m_i = m_A N_i + m_B (1 - N_i)$$

where $\{N_i\}$ are a set of random occupation variables for the solute A in the solvent B. N_i is a kind of indicator function

which carries all the configuration dependence information. In the absence of short-range order the various N_i's are independent random variables with probability densities,

$$p(N_i) = c\,\delta(N_i - 1) + (1 - c)\,\delta(N_i) \tag{2.31}$$

$$= -\frac{1}{\pi} \operatorname*{Im}_{\eta \to 0^+} \left\{ \frac{c}{N_i + i\eta - 1} + \frac{1 - c}{N_i + i\eta} \right\}$$

$$= -\frac{1}{\pi} \operatorname*{Im}_{\eta \to 0^+} \left\{ \frac{c}{N' - 1} + \frac{1 - c}{N'} \right\}, \quad N' = N_i + i\eta$$

$$= -\frac{1}{\pi} \operatorname*{Im}_{\eta \to 0^+} \left\{ \frac{1}{N' - c - \dfrac{c(1 - c)}{N' - (1 - c)}} \right\}$$

$$= -\frac{1}{\pi} \operatorname*{Im}_{\eta \to 0^+} \left\{ \frac{1}{N' - a_1 - \dfrac{b_1^2}{N' - a_2}} \right\} \tag{2.31}$$

where $a_1 = c$, $a_2 = (1 - c)$, $b_1^2 = (1 - c)c$. A representation of the matrix $\underline{M}$ is thus a 2 x 2 matrix

$$\begin{bmatrix} c & \sqrt{c(1 - c)} \\ \sqrt{c(1 - c)} & 1 - c \end{bmatrix} \tag{2.32}$$

with eigenvalues 0 and 1. Its eigenstates $|f_1\rangle$ and $|f_2\rangle$ describe occupancies corresponding to these eigenvalues.

We now introduce the "disorder field". To each variable N_i we have associated a vector space $\mathcal{V}_i$ and a representation of a self-adjoint operator $\underline{M}_i$ corresponding to the probability density of that variable in some basis $\{|f_n^i\rangle\}$. If we had taken the set of eigenvectors $\{|h_n^i\rangle\}$ of $\underline{M}_i$ as our basis then each $|h_n^i\rangle$ in $\mathcal{V}_i$ would correspond to one particular value taken

by the variable N_i. In general any element in $\mathcal{P}_i$ is a linear combination of the $\{|\, h_n^i >\}$. $\mathcal{P}_i$ with its basis and operator $\underline{M}_i$ thus contains all possible informations about the configurations of the variable N_i.

The product space $\Psi = \prod_i \otimes \mathcal{P}_i$ can now be constructed which contains all possible states of the set $\{N_i\}$ i.e. all configurations of the disordered system. The basis in the product space is

$$|f> = \{|f_i^1>\} \otimes \{|f_i^2>\} \otimes \ldots \tag{2.33}$$

and if $\underline{g}^{(\underline{M}_i)}(Z) = (Z\,\underline{I} - \underline{M}_i)^{-1}$

then

$$P(\{N_i\}) = -\frac{1}{\pi}\, \mathrm{Im} <f_o |\, \underline{G}(Z)\, |\, f_o>$$

where

$$|f_o> = |f_o^1> \otimes |f_o^2> \otimes |f_o^3> \otimes \ldots \tag{2.34}$$

and

$$\underline{G}(Z) = \underline{g}^{(\underline{M}_1)}(Z) \otimes \underline{g}^{(\underline{M}_2)}(Z) \otimes \underline{g}^{(\underline{M}_3)}(Z) \otimes \ldots$$

We call Ψ the disorder field. It is clear from the way it is constructed that it contains complete information about the statistical behaviour of the system. The information about probability of configurations is described by the operators $\underline{M}_i$ defined on the field.

We now describe the configuration averaging procedure. Let us first consider a function f(s) of one variable only. Its average is

$$\bar{f} = \int_{-\infty}^{\infty} f(s)\, p(s)\, ds$$

$$= \int_{-\infty}^{\infty} f(s) \{ -\frac{1}{\pi} \operatorname{Im}_{Z \to s + i0^+} g_{oo}^{(\underline{M})}(Z) \}\, ds$$

Assuming now that $f(Z)$ is a function of a complex variable Z and has no singularities on the real axis, in the neighbourhood of the branch cut of the function $g_{oo}^{(\underline{M})}(Z)$,

$$\bar{f} = -\frac{1}{2\pi i} \oint f(Z)\, g_{oo}^{(\underline{M})}(Z)\, dZ \qquad (2.35)$$

The contour over which the integration is carried out is taken into account the branch cut of $g^{(\underline{M})}(Z)$ along the real axis and not including any singularities of $f(Z)$. Since $\underline{M}$ is a Hermitian operator on we can write,

$$\bar{f} = -\frac{1}{2\pi i} \oint f(Z)\, dZ \, \langle f_o | \int_{-\infty}^{\infty} (Z - h)^{-1}\, d\underline{p}(h) \, | f_o \rangle$$

where we have written $\underline{g}^{(\underline{M})}(Z) = \int_{-\infty}^{\infty} (Z - h)^{-1}\, d\underline{p}(h)$, $\underline{p}(h)$ being the spectral projection operator of $\underline{M}$. Thus,

$$\bar{f} = \langle f_o | \int_{-\infty}^{\infty} f(h)\, d\underline{p}(h) \, | f_o \rangle$$

$$= \langle f_o | \, \underline{f}(\underline{M}) \, | f_o \rangle \qquad (2.36)$$

where $\underline{f}(\underline{M})$ is the same function of $\underline{M}$ as f is of s. The average has been expressed as a representation of a suitably constructed operator.

The generalisation to a function of several variables is straightforward with one $\underline{M}^i$ associated with each N_i. In case $f(N)$ is itself a matrix element of the kind say $\langle \bar{r}_1 | \, \underline{F}(s) \, | \bar{r}_j \rangle$,

$\underline{F} \in \mathcal{H}$, state vectors $|\bar{r}_i, f_o\rangle = |\bar{r}_i\rangle \otimes |f_o\rangle$ are defined on the augmented product space $\Omega = \mathcal{H} \otimes \Psi$ and the average becomes

$$\bar{F} = \langle \bar{r}_i \; f_o | \int_{-\infty}^{\infty} \{ \mathrm{Im}\, G^{(\underline{M})}(h + i0^+) \} \; F(h)\, dh \; | \bar{r}_i \; f_o \rangle \tag{2.37}$$

an matrix element in the expanded space Ω.

Now we are in position to use 'augmented space' in the vibrational study of substitutionally disordered binary alloys which is discussed in the following section.

2.8 Lattice Green's Function in 'Augmented Space'

We wish to calculate the configuration averaged one-phonon Green's function

$$\langle \underline{G}_{ij}(w) \rangle = \iint \ldots \int \underline{G}_{ij}(\{N_i\}, w) \prod_i p(N_i)\, dN_i \tag{2.38}$$

where the displacement-displacement Green's function, defined in (1.20), for a binary harmonic alloy $A_c B_{1-c}$ with nearest neighbour forces is

$$\underline{G}_{ij}(\{N_i\}, w) = \langle \bar{r}_i | \; \underline{\underline{K}}^{-1} \; | \bar{r}_j \rangle \tag{2.39a}$$

with

$$\underline{\underline{K}} = \sum_i \left(\underline{m}(N_i)\, w^2 - \sum_{l \neq i} \underline{\Phi}_{il}(N_i, N_l) \right) \underline{P}_i$$

$$+ \sum_{i \neq j} \sum \underline{\Phi}_{ij}(N_i, N_j)\, \underline{T}_{ij} \; ; \quad \underline{\underline{K}} \in \mathcal{H} \tag{2.39b}$$

Here $|\bar{r}_i\rangle$ is a basis for the Hilbert space $\mathcal{H}$ and the integration over $p(N_i)\, dN_i$ constitutes averaging overall possible configurations of the disordered system. $\underline{P}_i = |i\rangle\langle i|$ and

$T_{ij} = |i\rangle\langle j|$ are the projection and transfer operators in the Hilbert space on the tight-binding basis. We have incorporated in (2.39b) the sum rule $\sum_j \phi_{ij}(N_i, N_j) = 0$ essential to eliminate the $w = 0$ mode corresponding to bodily translations of the system as a whole (conservation of momentum). This sum rule was earlier cumbersome to incorporate in the traditional CPA calculations. The consequence is the environmental disorder which couples diagonal and off-diagonal disorder in the Hamiltonian $\underline{\underline{K}}$ (second term on the right hand side of eq. (2.39b)). As a result, the diagonal element $\underline{K}_{ii}$, and hence $\underline{G}_{ii}$, depends on the occupation of neighbouring sites. $\{\underline{m}(N_i)\}$ and $\{\phi_{ij}(N_i, N_j)\}$ are the set of random variables described by

$$\underline{m}(N_i) = m_A N_i \underline{I} + m_B(1 - N_i)\underline{I}$$

$$\phi_{ij}(N_i, N_j) = \underline{\phi}^{AA} N_i N_j + \underline{\phi}^{BB}(1 - N_i)(1 - N_j) + \underline{\phi}^{AB}\{N_i(1 - N_j) + N_j(1 - N_i)\} \qquad (2.40)$$

where $\{N_i\}$ are a set of random 'occupation' variables for the solute A in the solvent B. In the absence of SRO the various N_i's are independent random variables with probability density

$$p(N_i) = c\,\delta(N_i - 1) + (1 - c)\,\delta(N_i) \qquad (2.41)$$

using (2.40), we may rewrite (2.39b) in more useful form

$$\underline{\underline{K}} = \underline{\underline{K}}_B + \sum_i m w^2 \underline{I} N_i \underline{P}_i - \sum_i \Big(\sum_{l \neq i} (\underline{\phi}^{(1)}(N_i + N_l) + \underline{\phi}^{(2)} N_i N_l)\Big) P_i + \sum_i \sum_j (\underline{\phi}^{(1)}(N_i + N_j) + \underline{\phi}^{(2)} N_i N_j)\,\underline{T}_{ij} \qquad (2.42)$$

where $m = m_A - m_B$, $\underline{\underline{\phi}}^{(1)} = \underline{\underline{\phi}}^{AB} - \underline{\underline{\phi}}^{BB}$; $\underline{\underline{\phi}}^{(2)} = \underline{\underline{\phi}}^{AA} + \underline{\underline{\phi}}^{BB} - 2\underline{\underline{\phi}}^{AB}$ and $\underline{\underline{K}}_B$ is the non random operator for the pure solvent B,

$$\underline{\underline{K}}_B = \sum_i (m_B w^2 \underline{\underline{I}} - \underline{\underline{\phi}}^{BB}_{oo}) \underline{\underline{P}}_i + \sum_{ij} \underline{\underline{\phi}}^{BB} \underline{\underline{T}}_{ij} \qquad (2.42a)$$

The operator $\underline{\underline{K}}$ is now in a form appropriate for the 'augmented space' transformation. Corresponding to each N_i there is a operator $\underline{\underline{M}}^{(i)}$ in a two dimensional vector space $\mathcal{V}^{(i)}$. A representation of $\underline{\underline{M}}^{(i)}$ in a basis $\{|v^i_o\rangle, |v^i_1\rangle\}$ is

$$\begin{bmatrix} c & \sqrt{c(1-c)} \\ \sqrt{c(1-c)} & 1-c \end{bmatrix} \quad ; \quad \text{(Mookerjee, 1973)}$$

where c is the concentration of the solute A. The augmented space operators, now, are

$$\tilde{\underline{\underline{K}}} = \sum_i (\tilde{\underline{\underline{m}}}_i w^2 - \sum_{l \neq i} \tilde{\underline{\underline{\phi}}}_{il}) \underline{\underline{P}}_i + \sum_{ij} \tilde{\underline{\underline{\phi}}}_{ij} \underline{\underline{T}}_{ij}$$

$$= \underline{\underline{K}}_B \otimes \underline{\underline{I}} + mw^2 \underline{\underline{I}} \sum_i \underline{\underline{P}}_i \otimes \underline{\underline{M}}^{(i)} \otimes \underline{\underline{I}}^{(i)}$$

$$- \sum_i \Big(\sum_{l \neq i} (\underline{\underline{\phi}}^{(1)} (\underline{\underline{M}}^{(i)} + \underline{\underline{M}}^{(l)}) + \underline{\underline{\phi}}^{(2)} \underline{\underline{M}}^{(i)} \otimes \underline{\underline{M}}^{(l)}) \Big) \otimes \underline{\underline{P}}_i \otimes \underline{\underline{I}}^{(i)}$$

$$+ \sum_i \sum_j (\underline{\underline{\phi}}^{(1)} (\underline{\underline{M}}^{(i)} + \underline{\underline{M}}^{(j)}) + \underline{\underline{\phi}}^{(2)} \underline{\underline{M}}^{(i)} \otimes \underline{\underline{M}}^{(j)}) \otimes \underline{\underline{T}}_{ij} \otimes \underline{\underline{I}}^{(ij)} \qquad (2.43)$$

$\tilde{\underline{\underline{K}}} \in \Omega$, $\underline{\underline{I}}^{(i)}$, $\underline{\underline{I}}^{(ij)}$ in the above equation indicate identity operators in all subspaces $\mathcal{V}^{(k)}$ except those superscripted.

The configurationally averaged Green's function (2.38) is, then given by

$$\langle \underline{G}_{ij}(w) \rangle = \langle \bar{r}_i \quad \tau^{\circ} \mid \tilde{\underline{K}}^{-1} \mid \bar{r}_j \quad \tau^{\circ} \rangle \qquad (2.44)$$

with $\quad |\tau^{\circ}\rangle = \prod_i^{\otimes} |v_{\circ}^i\rangle .$

or in terms of $\tilde{m}\,\underline{I}$, $\tilde{\underline{\emptyset}}$,

$$\langle \underline{G}_{ij}(w) \rangle = \langle \bar{r}_i \quad \tau^{\circ} \mid (\tilde{m}\, w^2\, \underline{\underline{I}} - \tilde{\underline{\emptyset}})^{-1} \mid \bar{r}_j \quad \tau^{\circ} \rangle \qquad (2.44a)$$

The expanded operators $\tilde{\underline{m}}$, $\tilde{\underline{\emptyset}}$ and $\tilde{\underline{K}}$ contain complete information about the system and are defined on the expanded Hilbert space $\Omega = \mathcal{H} \otimes \Psi$ where $\Psi = \prod_i^{\otimes} \mathcal{H}_i$. Description of the dynamical behaviour of the system is in the subspace $\mathcal{H}$, while that of the statistical behaviour is in Ψ, the disorder space. The configuration averaged Green's function is a particular representation in this expanded space Ω. The problem has thus been reduced to the determination of the matrix element of the operator $\tilde{\underline{\underline{K}}}$ in the augmented space. Notice that upto this stage of configuration averaging, no approximations are involved. Subsequently, in the determination of the matrix element in the augmented space herglotzicity retaining approximations may now be introduced systematically. In the next section we shall describe the Graphical method which will enable us to do just this.

2.9 The Graphical Method

The graphical method was introduced by Haydock (1972) for calculation of the Green's function. It will be used to generate the cluster CPA formalism for a general alloy system in Section 2.10.

By a graph we shall mean a set of 'vertices' connected by the 'links'. Let $\{|i>\}$ be any complete linearly independent basis in which the Hamiltonian is described. The overlap matrix $S_{ij} = <i|j>$ is a unit matrix in case the basis is orthonormal. Matrix element of an operator $\underline{M}$ are given by $M_{ij} = <i|\underline{M}|j>$. A graph is associated with every basis $\{|i>\}$. To every element $|i>$ of the basis set $\{|i>\}$ is associated a vertex v_i and to each distinct pair of elements $(|i>, |j>)$ a link or bond l_{ij} which may be directional (i.e. l_{ij} may not be equal to l_{ji}) or otherwise. To any operator $\underline{M}$ there corresponds a graph consisting of vertices and those links for which $M_{ij} \neq 0$. If we want to invert an operator $\underline{M}$, then the contribution of each vertex v_i, is defined as

$$k(v_i) = 1/M_{ii} \quad \text{and that of the link } l_{ij} \text{ as}$$

$$k(l_{ij}) = M_{ij}$$

A path Q_N of length N is defined as a series of ordered vertices and links i.e.

$$Q_N = \{ v_i \; l_{ij} \; v_j \; l_{jk} \; \ldots \; v_n \}$$

Contribution of a path is defined as

$$k(Q_N) = \prod_{\text{vertices}} k(v_i) \prod_{\text{links}} k(l_{ij})$$

A self-avoiding path of length N, $Q_N = \{v_i \; l_{ij} \; v_j \; \ldots \; v_n\}$ is a path such that $v_n = v_m$ with the only exception that v_i may be the same as v_n, in which case it is a self-avoiding closed polygonal path.

The renormalized contribution of a vertex v_n in a path Q_N is defined as

$$\tilde{k}(v_n) = \sum_{N=0}^{\infty} \sum_{Q'_N} k(Q'_N) \tag{2.45}$$

where Q'_N are all polygonal self-avoiding paths from v_N and back, on the graph from which the vertices $v_1 \ldots v_{N-1}$ have been removed. If $\underline{M}^{-1} = \underline{G}$ then the representation of $\underline{G}$ in some basis can be expressed (Haydock, 1972; Mookerjee, 1979) as follows:

$$G_{ij} = \sum_{N=0}^{\infty} \sum_{Q_N} \tilde{k}(Q_N) \tag{2.46}$$

where Q_N are all self-avoiding paths from v_i to v_j.

Now we make use of this technique to calculate the Green's function defined in Eq. (2.44) as the technique as such preserves the Herglozicity (Haydock, 1972). The essential approximation now involves ignoring or delinking the contribution of possible self-avoiding paths. The relation of these polygonal paths to the CPA has been discussed by Bishop and Mookerjee (1974) and Mookerjee (1975b) has demonstrated their relation to the multiple scattering diagrams. The philosophy of approximation is as follows.

We consider exactly all paths that involve only the spatial part of the augmented space i.e. $\mathcal{H}$. Such paths are connected to the lattice structure and must not be approximated or delinked without destroying some of the feature of the underlying lattice. In 2- and 3-dimensions the recursion method helps us to deal with this infinite set of paths.

If we want a cluster-CPA with $(\bar{r}_1, \bar{r}_2, \ldots \bar{r}_N)$ within the cluster, then all polygonal paths that do not completely lie in the subspace and involve these vertices and none others must also be exactly accounted for. These are related to the multiple scattering within the cluster.

Larger polygonal paths which involve sites within and without the cluster but which do not completely lie in the subspace $\mathcal{H}$ must be delinked. The type of delinking depends very much on the environment we wish to immerse our cluster in. Immersion in a VCA medium yields the travelling pseudo fermion approximation (generalization of the ATA) of Diehl and Leath (1979a). If we wish to immerse in a 1CPA medium, we simply delink all larger polygonal paths into a Cayley tree (Bishop and Mookerjee, 1974). The result is not self-consistent and in particular the bandwidth is the same as that of the 1CPA. If we wish to embed our cluster in a self-consistent cluster medium we partition the lattice in Tsukada type clusters, delink the environment itself into cluster paths and self-consistently calculate the effect. We shall describe this in detail below.

2.10 CCPA Self-Consistent Medium

Here we shall illustrate the generation of a self-consist medium in the CCPA for our phonon problem. For electronic problem, it is already used extensively by Srivastava (1982). To start with we consider the 2CPA. The generalization of bigger clusters will be dealt with subsequently.

A graph is constructed according to the delinking procedure described in the previous section which has got the structure

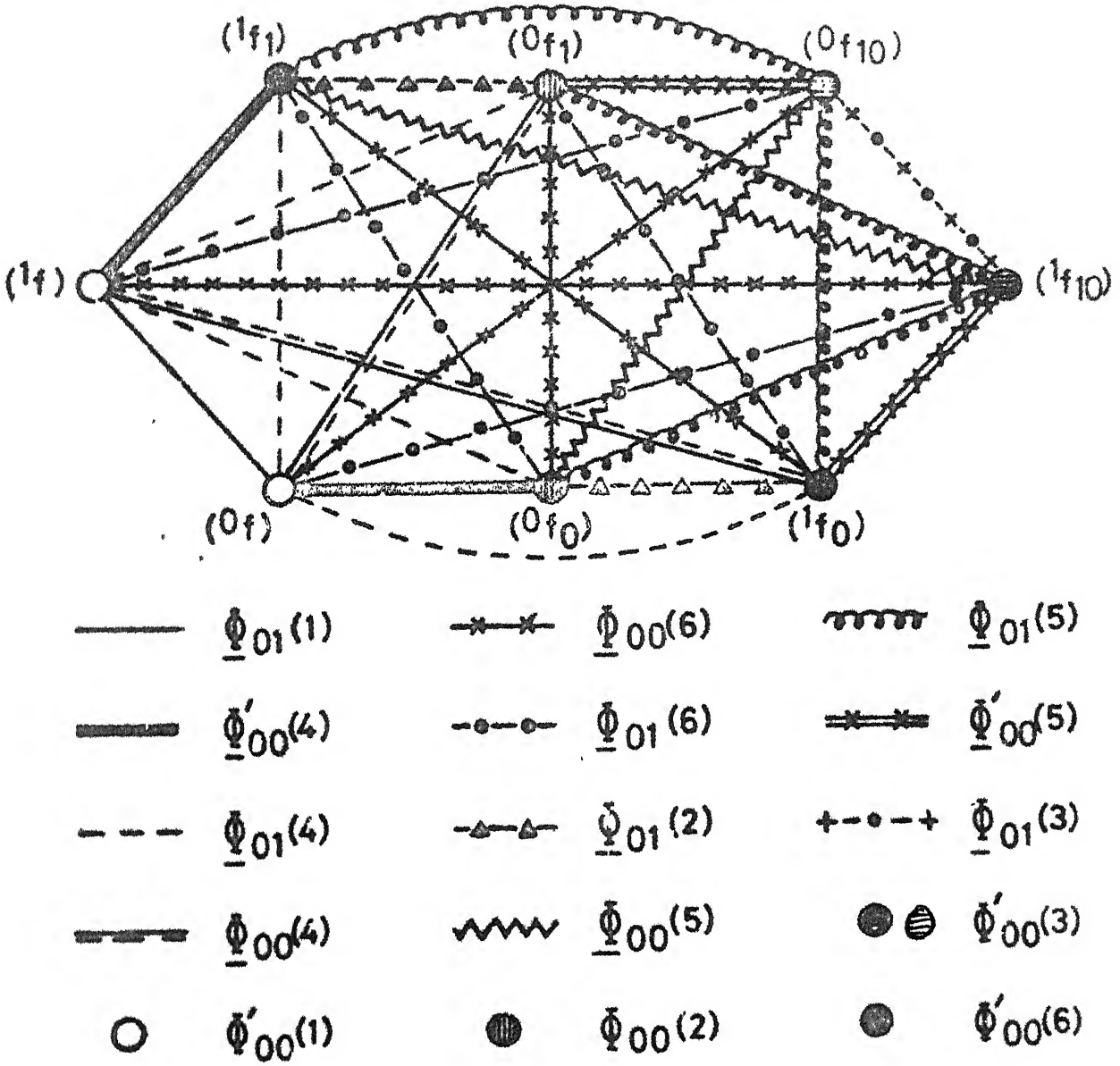

FIG. 2-1 (continued)

(see next page for details of symbols)

Dictionary of symbols used in Figure 2.1.

$$\mathcal{Q}_{01}(1) = \mathcal{Q}_{01}^{BB} + 2c\,\mathcal{Q}_{01}^{(1)\prime} + c^2\,\mathcal{Q}_{01}^{(2)}$$

$$\mathcal{Q}'_{00}(4) = \sqrt{c(1-c)}\,(m\,w^2\,\underline{I} + \mathcal{Q}_{00}^{(1)} + c\,\mathcal{Q}_{00}^{(2)})$$

$$\mathcal{Q}_{01}(4) = \sqrt{c(1-c)}\,(\mathcal{Q}_{01}^{(1)} + c\,\mathcal{Q}_{01}^{(2)})$$

$$\mathcal{Q}_{00}(4) = \sqrt{c(1-c)}\,(\mathcal{Q}_{00}^{(1)} + c\,\mathcal{Q}_{00}^{(2)})$$

$$\mathcal{Q}_{00}(6) = c(1-c)\,(\mathcal{Q}_{00}^{BB} + \mathcal{Q}_{00}^{(1)} + c(1-c)\,\mathcal{Q}_{00}^{(2)})$$

$$\mathcal{Q}_{01}(6) = c(1-c)\,(\mathcal{Q}_{01}^{BB} + \mathcal{Q}_{01}^{(1)} + c(1-c)\,\mathcal{Q}_{01}^{(2)})$$

$$\mathcal{Q}_{01}(2) = (\mathcal{Q}_{01}^{BB} + \mathcal{Q}_{01}^{(1)} + c(1-c)\,\mathcal{Q}_{01}^{(2)})$$

$$\mathcal{Q}_{00}(5) = \sqrt{c(1-c)}\,(\mathcal{Q}_{00}^{(1)} + (1-c)\,\mathcal{Q}_{00}^{(2)})$$

$$\mathcal{Q}_{01}(5) = \sqrt{c(1-c)}\,(\mathcal{Q}_{01}^{(1)} + (1-c)\,\mathcal{Q}_{01}^{(2)})$$

$$\mathcal{Q}'_{00}(5) = \sqrt{c(1-c)}\,(m_B w^2\,\underline{I} + \mathcal{Q}_{00}^{(1)} + (1-c)\,\mathcal{Q}_{00}^{(2)})$$

$$\mathcal{Q}_{01}(3) = (\mathcal{Q}_{01}^{BB} + 2(1-c)\,\mathcal{Q}_{01}^{(1)} + (1-c)^2\,\mathcal{Q}_{01}^{(2)})$$

$$\mathcal{Q}'_{00}(1) = (m_B w^2\,\underline{I} + \mathcal{Q}_{00}^{BB}) + c(m\,w^2\,\underline{I} + \mathcal{Q}_{00}^{(1)} + c\,\mathcal{Q}_{00}^{(2)})$$

$$\mathcal{Q}'_{00}(2) = (m_B w^2\,\underline{I} + \mathcal{Q}_{00}^{BB}) + ((1-c)(mw^2\,\underline{I} + c\,\mathcal{Q}_{00}^{(2)}) + \mathcal{Q}_{00}^{(1)})$$

$$\mathcal{Q}'_{00}(3) = (m_B w^2\,\underline{I} + \mathcal{Q}_{00}^{BB}) + (1-c)(mw^2\,\underline{I} + 2\mathcal{Q}_{00}^{(1)} + (1-c)\,\mathcal{Q}_{00}^{(2)})$$

$$\mathcal{Q}'_{00}(6) = (m_B w^2\,\underline{I} + \mathcal{Q}_{00}^{BB}) + (c(mw^2\,\underline{I} + (1-c))\mathcal{Q}_{00}^{(2)} + \mathcal{Q}_{00}^{(1)})$$

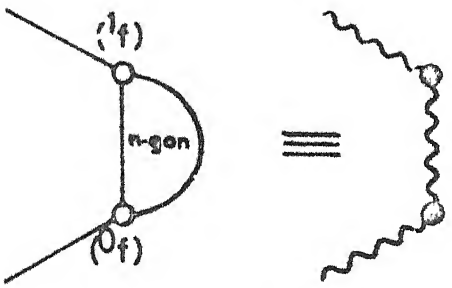

$\bigcirc = \Sigma_0$

$\sim = \Sigma_1$

FIG. 2·2a

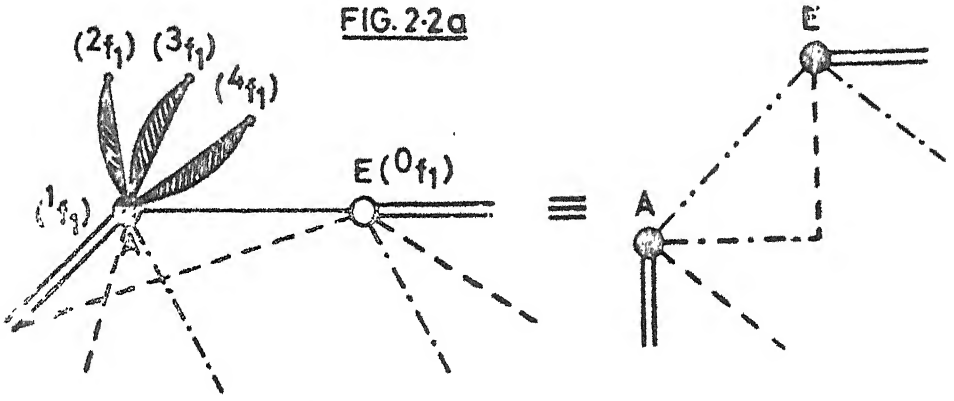

represents an octagon decoration as in Fig.2·1

$\bigcirc = \sigma_0$

$\cdots\!-\!\cdots = \sigma_1$

FIG.2·2b

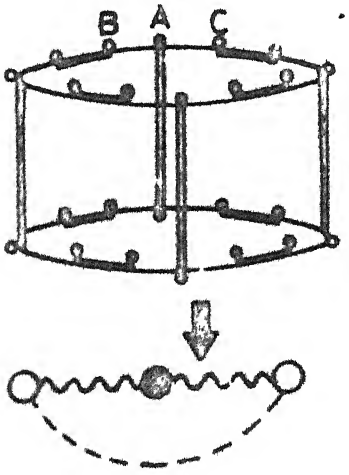

$\bullet = \Sigma_0$

$\circ = \Sigma'_0$

$\sim = \Sigma_1$

$- - - = \Sigma_2$

FIG.2·2c

and HK. Once the renormalization is accounted for, the octagon is effectively isolated. The renormalized vertices $\underline{\sigma}_o(w)$ and links $\underline{\sigma}_1(w)$ are found as follows. Let us divide the lattice as follows into two subspaces (1) an unrenormalized bond AE, which we shall call system 1. It has a Hamiltonian $\underline{\underline{K}}^{(1)} = \sum_{i=A,E} (m_i w^2 - \phi_{oo}^{(i)})\underline{P}_i + \sum_{ij=A,E} \phi_{ij}(\chi)\,\underline{T}_{ij}(\chi)$ where χ is the direction vector of bond AE. (2) A lattice L, which is the original lattice minus the link AE, and in which all bonds and sites are renormalized by $\underline{\underline{\Sigma}}$. This has a Hamiltonian

$$\underline{\underline{K}}^{(2)} = \sum_{i\neq A,E} \underline{\Sigma}_o(w)\,\underline{P}_i + \sum_{i,j\neq A,E} \underline{\Sigma}_1(w;\chi)\,\underline{T}_{ij}(\chi) \qquad (2.48)$$

and (3) a linking Hamiltonian

$$\underline{\underline{K}}^{int} = \sum_{ij} \underline{\Sigma}_1(w,\chi)(\underline{T}_{iA}(\chi) + \underline{T}_{Ai}(\chi) + \underline{T}_{iE}(\chi) + \underline{T}_{Ei}(\chi) \qquad (2.49)$$

where χ is the direction vector corresponding to the bond ij subscripted in transfer operator $\underline{T}_{ij}$.

If we now use the notation $\underline{\underline{X}}^{-\underline{P}_Y}$ to denote the inverse of the operator $\underline{\underline{X}}$ in the subspace Y

$$\underline{\underline{G}}^{(1)} = \underline{\underline{P}}_1\,\underline{\underline{G}}\,\underline{\underline{P}}_1 = \left[w^2\,\underline{\underline{I}} - \underline{\underline{K}}^{(1)} - \underline{\underline{K}}^{(int)}\,\underline{\underline{G}}^{(2)}\,\underline{\underline{K}}^{(int)}\right]^{-\underline{\underline{P}}_1}$$

where $\underline{\underline{G}}^{(2)} = \left[w^2\,\underline{\underline{I}} - \underline{\underline{K}}^{(2)}\right]^{-\underline{\underline{P}}_2}$

with $\underline{\underline{P}}_1 + \underline{\underline{P}}_2 = \underline{\underline{I}}$ (2.50)

Examination of the equation (2.50) immediately indicates that the effect of the rest of the lattice hanging on to the bond AE is to change the Hamiltonian $\underline{\underline{K}}^{(1)}$ to $\underline{\underline{K}}^{(1)} + \underline{\underline{\sigma}}$ where the self-energy $\underline{\underline{\sigma}}$ is given by

$$\underline{\sigma}_{AA} = \underline{\sigma}_{EE} = \underline{\sigma}_{o} = \sum_{k,m \in N_A} \underline{\Sigma}_1(\hat{Ak})\ \underline{G}^{(2)}_{km}\ \underline{\Sigma}_1^{+}(\hat{mA})$$

$$\underline{\sigma}_{AE} = \underline{r}\ \underline{\sigma}_{EA} = \underline{\sigma}_1(\hat{AE}) = \sum_{\substack{k \in N_A \\ m \in N_E}} \underline{\Sigma}_1(\hat{Ak})\ \underline{G}^{(2)}_{km}\ \underline{\Sigma}_1^{+}(\hat{mE}) \qquad (2.51)$$

where N_A denotes a nearest neighbour of A and $\hat{AE}$ denotes the direction vector corresponding to bond AE. $\underline{r}$ is the inversion matrix with respect to bond AE.

(b) Let us now work on the renormalized, isolated octagon. As before let us divide the octagon into two subsystems: a bond B (0f, 1f), the rest of the octagon M.

$$\underline{\underline{\tilde{K}}}^{B} = \sum_{ij\ 0f,1f} \underline{\tilde{K}}_{ij}\ , \qquad \underline{\underline{\tilde{K}}}^{M} = \sum\sum_{ij \neq 0f,1f} \underline{\tilde{K}}_{ij}$$

$$\underline{\underline{\tilde{K}}}^{BM} = \sum_{i \in B} \sum_{j \in M} (\underline{\tilde{K}}_{ij} + \underline{\tilde{K}}_{ji})$$

As before, we have

$$\underline{\underline{G}}^{B} = \underline{\underline{P}}_B\ \underline{\underline{G}}\ \underline{\underline{P}}_B = \left[w^2\ \underline{\underline{I}} - \underline{\underline{\tilde{K}}}^{B} - \underline{\underline{\tilde{K}}}^{BM}\ \underline{\underline{G}}^{M}\ \underline{\underline{\tilde{K}}}^{BM}\right]^{-\underline{P}_B}$$

$$\underline{\underline{G}}^{M} = \left[w^2\ \underline{\underline{I}} - \underline{\underline{K}}^{M}\right]^{-\underline{P}_M}$$

This immediately shows how the octagon renormalizes the bond B. We have

$$\underline{\Sigma}_o = \underline{\tilde{K}}^{B}_{oo} + \sum_{j \neq o \neq k} \sum \underline{\tilde{K}}^{BM}_{oj}\ \underline{G}^{M}_{jk}\ \underline{\tilde{K}}^{BM}_{ko}$$

$$\underline{\Sigma}_1(\hat{AE}) = \underline{\tilde{K}}^{B}_{o1} + \sum_{j \neq o} \sum_{k \neq 1} \underline{\tilde{K}}^{BM}_{oj}\ \underline{G}^{M}_{jk}\ \underline{\tilde{K}}^{BM}_{k1} \qquad (2.52)$$

Equations (2.51) and (2.52) together provide a self-consistent set of equations for the calculations of the

self-energy $\underline{\underline{\Sigma}}$. The various Green functions involved can be easily calculated on a three-dimensional lattice using the recursion technique of Haydock et al. (see Appendix A). In the case when we are using frequency dependent effective Hamiltonians, the recursion has to be done separately for each value of frequency.

The cluster generalisation to arbitrary large clusters now follows exactly the same philosophy. Equations (2.51) and (2.52) remain the same. The only modification is the augmented space unit. For example, in the 3CPA the augmented space unit is the 24-gon (Figure 2.2c) (Mookerjee, 1973) and

$$\underline{\underline{\Sigma}} = \begin{bmatrix} \underline{\Sigma}_0 & \underline{\Sigma}_1 & \underline{\Sigma}_1 \\ \underline{\Sigma}_1 & \underline{\Sigma}_0' & \underline{\Sigma}_2 \\ \underline{\Sigma}_1 & \underline{\Sigma}_2 & \underline{\Sigma}_0' \end{bmatrix}$$

This has four independent components, but note that both (2.51) and (2.52) for this case also yield four equations:

$$\begin{aligned}
\underline{\Sigma}_0 &= \underline{\Sigma}_{AA} = \tilde{\underline{K}}^{B}_{AA} + \sum_{km} \tilde{\underline{K}}^{BM}_{Ak}\, \underline{G}^{M}_{km}\, \tilde{\underline{K}}^{BM}_{mA} \\
\underline{\Sigma}_0 &= \underline{\Sigma}_{BB} = \tilde{\underline{K}}_{BB} + \sum_{km} \tilde{\underline{K}}^{BM}_{Bk}\, \underline{G}^{M}_{km}\, \tilde{\underline{K}}^{BM}_{mB} \\
\underline{\Sigma}_1 &= \underline{\Sigma}_{AB}(\hat{AB}) = \tilde{\underline{K}}^{B}_{AB} + \sum_{km} \tilde{\underline{K}}^{BM}_{Ak}\, G^{M}_{km}\, \tilde{\underline{K}}^{BM}_{mB} \\
\underline{\Sigma}_2 &= \underline{\Sigma}_{BC}(\hat{BC}) = \tilde{\underline{K}}^{B}_{BC} + \sum_{km} \tilde{\underline{K}}^{BM}_{Bk}\, G^{M}_{km}\, \tilde{\underline{K}}^{BM}_{mC}
\end{aligned} \qquad (2.53)$$

As the cluster size increases, the augmented space graph itself becomes large and the augmented space unit which

renormalizes the cluster also becomes large. For clusters of size N, this unit is a $(N \times 2^N)$ - gon. However, the number of independent members in $\underline{\underline{\Sigma}}$ still remains relatively small and the G^M can be calculated by the recursion method with great facility even on quite large augmented space units. This fortunate marriage of the above method with the recursion technique reduces the calculation of quite large CCPAs to tractable problem.

The self-energy $\underline{\underline{\Sigma}}$, hence the CCPA, is cluster diagonal, a property essential to preserve Herglotzicity (Butler, 1973). The effective Hamiltonian is invariant with respect to cluster translation. However the exact effective Hamiltonian is translationally invariant. In contrast, in the CCPA's the self-energy at the cluster-centre and cluster-periphery are indeed different. Unless it is possible to construct clusters in which all the sites are equivalent (as in the 2CPA) this distinction is unavoidable and inherent in any cluster approximation (Tsukada, 1972).

The equations (2.51) and (2.52) form the basis of the self-consistent calculation of the self-energies $\underline{\Sigma}_o(w)$ and $\underline{\Sigma}_1(w)$. The philosophy behind the procedure is the standard one employed in all self-consistent coherent media calculations. The aim is to find an "effective" Hamiltonian

$$\underline{\underline{K}}_{eff} = \sum_i \underline{\Sigma}_o(w)\, \underline{P}_i + \sum_{ij} \underline{\Sigma}_1(w, \chi)\, \underline{T}_{ij}(\chi) \qquad (2.54)$$

such that $\left[w^2 \underline{\underline{I}} - \underline{\underline{K}}_{eff}\right]^{-1}$ is the configuration averaged resolvent. The $\underline{\underline{K}}_{eff}$ is found by determining the way in which the disorder 'renormalizes' diagonal term to $\underline{\Sigma}_o(w)$ and off-diagonal term to $\underline{\Sigma}_1(w)$, by immersing the cluster configuration in a

medium and ensuring that there is no extra scattering. The procedure, involving a self-consistent iterative method, is only useful if the iterations converge. We may start with the MCPA results as the zeroeth approximation, i.e. $\underline{\Sigma}_o^o(w) = \Sigma_{CPA}(w)\ \underline{I}$ and $\underline{\Sigma}_1^o(w) = \underline{\emptyset}$ and use these in (2.51)' to generate $\underline{g}_o^o$ and $\underline{g}_1^o$. These in turn may be now used in (2.52) to generate $\underline{\Sigma}_o^1(w)$ and $\underline{\Sigma}_1^1(w)$. The procedure is then iterated until there is convergence i.e. self-consistency is achieved.

Now we will apply this scheme on one-dimensional (Section 2.12) and on three-dimensional systems (Chapter III). Before this, we will discuss spectral functions and density of states evaluated by our scheme.

2.11 Spectral Functions and Density of States

The spectral function may be immediately deduced from (2.54). In K-space

$$K^{eff}_{k,k'} = \frac{1}{N} \sum_{ij} e^{i(\bar{k}.\bar{r}_i - \bar{k}'.\bar{r}_j)} \{ \underline{\Sigma}_o(w)\ \delta_{ij} + \underline{\Sigma}_1(w, \bar{\chi})\ \delta_{j,i+\bar{\chi}}$$

$$= \delta_{kk'}\ \underline{\Sigma}_o + \underline{\Sigma}_1(k) \quad , \quad \Sigma_1(k) = \sum_{\chi} e^{i\bar{k}.\bar{\chi}}\ \underline{\Sigma}_1(w, \bar{\chi})$$

The effective Hamiltonian is diagonal in the K-indices and therefore the spectral function is

$$A(k, w) = -\frac{1}{\pi} \mathrm{Im} \left[w^2\ \underline{I} \cdot \underline{\Sigma}_o - \underline{\Sigma}_1(k) \right]^{-1} \qquad (2.55)$$

The inverse being taken over the 3 x 3 space of the longitudinal and transverse branches. The spectral functions are peaked at the natural frequencies of the alloy and the width at half

maximum (FWHM) is proportional to the inverse life time of the state with that energy. For the CCPA, the widths are branch dependent and also dependent on the direction of k. This is in direct contrast to the MCPA, where $\underline{\Sigma}_o$ is diagonal and $\underline{\Sigma}_1 = \underline{\Phi}(k)$ is real or the imaginary part of $H^{eff}(k)$ is branch and k-independent. Thus the spectral functions allow us to construct the dispersion curves for the alloy and the accompanying widths. Maxima in widths indicate existence of resonance, while double peaked spectral functions indicate strong hybridization. We shall extract these information for the alloys under consideration to compare with neutron scattering experiments (Chapter III).

The configuration averaged density of states is given by

$$\rho(w) = -\frac{2w}{3\pi} \operatorname*{Im}_{Z \to w^2 + i0^+} \left[\mathrm{Tr} \; \langle \bar{r}_i \,|\, \underline{m}_i \, \underline{\underline{K}}^{-1}(Z) \,|\, \bar{r}_i \rangle \right]$$

$$= -\frac{2w}{3\pi} \operatorname*{Im}_{Z \to w^2 + i0^+} \mathrm{Tr} \left\{ m_B \left[\langle \bar{r}_i \,|\, \underline{\underline{K}}^{-1} \,|\, \bar{r}_i \rangle \right] + (m_A - m_B) \left[\langle r_i \,|\, N_i \, \underline{\underline{K}}^{-1} \,|\, r_i \rangle \right] \right\}$$

with

$$\underline{m}_i = m_B \, \underline{I} + (m_A - m_B) \, N_i \, \underline{I}$$

From (2.44), the terms within the brackets may be written as

$$m_B \langle r_i, \tau^o \,|\, \underline{\underline{K}}^{-1} \,|\, r_i, \tau^o \rangle + (m_A - m_B) \langle r_i, \tau^o \,|\, \underline{M}^{(i)} \times \underline{\underline{K}}^{-1} \,|\, r_i, \tau^o \rangle$$

Using (2.32), if $\bar{m} = cm_A + (1 - c)m_B$ and $\delta m = (m_A - m_B)\sqrt{c(1 - c)}$ it becomes,

$$\bar{m} \langle \bar{r}_i, \tau^o | \underline{\underline{K}}^{-1} | \bar{r}_i, \tau^o \rangle + \Delta m \langle \bar{r}_i, \tau^o_{(i)} | \underline{\underline{K}}^{-1} | \bar{r}_i, \tau^o_{(i)} \rangle \tag{2.56}$$

where

$$|\tau^o_{(i)}\rangle = \prod_{j \neq i} |v^j_o\rangle \otimes |v^i_i\rangle = |i_{f_i}\rangle \quad \text{in our notation.}$$

We have already discussed the calculation of the first term in detail. For the second term, let us go back to (2.52) which algebraically expresses the renormalisation of a bond and its terminal sites by 2CPA octagon (Figure 2.2a). We shall now divide the octagon into two subsystems B': (Of, Of_o, 1f, $1f_1$) and the rest M'. Thus M' now renormalises B' as shown:

$$\underline{\Sigma}_{o_f, o_f} = \underline{\Sigma}_o = \underline{\tilde{K}}^{B'}_{oo} + \sum_{j \neq o \neq k} \underline{K}^{B'M'}_{oj} \, G^{M'}_{jk} \, \underline{K}^{M'B'}_{ko} = \underline{\Sigma}_{1_f, 1_f}$$

$$\underline{\Sigma}_{o_{f_o}, o_{f_o}} = \underline{\Sigma}'_o = \underline{\tilde{K}}^{B'}_{oo} + \sum_{j \neq o' \neq k} K^{B'M'}_{o'j} \, G^{M'}_{jk} \, \underline{K}^{M'B'}_{ko'} = \underline{\Sigma}_{1_{f_1}, 1_{f_1}}$$

$$\underline{\Sigma}_{o_f, 1_f}(\hat{AE}) = \underline{\Sigma}_1 = \underline{\tilde{K}}^{B'}_{o1} + \sum_{j \neq o} \sum_{k \neq 1} \underline{K}^{B'M'}_{oj} \, \underline{G}^{M'}_{jk} \, \underline{K}^{M'B'}_{k1} =$$

$$= \underline{\Sigma}_{1_f, o_f}(\hat{AE})$$

$$\underline{\Sigma}_{o_f, 1_f}(\hat{AE}) = \underline{\Sigma}'_1 = \underline{K}^{B'}_{o'1'} + \sum_{j=o'} \sum_{k \neq 1'} \underline{K}^{B'M'}_{o'j} \, \underline{G}^{M'}_{jk} \, \underline{K}^{M'B'}_{k1'}$$

$$= \underline{\Sigma}_{1_{f_1}, o_{f_o}}(\hat{AE})$$

$$\underline{\Sigma}_{o_f,1_{f_1}}(\hat{\Lambda E}) = \underline{\Sigma}_2 = \underline{\tilde{K}}^{B'}_{o1'} + \sum_{j\neq o}\sum_{k\neq 1'} K^{B'M'}_{oj}\, G^{M'}_{jk}\, \underline{K}^{M'B'}_{k1'}$$

$$= \underline{\Sigma}_{1_{f_1},o_f}(\hat{\Lambda E}) \qquad (2.57)$$

On the renormalized lattice, now we have two states (i_f, i_{f_i}) per site. Let us indicate them by f and f_i.

$$\underline{K}_{eff} = \sum_i \{ \underline{\Sigma}_o P_{i_f} + \underline{\Sigma}'_o P_{i_{f_i}} \} + \sum_{ij} \{ \underline{\Sigma}_1 T_{if;jf}$$

$$+ \underline{\Sigma}'_1 T_{if_i,\, jf_j} + \underline{\Sigma}_2 (T_{if,jf_j} + T_{if_i,jf}) \} \qquad (2.58)$$

$\langle if_i | \underline{\underline{K}}^{-1} | if_i \rangle$ may now be calculated from (2.58) by recursion starting from $|o\} = |o_{f_o}\rangle$ and performing at each frequency.

2.12 Results on Linear Chains

Here we present the results of the linear chain for a preliminary comparison with earlier work. We choose the mass and off-diagonal parameters in such a way that we may compare our results with those of Myles and Dow (1979a,b) and Diehl et al. (1979). It must be emphasised here that it is not necessary to limit our choice to these special values, but any arbitrary choice is possible.

Figure 2.3 shows the results for very small mass and off-diagonal disorders. The results are very similar to all earlier works. In Figure 2.4 we show results for mass disorder only, and we may compare our results with those of Myles and Dow (Figure 7). One immediately notices the following points: most of the fine peak structure is almost identical for clusters of

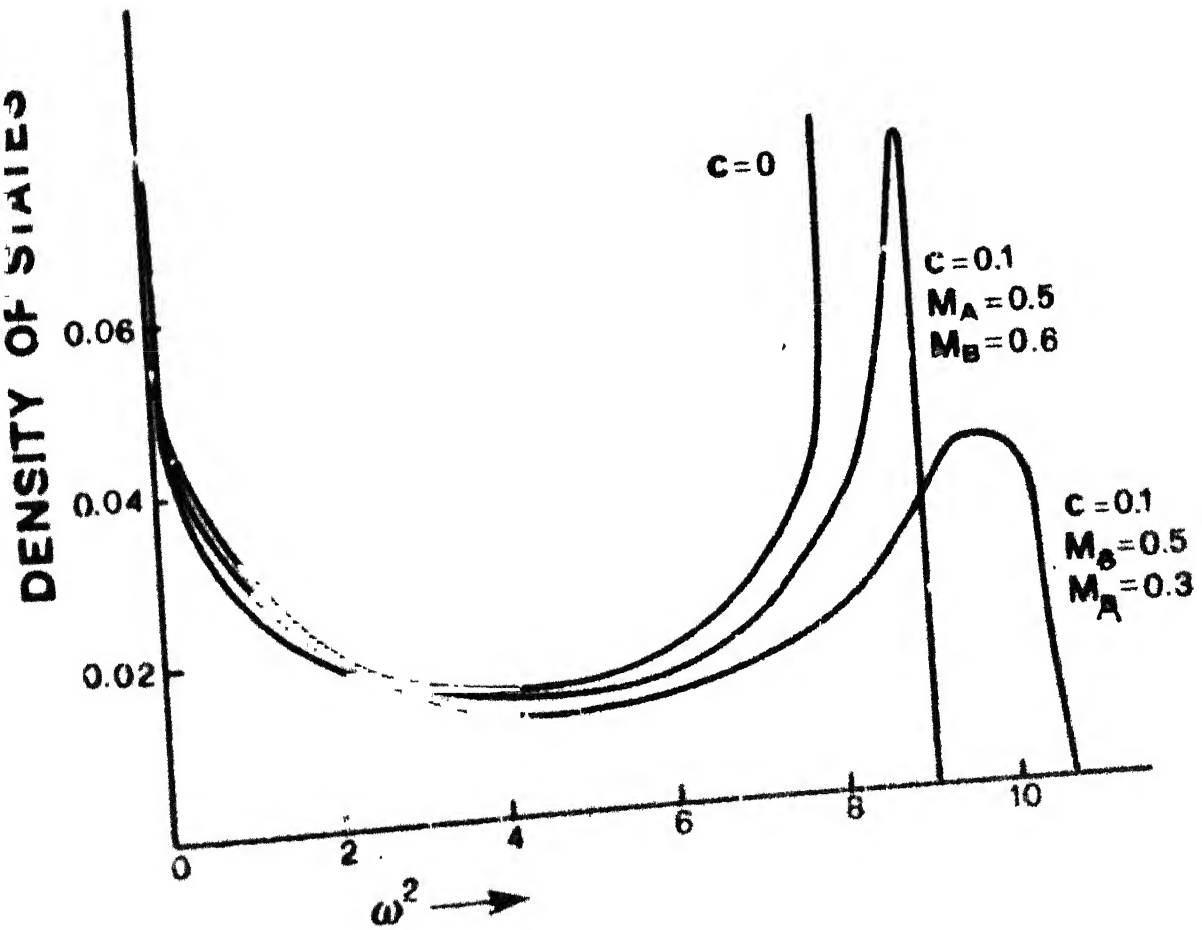
DENSITY OF STATES
0.06
0.04
0.02
0
2
4
6
8
10
ω^2 →
c = 0
c = 0.1
M_A = 0.5
M_B = 0.6
c = 0.1
M_B = 0.5
M_A = 0.3

FIG. 2-3

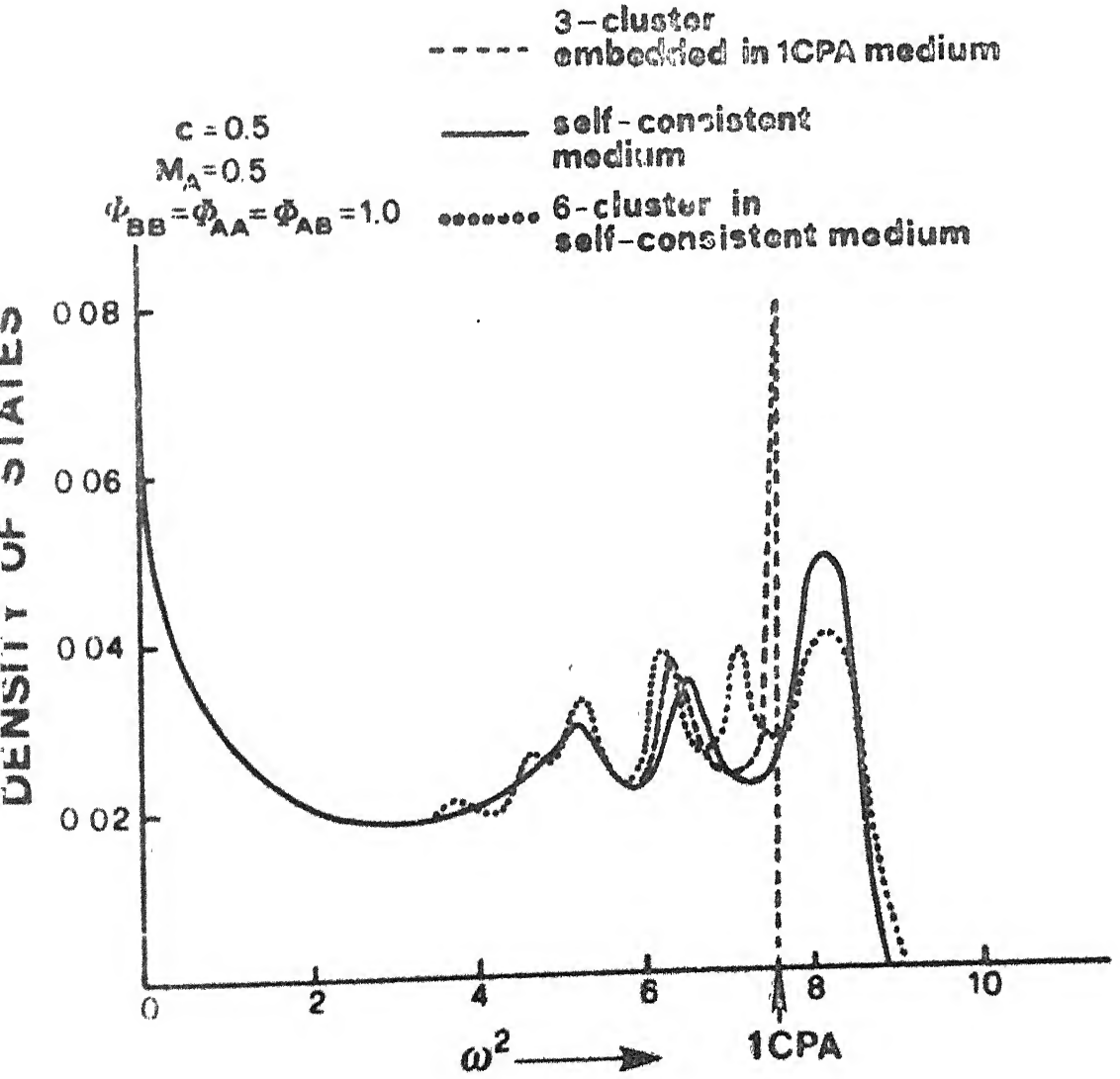
3-cluster
embedded in 1CPA medium
c = 0.5
M_A=0.5
$\Phi_{BB}=\Phi_{AA}=\Phi_{AB}$=1.0
self-consistent
medium
6-cluster in
self-consistent medium
DENSITY OF STATES
0 08
0 06
0 04
0 02
0
2
4
6
8
10
ω^2
1CPA

FIG.2·4

the same size. Significant differences only occur near the band edges. The band width in the self-consistent field is greater than that given by the 1CPA environment. Moreover, the sharp cut-off introduced by the artificial 1CPAenvironment is absent, as well as the sharp unphysical peak there introduced by the squeezing in of the states into the MCPA band. It is obvious from the trends that larger clusters will reproduce the detailed peak structure more accurately, and the position and structure near the band edges also improve with the size of the cluster taken.

Figures 2.5 and 2.6 are to be compared with Diehl et al. (1979, Figures 3c and b) respectively. The underlying histogram is that calculated "exactly" by Dean (1961) and Payton and Visscher (1968) for chains up to 100,000 atoms. Again, the method presented here is a significant improvement on the travelling pseudofermion generalization. The band edges are much better reproduced, as well as the structure near the band edges, especially in those cases where there is an impurity band with considerable structure. Agreement with the "exact" histogram results is not bad, and it is obvious that the two will converge as the size of the cluster is increased.

We have put forward a formalism for calculation of averaged density of states with effect of random clustering. The formalism retains the analytic properties of the resolvent, which is crucial to a satisfactory density of states calculation and does so for all ranges of disorder and energy. Moreover, it provides a tractable method of obtaining the self-consistent

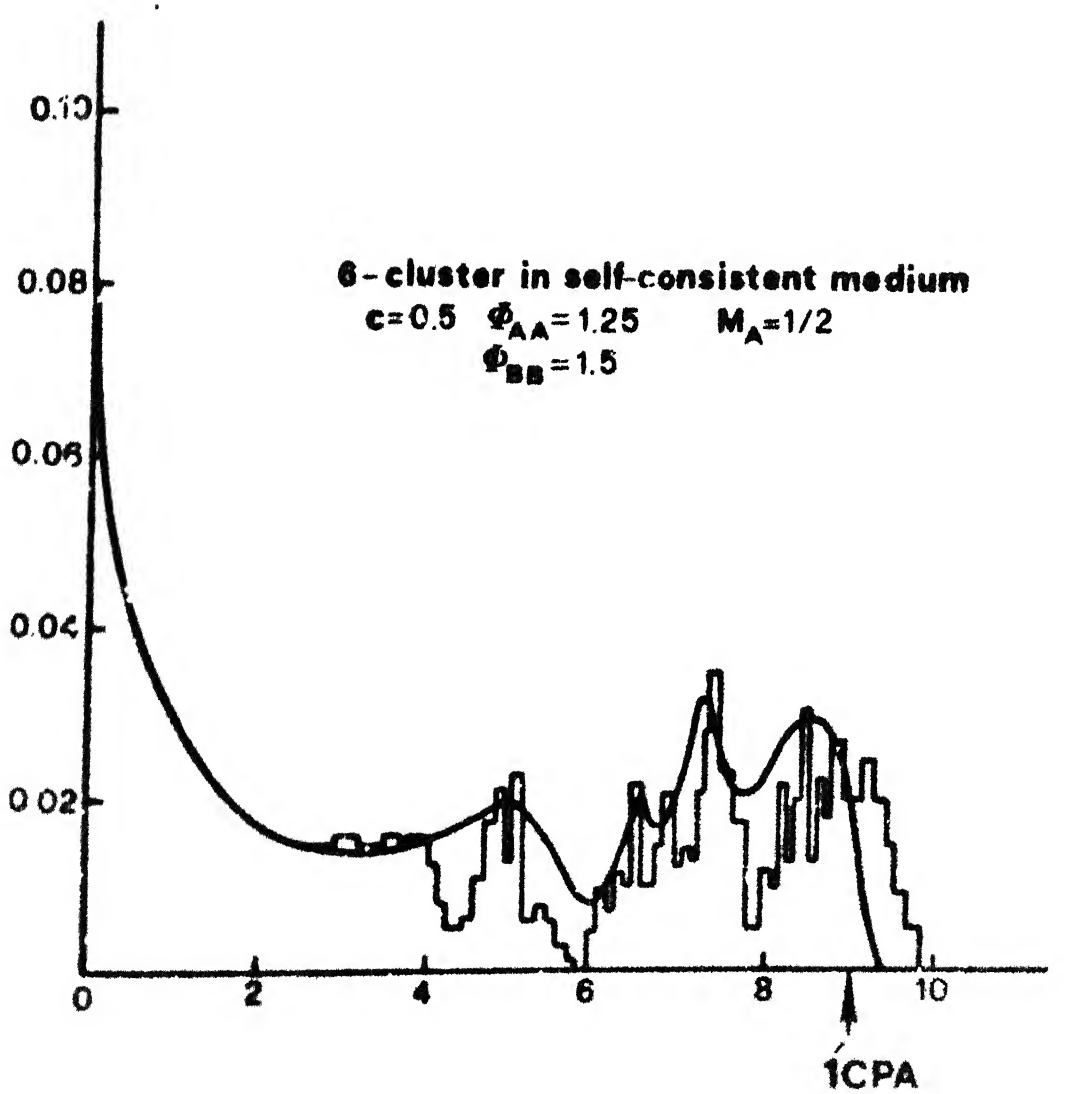
0.10
0.08
0.06
0.04
0.02
0
2
4
6
8
10
6-cluster in self-consistent medium
c=0.5 Φ_{AA}=1.25 M_A=1/2
Φ_{BB}=1.5
ICPA

FIG. 2-5

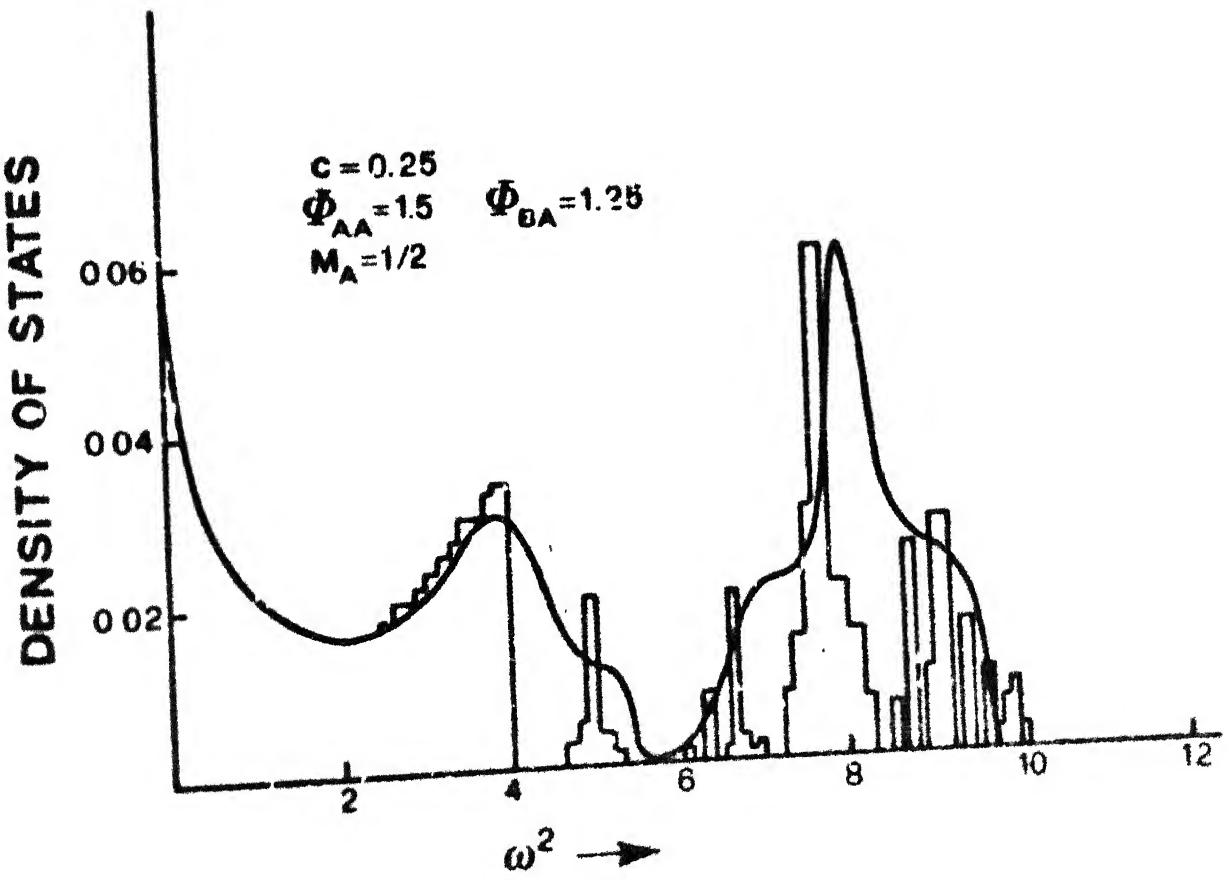
DENSITY OF STATES
c = 0.25
Φ_{AA}=1.5
Φ_{BA}=1.25
M_A=1/2
0 06
0 04
0 02
2
4
6
8
10
12
ω^2 →

FIG. 2·6

medium, which is a natural and unambiguous extension of the single site CP ideas. The formalism is equally applicable without much calculational complexity to three-dimensional systems. We are now in a position to apply the formalism to actual physical situations: for example, to FCC transition metal alloys in which much interest has been shown by experimentalists (Tsunoda et al, 1979; Bosi et al, 1980) due to large mass and force constant disorders (Chapter III).

Chapter III

Application of CCPA to FCC Structured Transition Metal Alloys

3.1 Introduction

The preliminary results of calculation for linear chains discussed in the previous chapter were encouraging and provided us with sufficient theoretical basis to apply the method of self-consistent cluster CPA to more realistic situation of transition metal alloys e.g. Ni-Pd, Ni-Cr and Ni-Pt. The choice is not arbitrary. In fact, these alloys form a continuous series of FCC solid solutions. The experimental results of vibrational properties of these alloys are available to compare with theoretical results. The mass change is dominating in Ni-Pd alloys; force constant change is large in Ni-Cr alloys due to large variation in effective charges, while, Ni-Pt alloys have large variations both in mass and force constants (Table 1). This sequence makes our choice for a systematic study of alloys with all types of disorders. The general augmented space formulation discussed in Chapter II, is developed, in particular for for nearest neighbour interactions only. Thus the FCC structured alloys have another advantage of being the applicants, as we can neglect other than 1^{st} nearest neighbour force constants in them without losing much structural features of physical properties (Chapter I). We note here that the inclusion of second and third near-neighbour force constants is, in practice, not difficult, as we are using the recursion technique to

Table 1 : General Properties of FCC Structured Metals (Ni, Pt, Pd and Cr)

	Ni	Pd	Pt	Cr
1. Atomic Number	28	46	78	24
2. Atomic mass (amu)	58.71	106.4	195.09	51.996
3. Free atom g.s.	$3d^8 4s^2$	$4d^{10}$	$5d^9 6s^1$	$3d^5 4s^1$
4. Lattice constant (fcc) at room temp. (A°)	3.524	3.8904	3.924	3.68 (fcc) (2.89)(bcc)
5. Elastic constants at 296°K (10^{12} dyn/cm)				
C_{11}	2.46	2.270	3.467	3.5
C_{12}	1.50	1.759	2.507	0.678
C_{44}	1.22	0.717	0.765	1.01
6. n-n force constants used (dyn/cm)				
	18474	22469	27987	37483
	19887	22185	31139	17453
	-1396	-3726	-6663	-13229

Table 2 : Recursion-Coefficients for FCC (Ni) Lattice

N	a_N	b_n^2	N	a_n	b_N^2
1	3.998	4.011	7	4.031	4.257
2	4.453	3.548	8	4.176	4.145
3	3.663	3.816	9	3.998	4.029
4	4.113	4.579	10	4.085	4.283
5	4.192	3.993	11	4.081	4.028
6	4.011	4.092	12	4.050	4.176

calculate the various Green's functions. The development of the use of real space symmetries (Kelly, 1980) makes such inclusion computationally possible.

Neutron inelastic scattering experiments have been extensively carried out for the vibrational properties of metals and alloys. The phonon line shapes, spectral functions, scattering cross-sections, width functions are among the experimental quantities which are, in general, studied. These physical quantities depends either upon $\underline{G}(w)$ or $\underline{G}(\underline{k}, w)$. So our aim will be to evaluate configurationally averaged $\underline{G}(w)$ and hence $\underline{G}(\underline{k}, w)$ in MCPA (Eq. 2.16) and 2CPA (Eq. 2.47). Later we compare theoretical dispersion relations, width functions, spectral functions and phonon density of states with experimental ones.

The theoretical calculations for G(w) in MCPA require the $G^{o}_{oo}(w)$ of pure metal, the mass ratio parameter and the impurity concentration (See Eq. 2.22). In 2CPA calculations we require apart from the quantities mentioned above, off-diagonal elements of $\underline{G}^{o}_{ij}$ of pure metal and force constant matrices for the host and impurity. Since our present 2CPA formalism is applicable in the first nearest-neighbour approximation; so we do all calculations of pure metals and MCPA in the same approximation in order to be consistent. Before considering any particular alloy we shall first discuss the force constant matrices for the host and impurities with the $\underline{G}^{o}(w)$ of pure metal.

3.2.1 Force Constant Matrices

The experimental results for the dispersion relations of 'gang of four' metals - Ni, Pd, Pt and Cr - are available

(Birgeneau et al, 1964; Dutton et al, 1972; Muller and Brockhouse, 1971; Feldmann, 1970). These results are used, in general, to fit for 3-5 neighbour force constant models to reproduce other physical quantities e.g. density of states, and Debye-Waller factor etc. We have seen that for these metals except Cr which is BCC in metallic form at normal temperature, the nearest neighbour force constant is very large in Born Von Karman models. So we choose nearest neighbour force constants model. In this model theoretical dispersion curves are given by equation (1.45). Using experimental points in Eq. (1.45) we find the force constants as a best fit to them. The values of best fit force constant matrices for these metals are given in Table 1 while the theoretical dispersion curves with experimental points are given in Figure 1.6 and Figures 3.1-3.3 for Ni, Pt, Pd and Cr metals respectively. It must be remembered that actual Cr is BCC. However Cr in dilution with Ni forms a FCC solid solution. These results are of a hypothetical Cr FCC solid. So the comparison of the theoretical dispersion curves with the experimental points is not justified.

3.2.2 Lattice Green's Functions

The knowledge of $\underline{G}^{o}(w)$ of a pure metal is best obtainable from the Eq. (1.44) which require $\underline{k}$-space calculations. Very accurate $\underline{k}$-space methods exist for the calculation of the Green's functions, for example, the ray integration technique (Chen, 1977) which was further extended by Choudhry (1981) to deal with off-diagonal Green's functions. Green's functions with vacancies

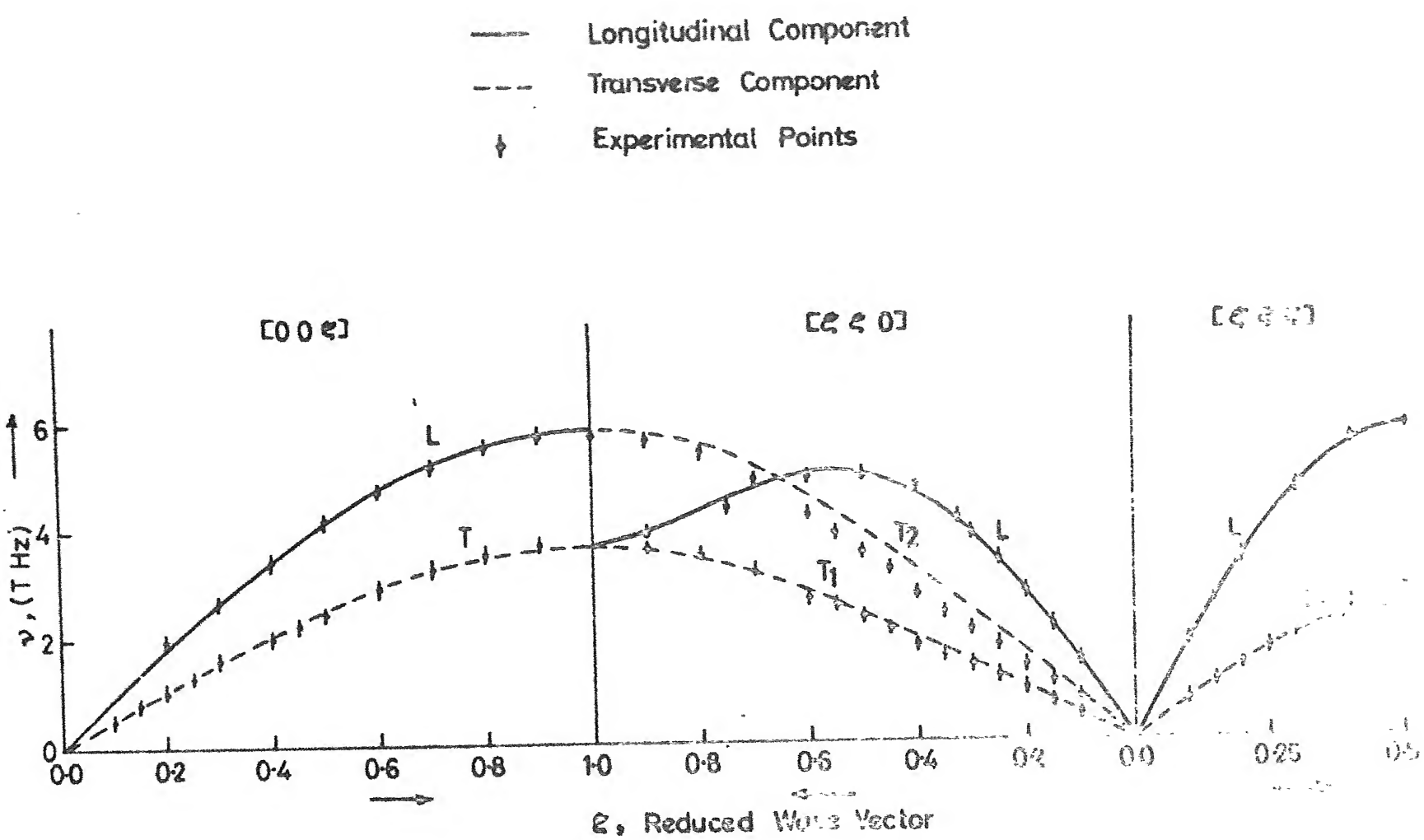

FIG. 3·1 Dispersion Curves for Platinum

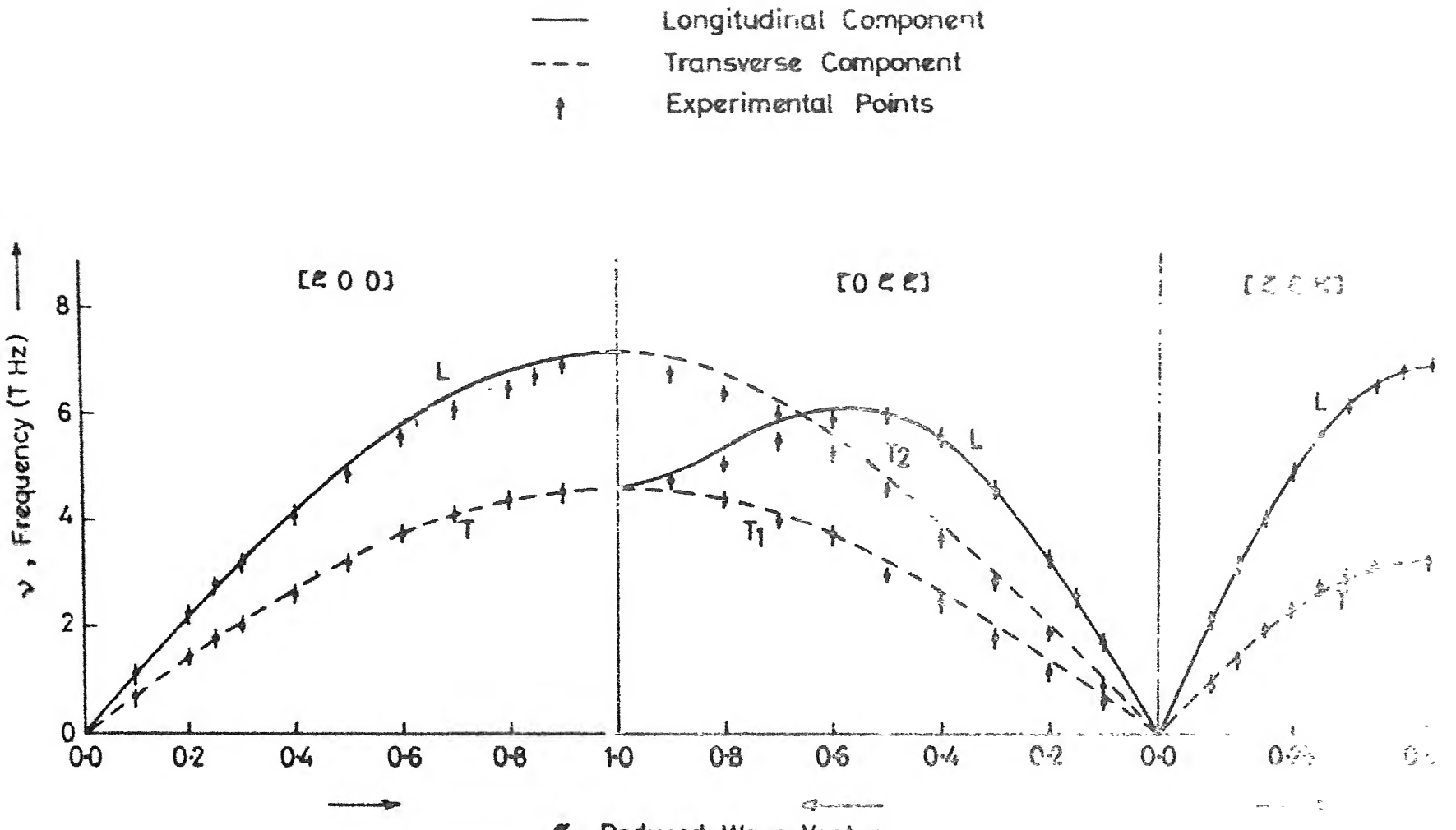

FIG.3·2 Dispersion Curves for Palladium along Principal [illegible]

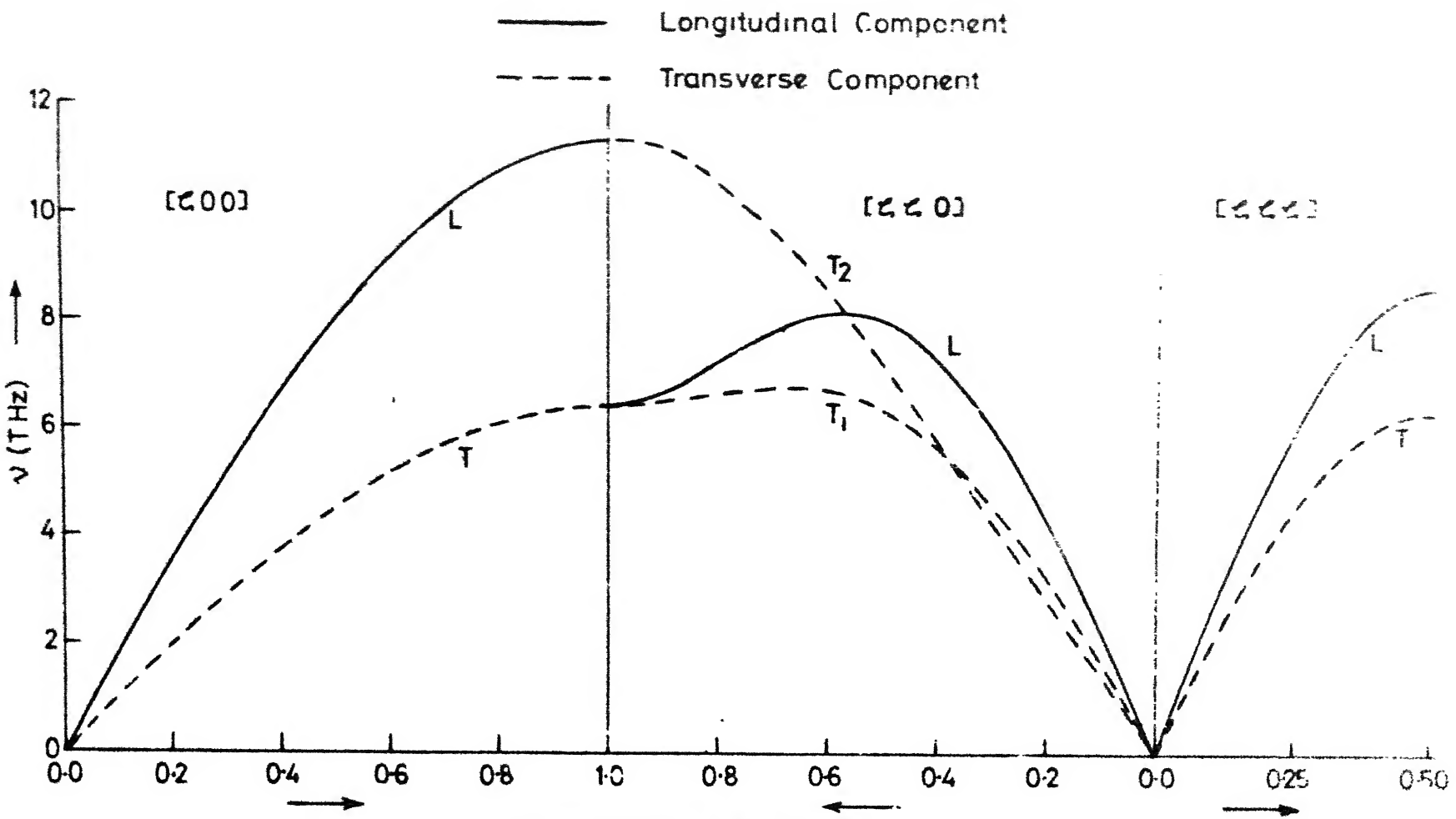

FIG.3·3 Dispersion Curves for FCC Structured Cromium

(as required in our methodology) may also be derived from these by isolated impurity techniques. But this requires high precision computational accuracy. Moreover the frequent use of $\underline{G}(w)$'s in self consistent equations (2.51) and (2.52) makes it unfeasible in practice.

Instead there is a very different approach for the calculation of Green's functions - 'Recursion' technique in real space (Haydock et al, 1972; 1975) (discussed in Appendix A). For comparison we draw the phonon density of states for Ni metal with varying number of continued fraction coefficients, Figure 3.4 (coefficients are given in Table II). The $\underline{k}$-space calculated density of states are given in Figure 3.5. The only difference between recursion density of states and $\underline{k}$-space density of states is that near Von-Hove singularities recursion density of states gives oscillatory behaviour. This nature can be smoothened out if the asymptotic part of the continued fraction coefficients is extrapolated in an efficient manner. Recently the asymptotic summation of continued fraction has been discussed by Kelly (private communication and SSP, Vol. 35). To get the continued fraction coefficients much faster one should exploit the real space symmetries (Kelly, 1980) but we so far have not been able to achieve this in particular for phonon case (though for electronic case these are being exploited in our group by Joshi (private communication)). Our interest, at present, is to include off-diagonal disorder effects in above alloys. We can leave these problems as future extension of this work.

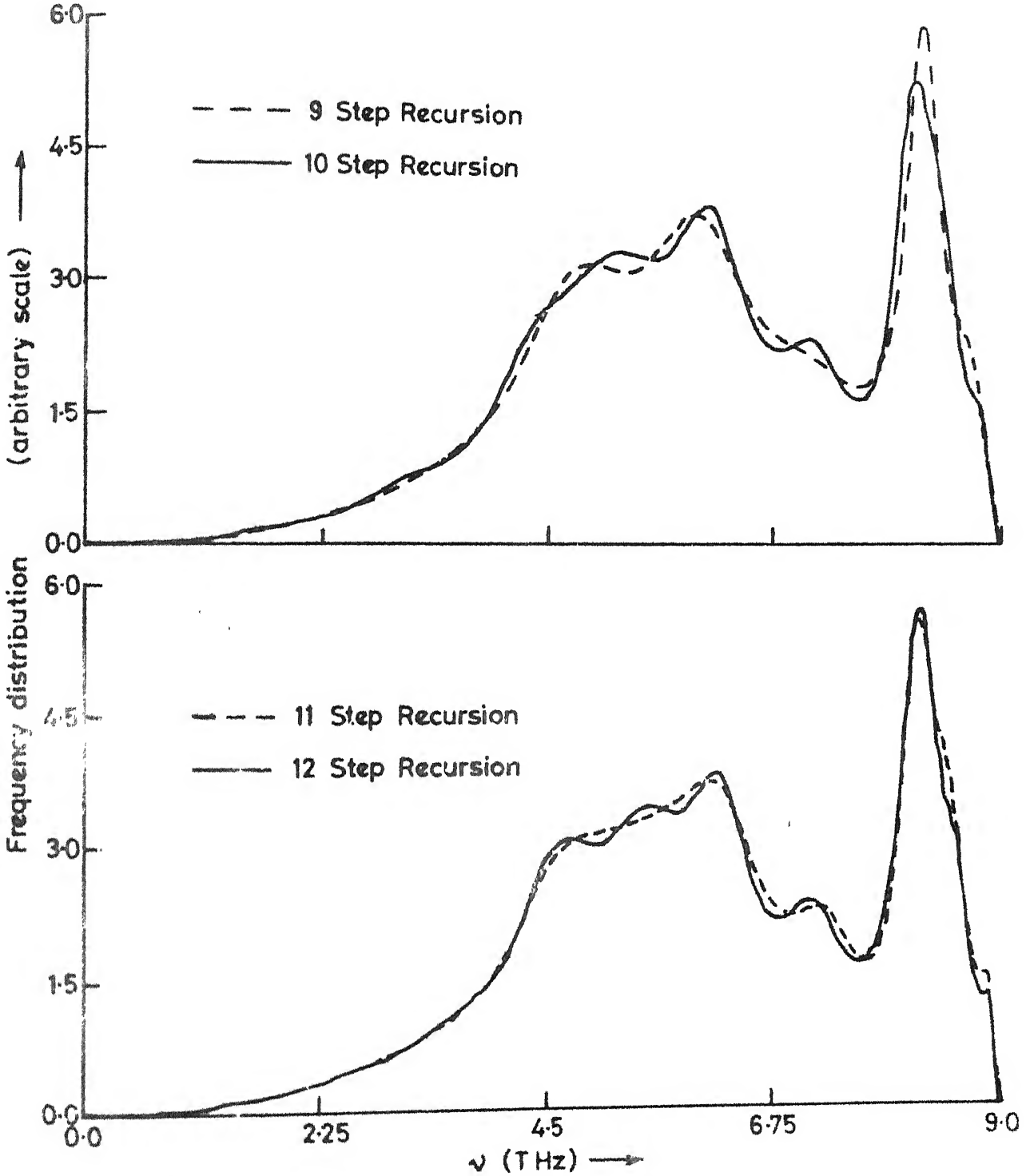

FIG.3·4 Frequency distribution for pure Ni

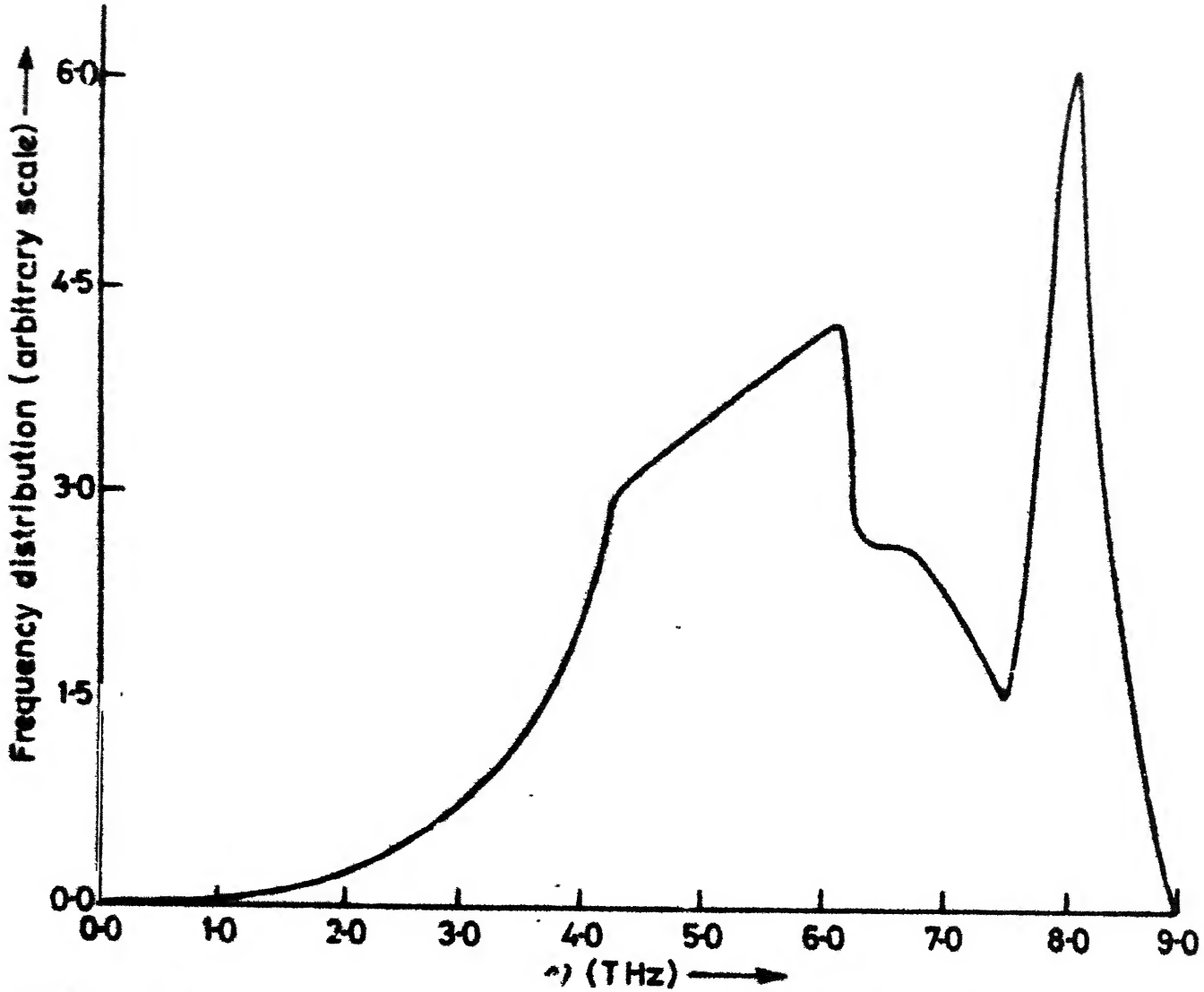

FIG.35 Frequency distribution for Ni metal from experimental points (k-space method)

Having known these input parameters we are, now in position to study these alloys in MCP and 2CP approximations. First we will discuss in detail Ni-Pd alloys, having large mass disorder. In the next section we discuss Ni-Cr alloys where force constant disorder is dominant. Finally we will discuss Ni-Pt alloys where both disorders are important. In the last section we will conclude the results.

3.3 Ni-Pd Alloy

We choose the $Ni_{55}Pd_{45}$ alloy for the application of 2CPA developed in Chapter II because this alloy has already been studied theoretically (Kamitakahara and Taylor, 1974) in MCPA and experimentally (Kamitakahara and Brockhouse, 1974) by inelastic neutron scattering. The properties of Ni and Pd have been summarized in Table 1. Ni and Pd form solid solutions of all concentrations and there are no indications of long-range order down to 0°C. The phase diagram of $Ni_{1-c}Pd_c$ shows that the liquidus and solidus touch at 45% Pd (Hansen, 1958). The dispersion curves of Ni and Pd are dominated by large, almost central nearest neighbour forces (Birgeneau et al, 1964; Muller and Brockhouse, 1968; 1971). Force constants in Pd are about 15% higher than Ni.

In Figure 3.6 we display the spectral functions obtained from 2CPA formulation in the highest symmetry directions ($[00\zeta]$, $[\zeta\zeta 0]$, $[\zeta\zeta\zeta]$). The first thing to note is that the spectral functions are (in contrast to Lorentzian shapes) often asymmetric near the resonances. The asymmetries

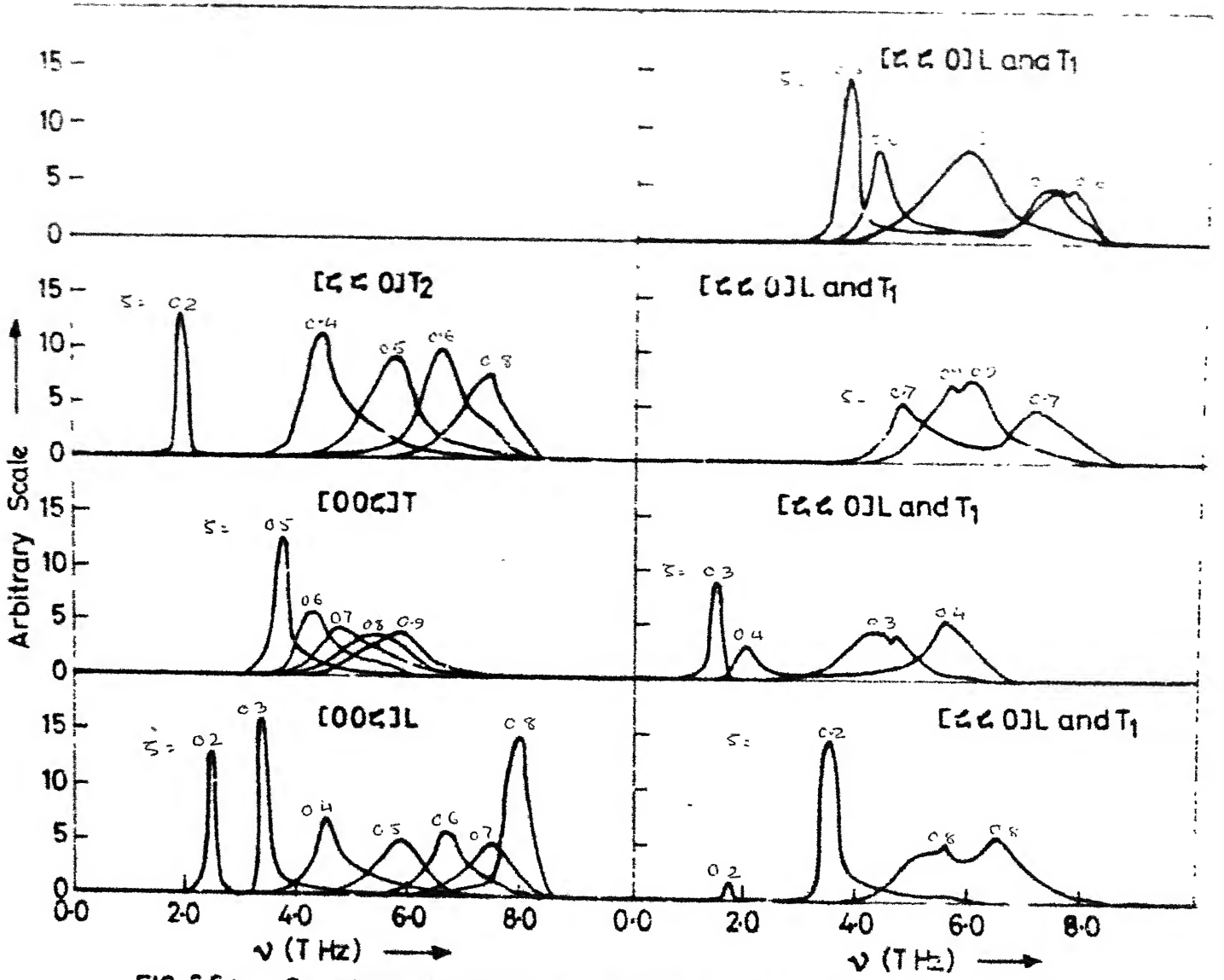

FIG.3-6a Spectral functions in 2 CPA for $Ni_{55}Pd_{45}$ (continued)

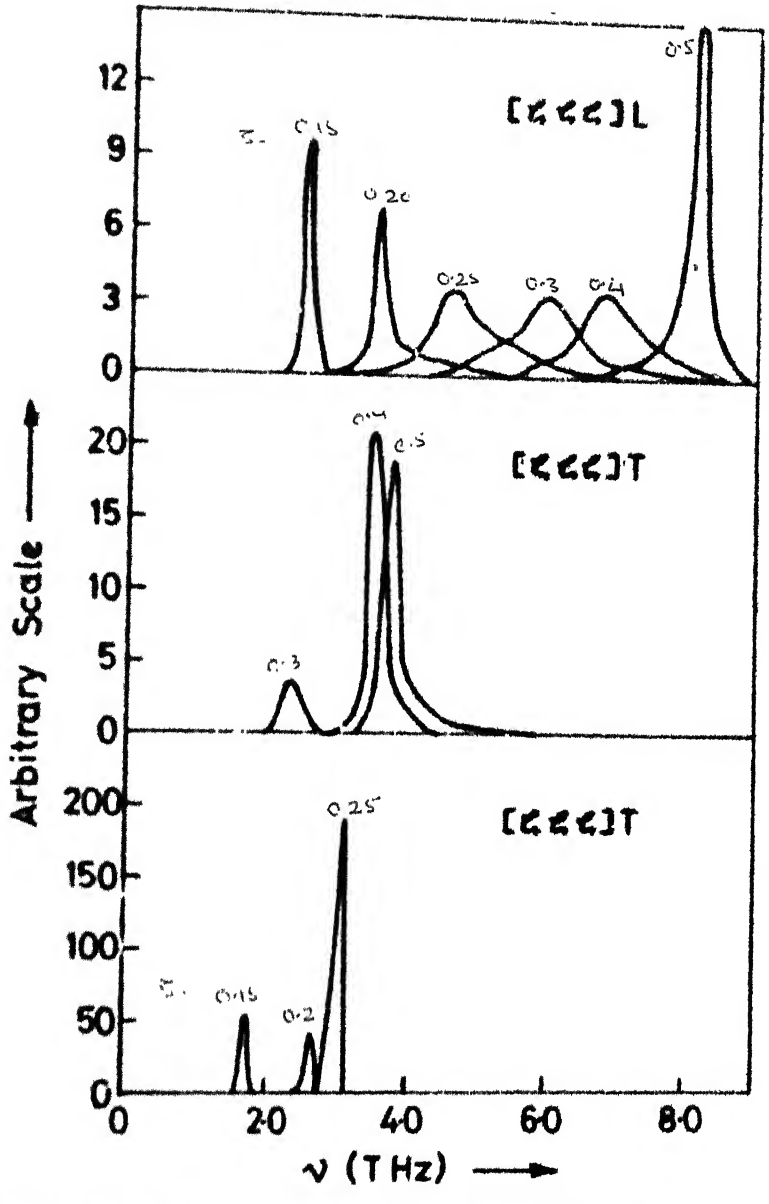

FIG.36b Spectral functions in 2 CPA for $Ni_{55}Pd_{45}$

occur near the resonance frequencies. In other words, the shape of a mode with a frequency slightly lower or higher than that of a resonance tends to have a second peak or wide tail over the resonance region. Experimentally, for some neutron groups corresponding to transverse phonons with frequencies just below the lower resonance, definite asymmetries to the right were observed. Such asymmetries are evident for $[\zeta\zeta\zeta]$ T and $[\zeta\zeta 0]$ T_1 branches (Kamitakahara and Brockhouse, 1974). In most cases the energy resolution is typically 0.5 THz and counting statistics are probably inadequate to detect other types of asymmetries. Secondly, the spectral functions have a pronounced branch dependence in contrast with the MCPA predictions.

In Figure 3.7 we display the natural disorder-induced widths (a consequence of spectral function of Figure 3.6) as a function of frequencies with the experimentally observed points from incoherent neutron scattering data by Kamitakahara and Brockhouse. Experimentally, there is a evidence of resonance, which is strongest in the $[\zeta\zeta\zeta]$ T branch and at 3 THz, strong in the $[\zeta\zeta 0]$ T_1 branch also at 3 THz. It is weaker but still evident in the $[\zeta\zeta 0]$ T_2 and $[00\zeta]$ T branches at slightly greater than 4 THz. In the $[\zeta\zeta 0]$ T_2 branch there is evidence of a second resonance at around 7 THz. There is some indication of two resonances in the $[\zeta\zeta\zeta]$ L branch but within experimental error the width could increase monotonically from origin to the zone boundary. In the $[00\zeta]$ L branch, there is no indication at all of resonances and the amplitude of the width is smaller than for the other branches.

Theoretically MCPA calculations predicts a branch

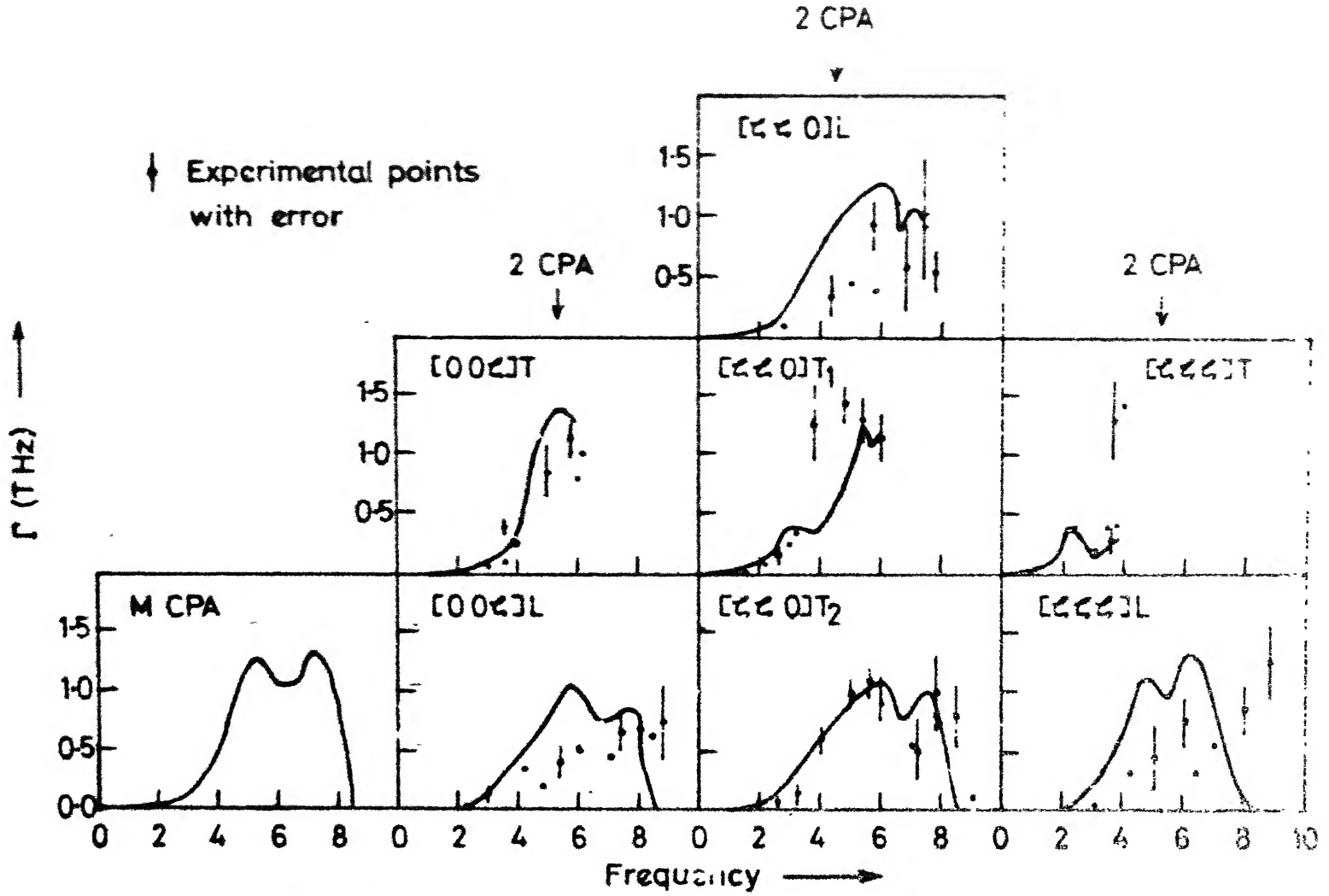

FIG.3·7 Width functions for $Ni_{55}Pd_{45}$

independent width shape because of diagonality and k-independence of the MCPA self-energy $\underline{\Sigma}$. The 2CPA calculations introduce both non-diagonality and k-dependence of $\underline{\Sigma}$ (2.55) and the predicted width shapes are strikingly similar to experimental results (Figure 3.7) except in $[\zeta\zeta\zeta]$ T and $[00\zeta]$ L directions. In our calculations we do not get large width in $[\zeta\zeta\zeta]$ T direction as experimentally observed. Though for $\zeta < 0.25$ there is very good matching. In $[00\zeta]$ L direction we still get two resonance widths while experimentally no resonance exists. But Bosi et al. (1978) got a high resonance width in $[00\zeta]$ L direction for the Pd-Pt alloy which has almost same mass ratio (1.836) as Ni-Pd alloy and hence, to some extent, supports our prediction.

The deviation from MCPA results is particularly noticeable in the concentrated alloy (45% of Pd). In these concentrated regimes, there is a high probability of clusters of Pd randomly occurring in the alloy, these clusters have an effect of introducing $\underline{k}$-dependence and off-diagonal $\underline{\Sigma}$'s (in fact the off-diagonal $\underline{\Sigma}_1$ has the same matrix structure as the force constant, dictated by the symmetries of the lattice (Chapter I)). For this alloy, such an effect also arises from disorder in the force constants which cannot be taken into account in MCPA. The 2CPA is the lowest order approximation in which it is possible to consider them consistently. It is difficult to guess which of these two effects dominate in the width function although the analysis of Ni-Cr alloy with dominant off-diagonal disorder indicates a predominant effect of the latter.

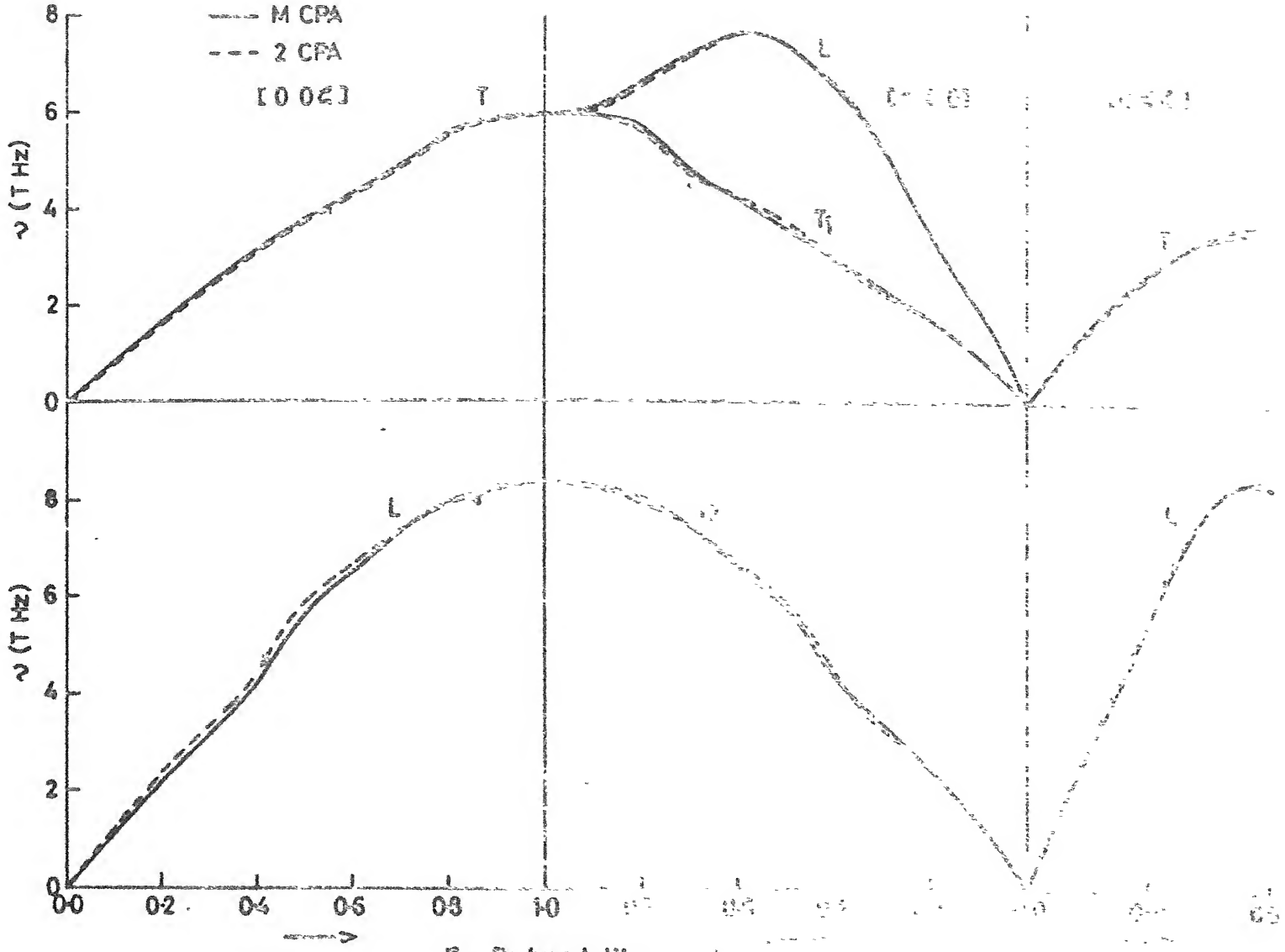

FIG.3.3 Dispersion Curves for

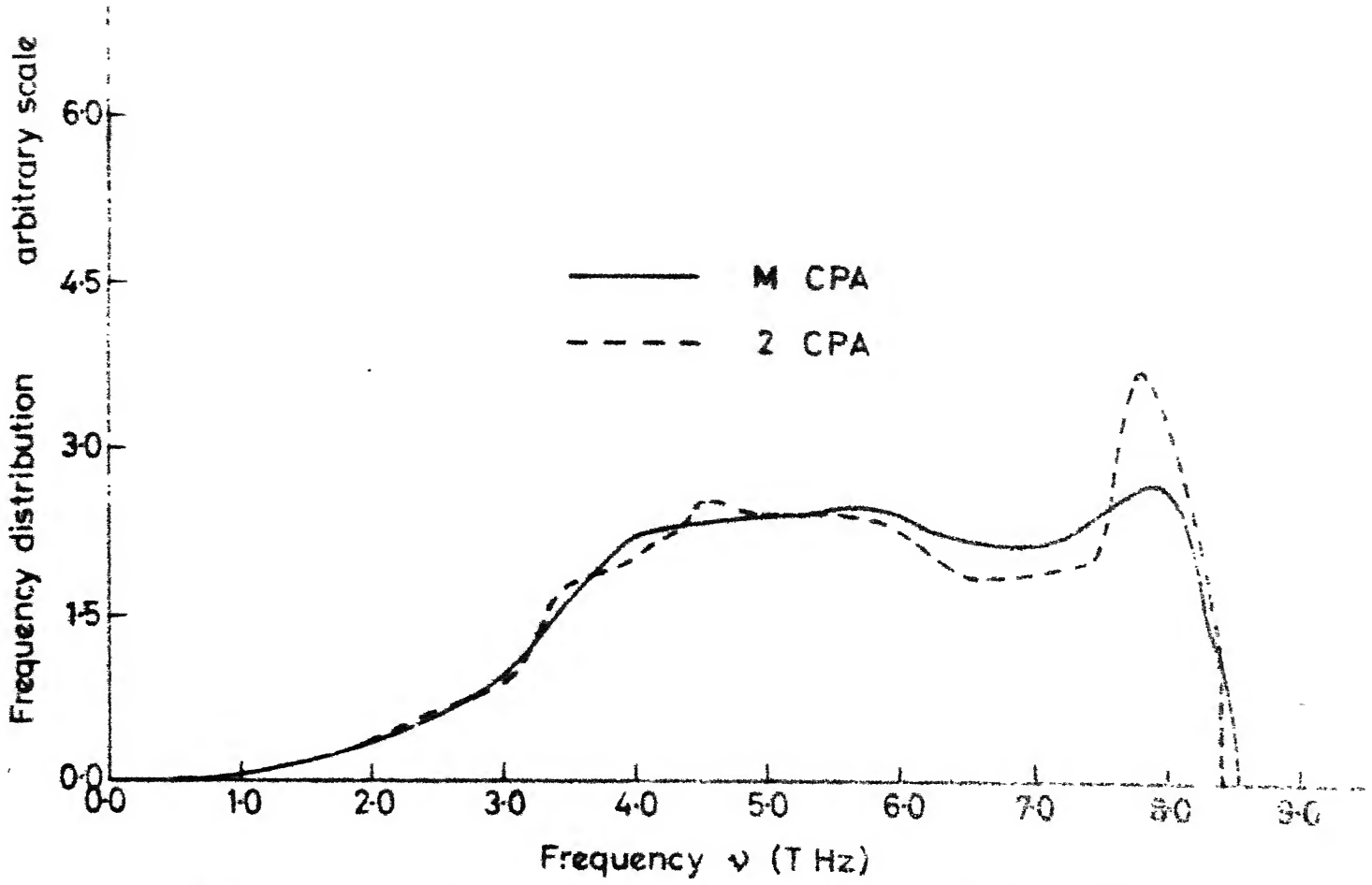

FIG 3.9 Frequency distribution for $Ni_{55}Pd_{45}$ alloy

In Figure 3.8 we plot the MCPA and 2CPA dispersion curves. The 2CPA further strengthens the evidence of a second resonance in $[\zeta\zeta 0]\, T_2$ branch at higher frequencies. The kinks in the transverse branches are also pronounced. Next we plot (in Figure 3.9) the u-u correlation function $\rho'(w)$ given by

$$\rho'(w) = -\frac{2w}{\pi} m_B \ll \mathrm{Tr}\,(\mathrm{Im}\,\underline{G}\,(1, 1; w)) \gg \qquad (3.1)$$

in MCPA and 2CPA. In a pure crystal this is the true density of states (see Chapter I). But it is the natural function to extract from incoherent neutron scattering cross-section results. Specific features appear in 2CPA. The enhancement of the peak around 7.8 THz is the main feature. We may understand this as due to impurity - cluster bands pulled out of the mean crystal density. Secondary structures appear around 3.5 THz where the resonance occurs. The effect of force constant disorder is not transparently apparent in Figure 3.9 except perhaps in slight lowering the band edges in reference to MCPA calculation.

3.4 Ni-Cr Alloy

Theoretically it is not a good system to study because of BCC structure of pure Cr metal. But when it is alloyed with Ni it forms a continuous series of FCC alloys upto 30% of Cr. In Ni-Cr system, the components have masses which are close enough to eliminate any appreciable effects of mass disorder while at the same time the number of outer electrons (d and s electrons outside the A-core) changes from six to ten and hence the effect of force-disorder dominates. Moreover, $Ni_{89}Cr_{11}$ is experimentally

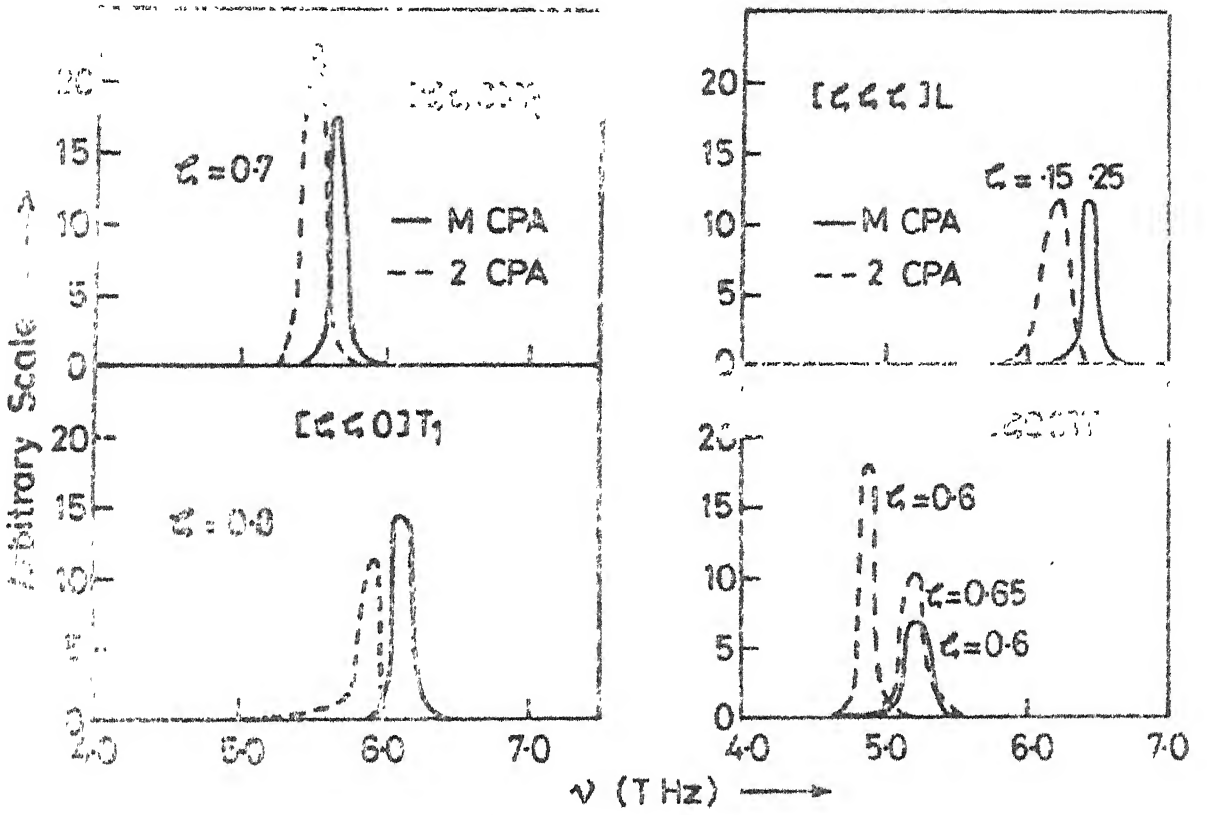

FIG.3·10 Spectral functions for $Ni_{88}Cr_{12}$

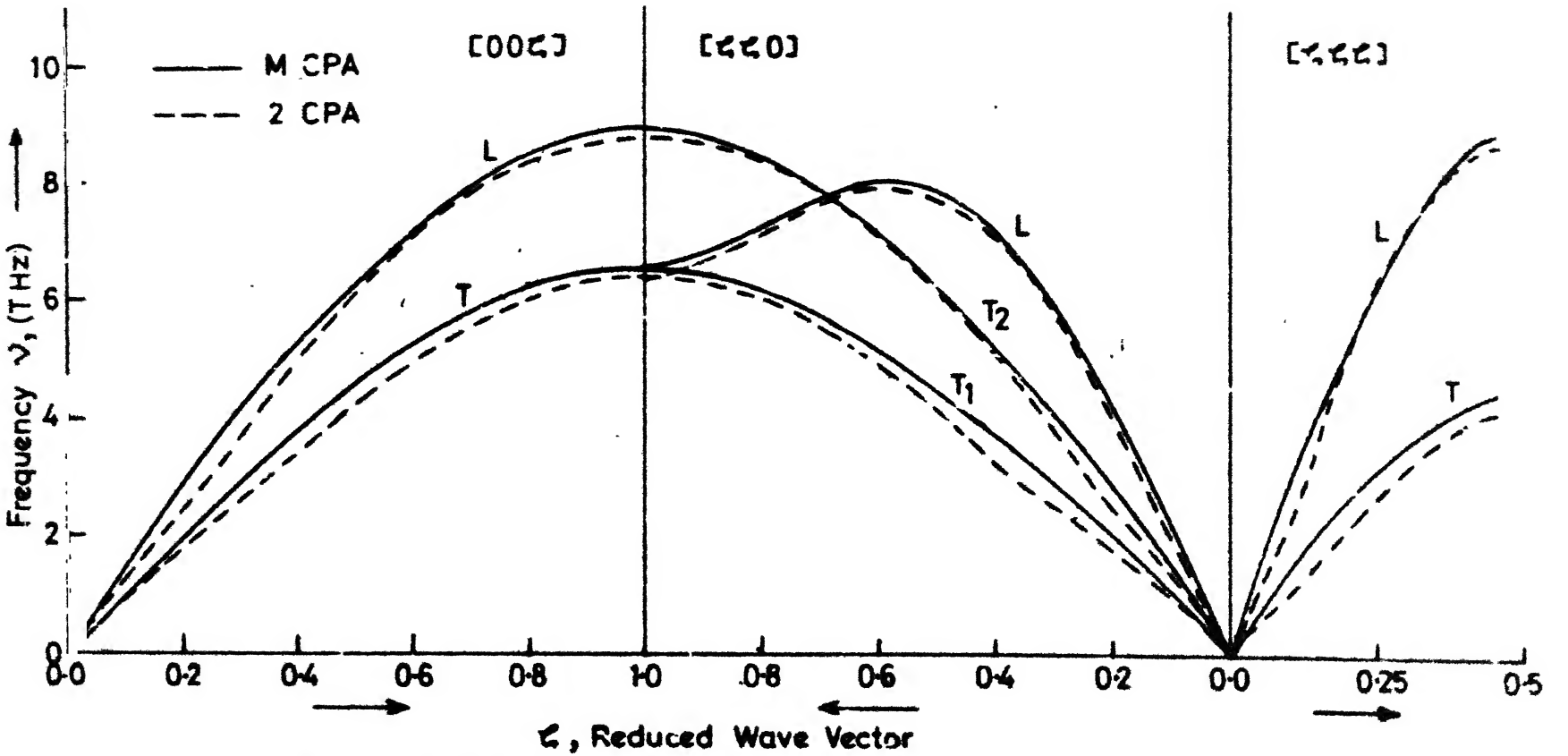

FIG.3·11 Dispersion Curves for $Ni_{88}Cr_{12}$

studied by Bosi et al. (1980) to see the effect of force constant disorder. That is why we have chosen this system for the application of our theory. Our calculations are on Ni-Cr model system in which Cr is treated as FCC metal because of the requirement of our theory. We construct a hypothetical FCC Cr in such a way that its BCC elastic constants are related to FCC force constants in nearest neighbour approximation:

$$C_{11} + 2C_{12} = 4(f_l - f_{t'} - f_t)/a$$

$$C_{11} - C_{12} = (f_l + 5f_{t'} + 2f_t)/a$$

$$C_{44} = (f_l + f_{t'} + 2f_t)/a$$

The values of C_{11}, C_{12}, and C_{44} are taken from Leibfried and Breuer (1978). The calculated values are listed in Table 1 and the dispersion curves are given in Figure 3.3.

Having done this, we carry out the MCPA and 2CPA calculations and display the some spectral functions (Figure 3.10), dispersion curves (Figure 3.11) and the frequency distribution function (Figure 3.12). In this case the widths are small in all directions. This is expected, as clear-cut resonances are features of large mass disorder. There is evidence of $\underline{k}$ and branch dependence, as also asymmetry in certain directions. This strengthens our argument that force constant disorder is responsible for the asymmetry of line shapes and ultimately for their strong $\underline{k}$- and w-dependence. The same effect can be seen in the dispersion curves and in the frequency distribution function. The dispersion curves are lowered and distorted near 2.5-4.5 THz range in all directions. The lowering of

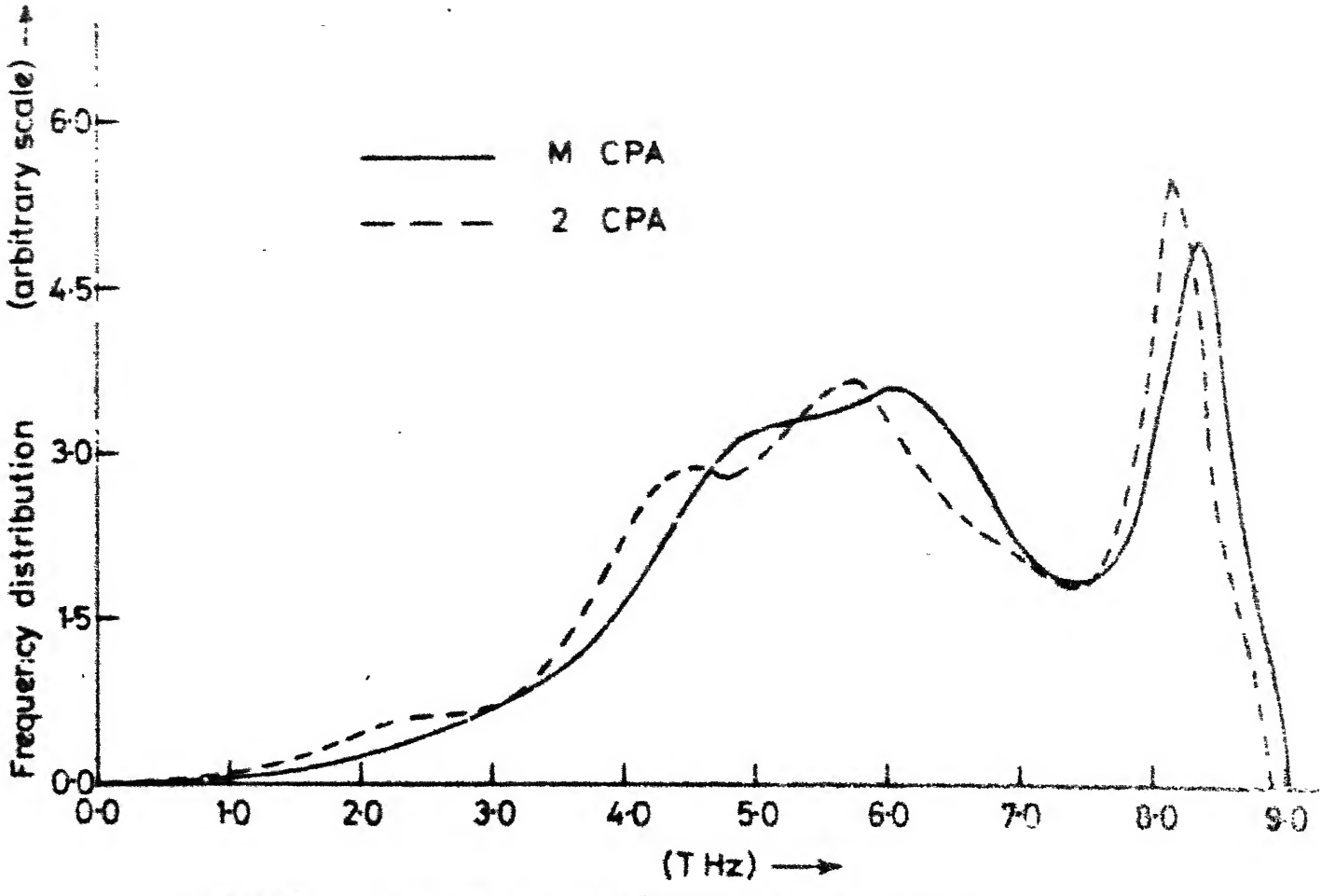

FIG.3-12 Frequency distribution for $Ni_{88}Cr_{12}$

dispersion curves near edges of symmetry directions is observable in the maximum limit of density of states which is reduced. considerably. Near the broadening region (5-6 THz) of spectral functions, frequency distribution gives a peak while at lower (higher) values of this region the distribution is reduced compared to MCPA.

3.5 Ni-Pt Alloys

Being encouraged by the right trend of theoretical results towards the experimental results in the Ni-Pd and Ni-Cr alloys, where either of two disorders - diagonal and off-diagonal dominates, we now apply our formulation to Ni-Pt alloys where both disorders are predominant. The melting points of these alloys are nearly constant over a wide range of concentration and hence these alloys also form a continuous series of FCC solid solutions. The extra characters of these alloys are their atomic ordering at 3:1 and 1:1 compositions and hence are under the influence of atomic short range ordering (Hansen, 1958). The nearest neighbour force constant of Pt is roughly 50% larger than that of Ni. Tsunoda et al. (1979) have studied this system thoroughly covering the full range of concentration by inelastic neutron scattering. We, therefore, discuss this in detail for different concentrations (c = 0.05, 0.30, and 0.50) successively.

3.5.1 $Ni_{95}Pt_{05}$

In Figure 3.13 we plot the dispersion curves in the $[00\zeta]$ L and $[00\zeta]$ T directions for MCPA and 2CPA. The insets are enlarged for both components which explain the effect of

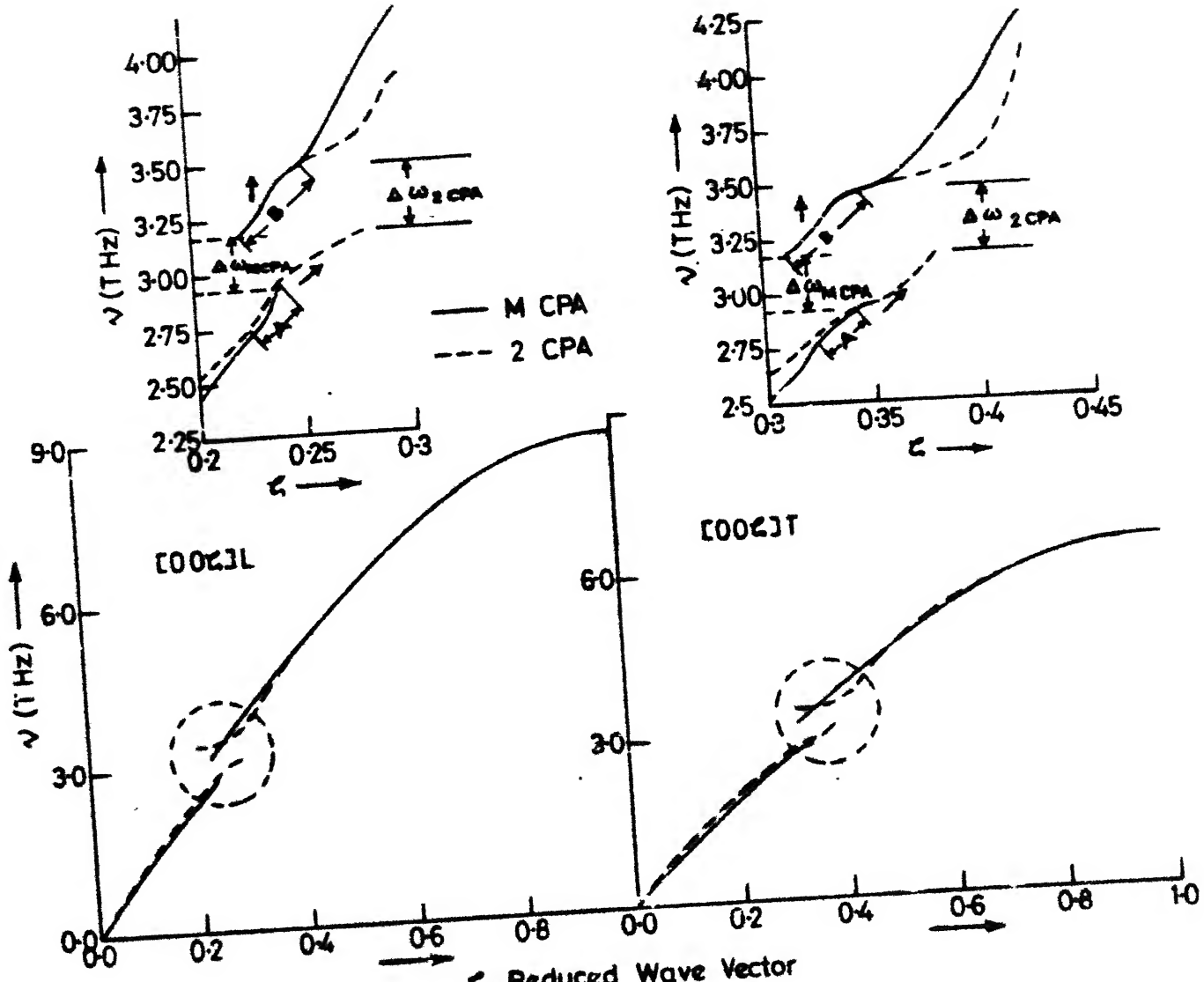

FIG.3·13 Dispersion curves for $Ni_{95}Pt_{05}$

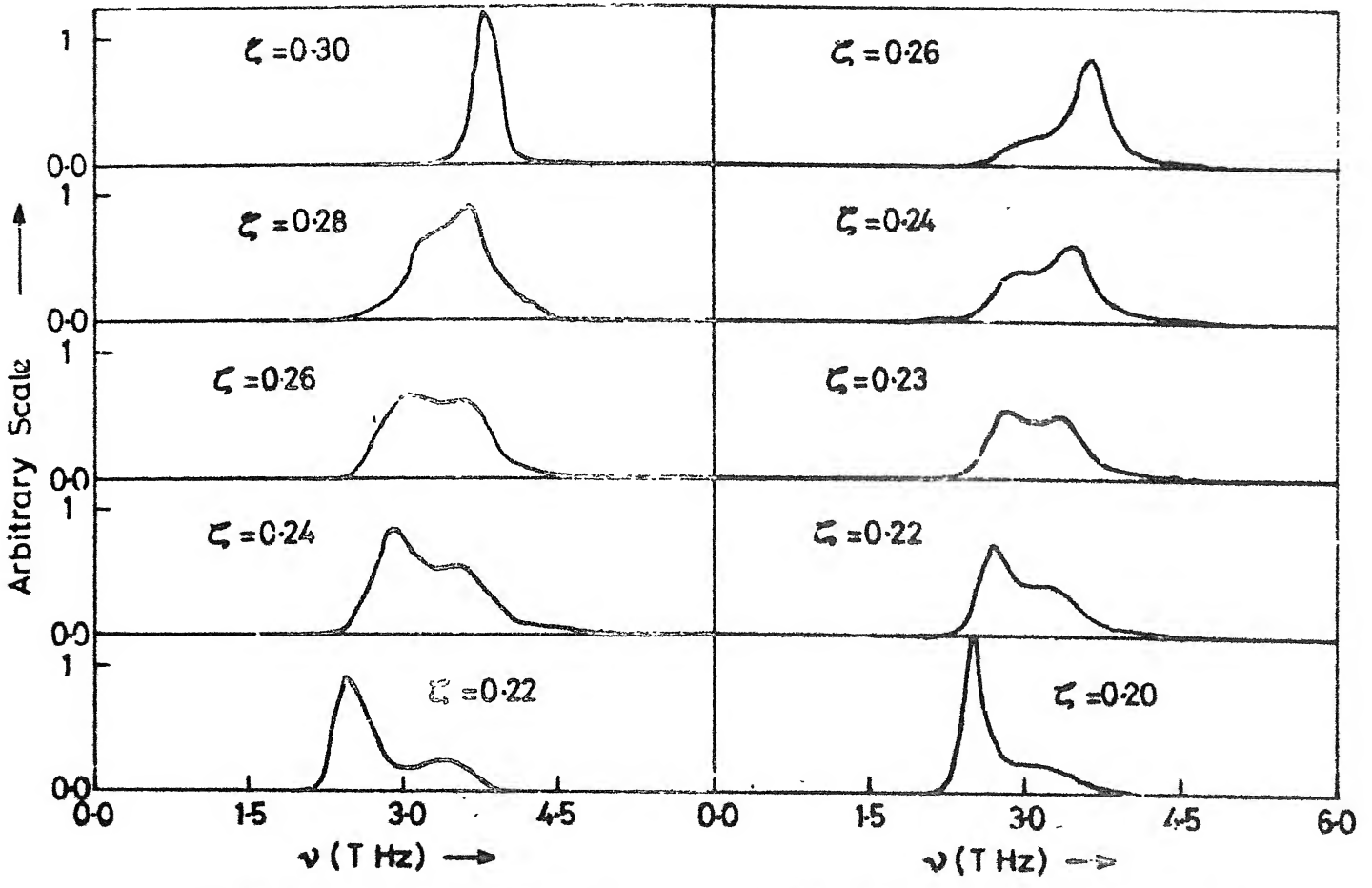

2 CPA line shapes for $Ni_{95}Pt_{05}$ in [00ζ] L direction

M CPA line shapes for $Ni_{95}Pt_{05}$ in [00ζ] L direction

FIG.3·14

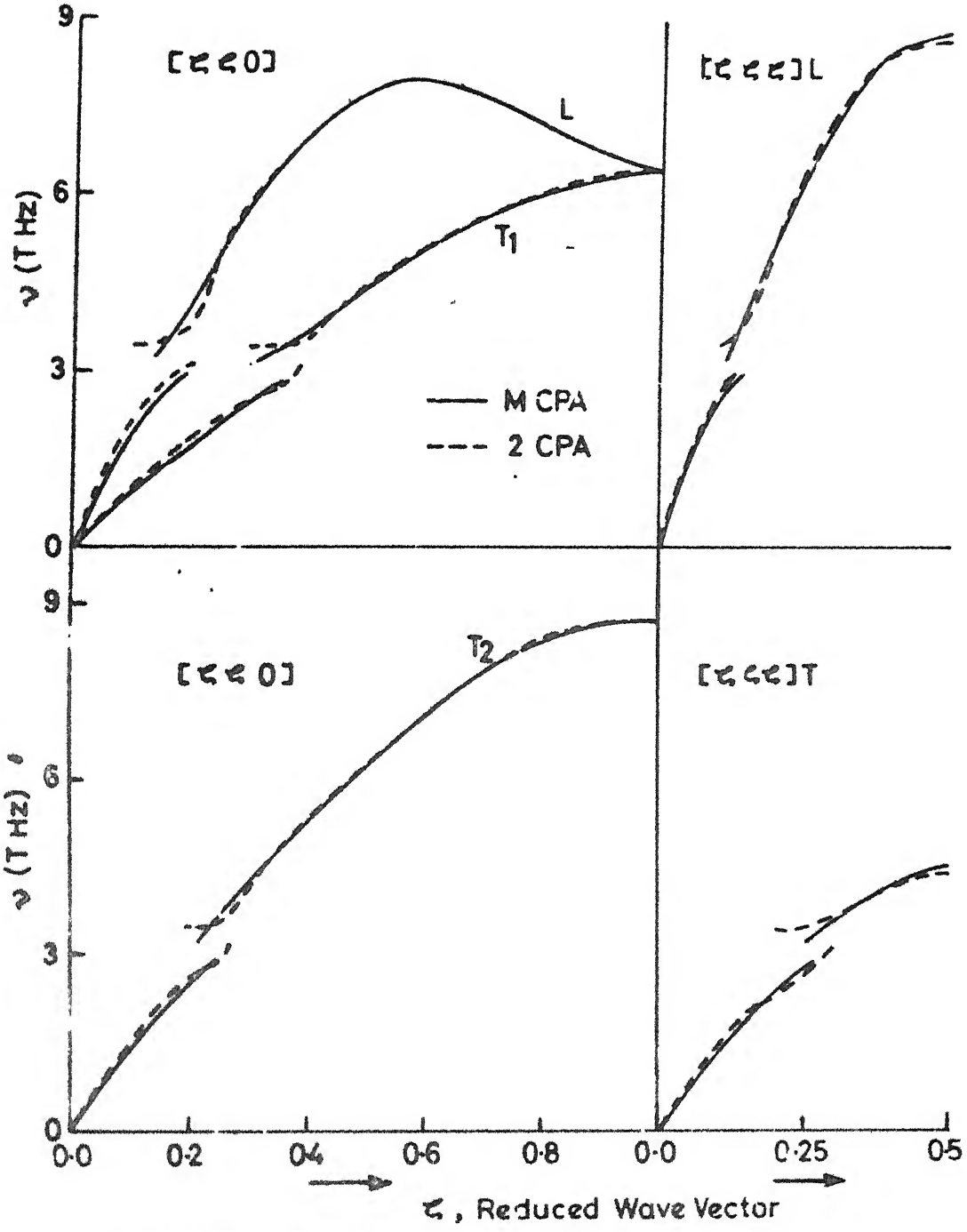

FIG. 3·15 Dispersion Curves for $Ni_{95}Pt_{05}$

environmental disorder. The portion A of MCPA is stretched to higher values of ζ in 2CPA, while portion B of MCPA is pushed up to higher frequencies in 2CPA. This pushing and pulling is the consequence of hybridization of ideal phonon lines with the resonance mode which is possible only if $\underline{\underline{\Sigma}}$ has strong $\underline{k}$- and w-dependence (Dederichs and Zeller, 1980). The ultimate effect is the increment in the energy gap with the resonance frequency. The anamolies corresponding to the resonance modes of Pt occurs at nearly the same frequency of 3.05 THz in MCPA for both components, while it is near 3.32 THz in 2 CPA calculations. The experimentally observed frequency mode is 3.3 THz almost equal to our prediction. At this frequency both components have double peak structure. Some of the spectral functions (line shapes) for the $[00\zeta]$ L branch are given in Figure 3.14 after the calculation by MCPA and 2CPA. For other two directions $[\zeta\zeta 0]$ and $[\zeta\zeta\zeta]$ dispersion curves are given in Figure 3.15. In MCPA the resonance frequency appears to be insensitive to the phonon propagation direction. In 2CPA we also obtain same nature except in $[\zeta\zeta\zeta]$ L direction (where resonance mode occurs at about 3.27 THz). Since at this low concentration one cannot, from experimental results, claim the dependence or independent of k-vector in the resonance mode, so we shall later use our formulation for higher concentrations to see the directional dependence effects. in Figure 3.16 we display the MCPA and 2CPA frequency distribution functions along with the partial density of states in the inset calculated by Tsunoda et al. by inelastic neutron scattering experiment. The experimental partial density of states are

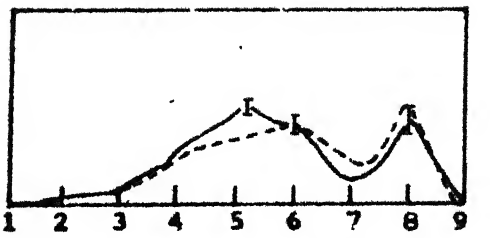

Phonon density of states from experiments by Tsunoda et al. with the partial density of states (broken curve) of Ni in the $Ni_{95}Pt_5$ calculated with the MCPA.

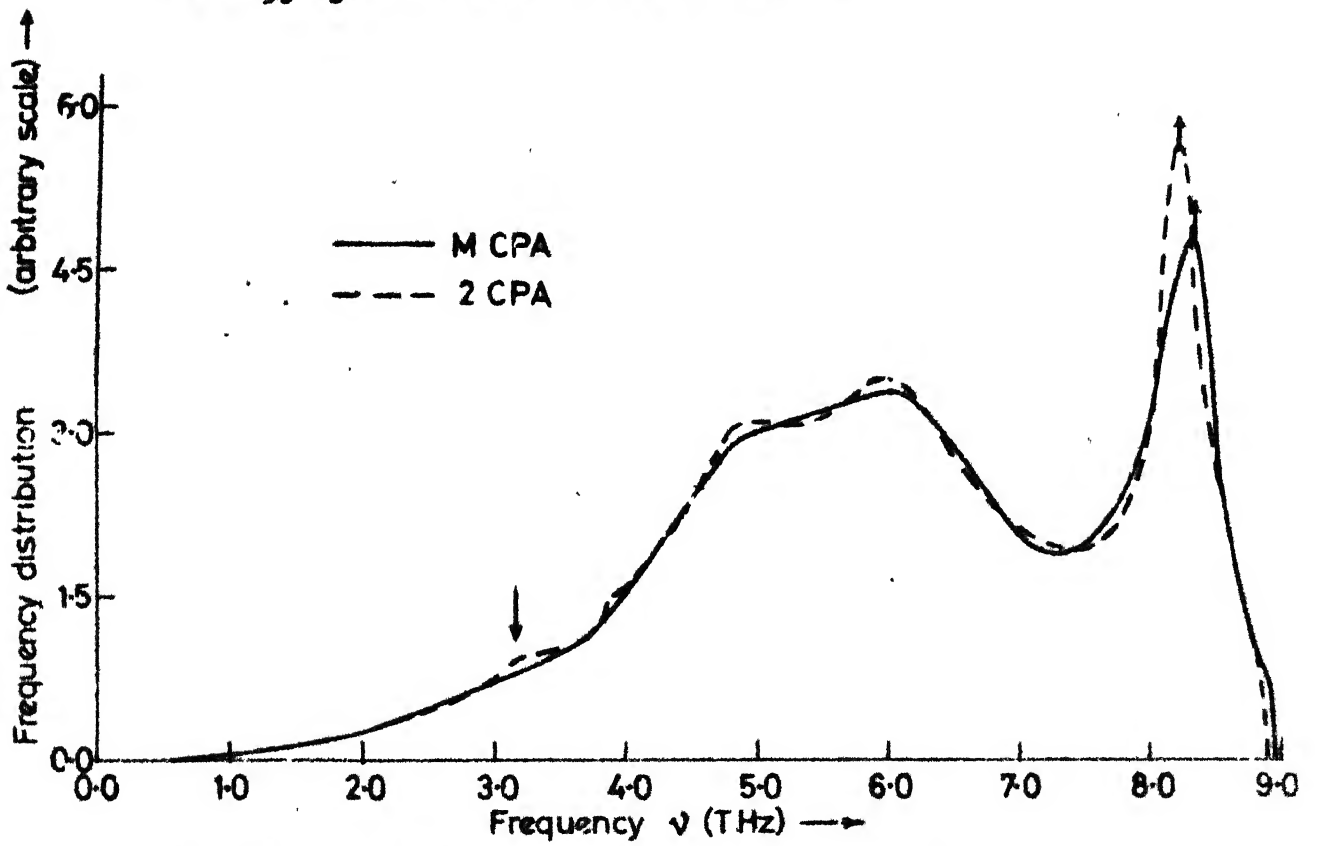

FIG. 3·16 Frequency distribution for $Ni_{95}Pt_{95}$ alloy

increased in frequency range 4-6 THz. Similar effect can be seen in frequency distribution function in the same region for 2CPA. Moreover, second peak is also increased and near the resonance frequency there is a kink in 2CPA. As far as the maximum frequency is concerned there is not much change in 2CPA calculations except a slight lowering of the band width.

3.5.2 $Ni_{70}Pt_{30}$

The dispersion curves along the $[00\zeta]$, $[\zeta\zeta 0]$ and $[\zeta\zeta\zeta]$ directions are displayed in Figure 3.17 for MCPA and 2CPA. The resonant behaviour observed for c = 0.05 is strongly enhanced in this system. For the $[00\zeta]$ T branch the phonon spectral functions (line shapes) becomes well separated double peaks in the region from $\zeta = 0.15$ to the zone boundary in MCPA; from $\zeta = 0.30$ to the zone boundary in 2CPA; while from $\zeta = 0.40$ to the zone boundary experimentally. For $\zeta > 0.5$, both the MCPA and 2CPA indicate that the 00ζ T branch increases with ζ to the zone boundary, whereas the experimental branch seems to decrease in this region. This leads to a difference in interpreting the position of the resonance mode. Tsunoda et al. interpret this as the mean between the maximum energy at $\zeta \simeq 0.5$ on either side of which $[00\zeta]$ T branch decreases, and the lowest energy of the upper $[00\zeta]$ T branch. This gives a value of 3.5 THz. But in the MCPA and 2CPA we interpret this as the mean between the maximum of the lower T branch at the zone boundary and the minimum of the upper T branch. It is 3.75 THz in MCPA while 4.1 THz in 2CPA. However, if we take the maximum of the lower T branch at around $\zeta = 0.45$ beyond which the peak value of spectral

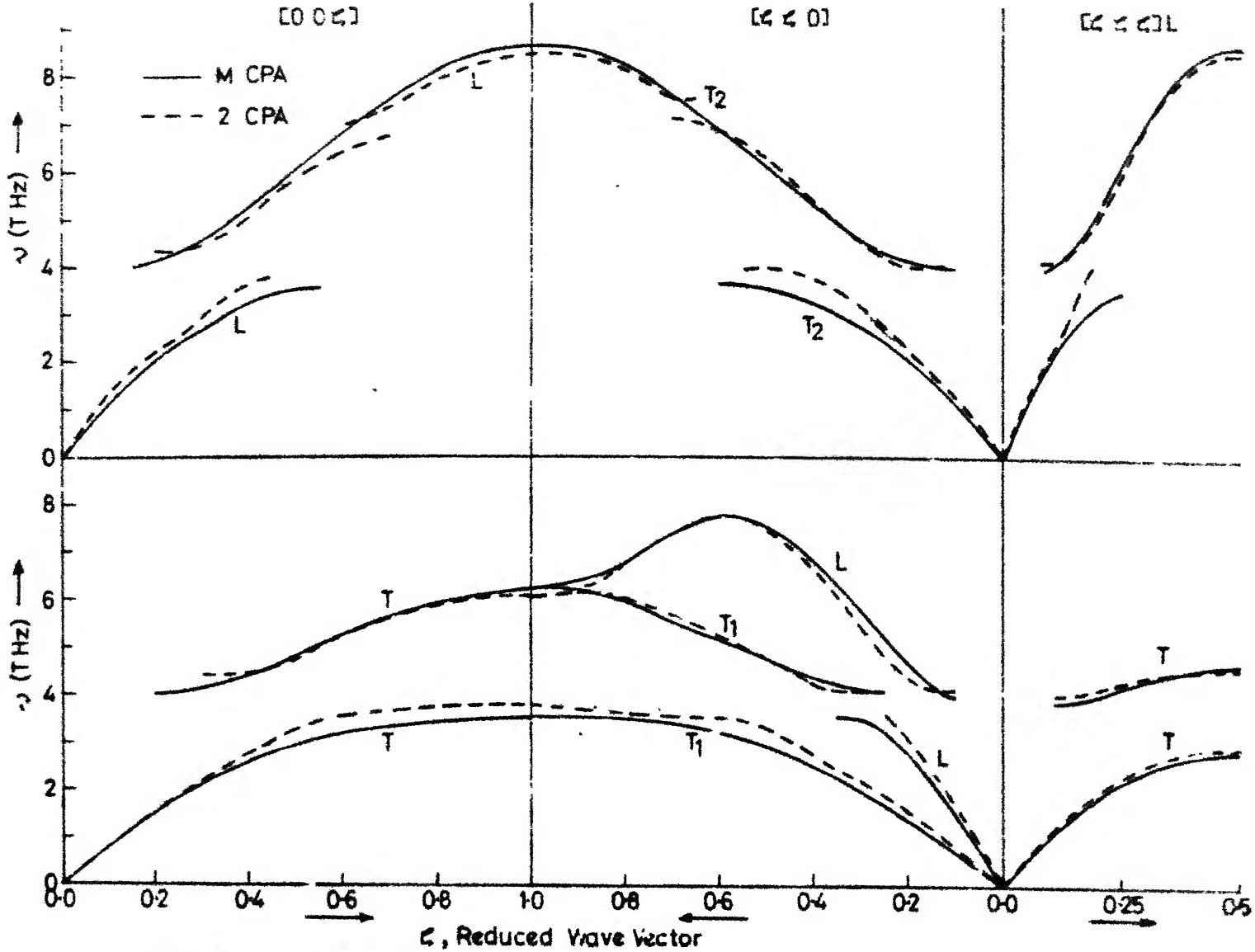

FIG.3-17 Dispersion Curves for $Ni_{70}Pt_{30}$

function is decreasing, we shall get 3.6 THz a mean resonance value in the 2CPA in good agreement with the experimental value. Another feature in the 2CPA result is a sudden shift upward in the lower spectral peak around $\zeta \simeq 0.45$ in the T branch and similar shifts in other branches ($[\zeta\zeta 0]$ T_1 and L branches). The widths here are very large and the peak values themselves low so that individual interpretations become difficult to compare.

For the $[00\,\zeta]$ L branch, MCPA calculation predicts the existence of a resonance mode at $\nu \simeq 7$ THz in addition to the main resonance at $\nu \simeq 3.75$ THz but at the secondary resonance the calculation shows only an asymmetric line shape with a large width. In 2CPA calculation we obtain large hybridization at $\nu \simeq 4.1$ THz ($\zeta = 1.5$-4.5 THz) and smaller secondary splitting near $\zeta \simeq 0.65$ and $\nu \simeq 6.8$ THz while observed splits are near $\zeta \simeq 0.35$, $\nu \simeq 4.0$ THz and $\zeta \simeq 0.6$, $\nu \simeq 6.0$ THz. Near secondary resonance 2CPA shows an asymmetric spectral functions of large width but with a dip resulting in the splitting. In fact, as discussed earlier in Ni-Pd case, such a secondary resonance is due to more scattering induced by impurity at higher frequencies causing resonance modes to decay into the host bands with the strength being proportional to the host phonon density of states and hence increasing the line widths.

The dispersion curve of $[\zeta\zeta 0]$ T_1 has the almost same nature as $[00\,\zeta]$ T except that resonance is at about 3.65 THz in 2CPA. The $[\zeta\zeta 0]$ L component has one resonance mode only at $\zeta = (1.0 - 2.5)$ [redacted] and $\nu \simeq 3.9$ THz in 2CPA. The absence of second resonances in this branch and $[\zeta\zeta\zeta]$ L are understandable if we consider the maximum limit of impurity density of states

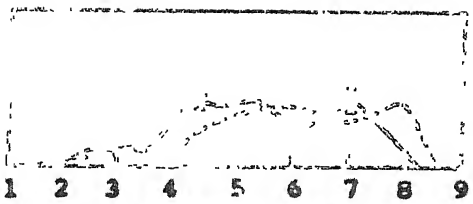

Phonon density of states from experiments by Tsunoda et al. with the partial density of states (broken curve) of Ni in the $Ni_{70}Pt_{30}$ calculated with the MCPA.

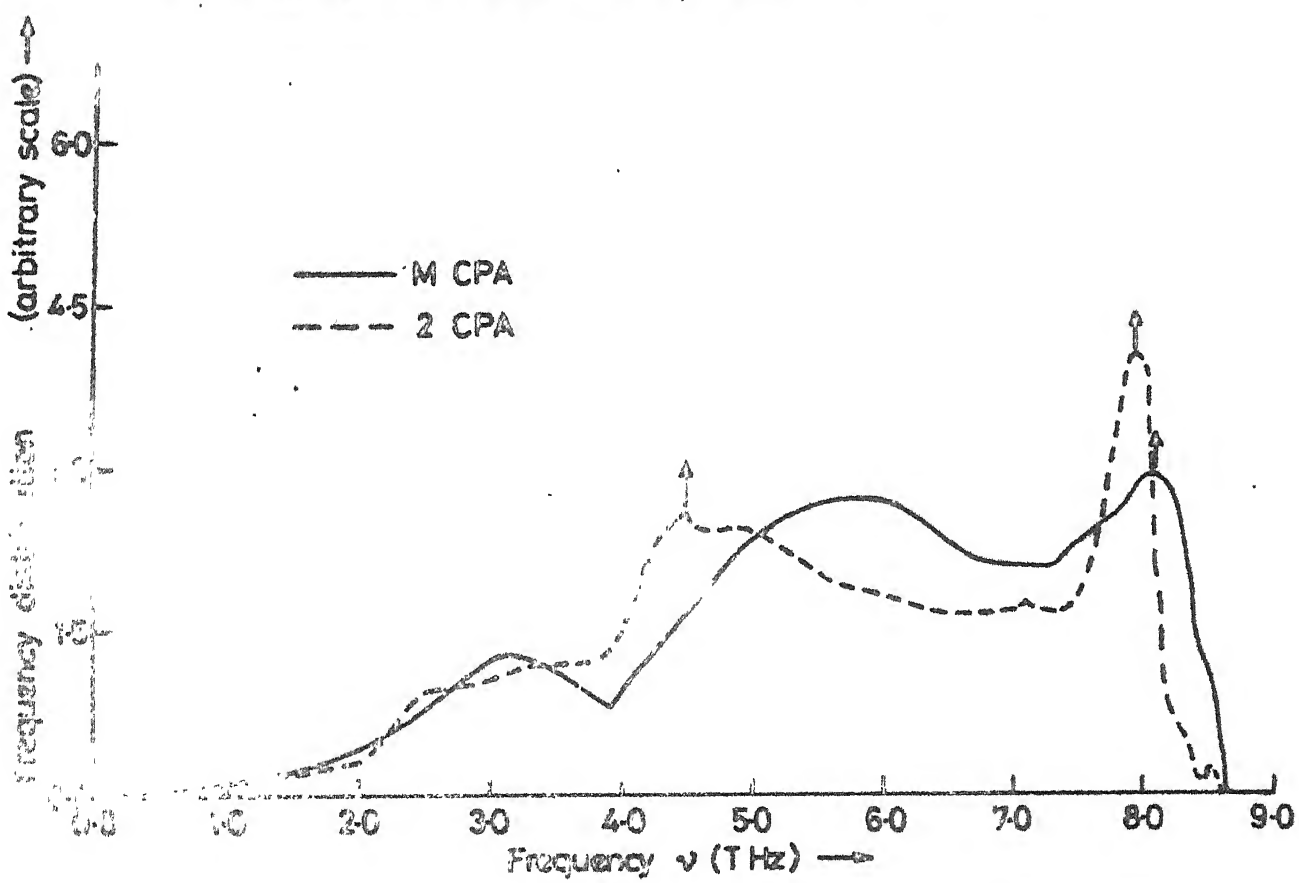

FIG. 3·18 Frequency ... for $Ni_{70}Pt_{30}$ alloy

which is approximately 6 THz. The introduction of large concentration of impurities will affect the Ni-Ni force constant much and hence the high frequency range of pure density of states (6-8 THz) with the result that a second resonance appears around 6 THz. But at higher ζ (> 0.4) in these branches the higher frequencies of host atom dominate not being affected very much by impurity atoms. We do get second resonance in $[\zeta\zeta 0]$ T_2 branch which is not observed in experiments. In $[\zeta\zeta\zeta]$ T branch MCPA and 2CPA show double peak structure in almost entire region one below ~ 3.5 THz and one above it. The resonance frequency is ~ 3.4 THz in MCPA, ~ 3.5 THz in 2CPA while 3.5 THz is experimentally observed. In $[\zeta\zeta\zeta]$ L branch 2CPA resonance width decreases (~ 0.4 THz) while in MCPA width is $\sim$ 0.5 THz).

In Figure 3.18 we display the frequency distribution function for MCPA and 2CPA with the experimental partial density of states in the inset. The experimental observation shows the sudden increment in density of states at about 4.0 THz (a primary resonance mode region) and pushing in the band limit at higher frequencies. The same nature we get by 2 CPA calculation. There is sharp enhancement of frequency distribution at about 4.0 THz and at about 7.6 THz and band is also reduced. In a partial density of states for the host atom calculation, the impurity peaks near the band edges will be removed. The remainder of the frequency distribution function in the 2CPA is in excellent agreement with the experimental curve shown in the inset.

The 2CPA calculations show the branch dependence of resonance mode in better way than by MCPA. The trend being in

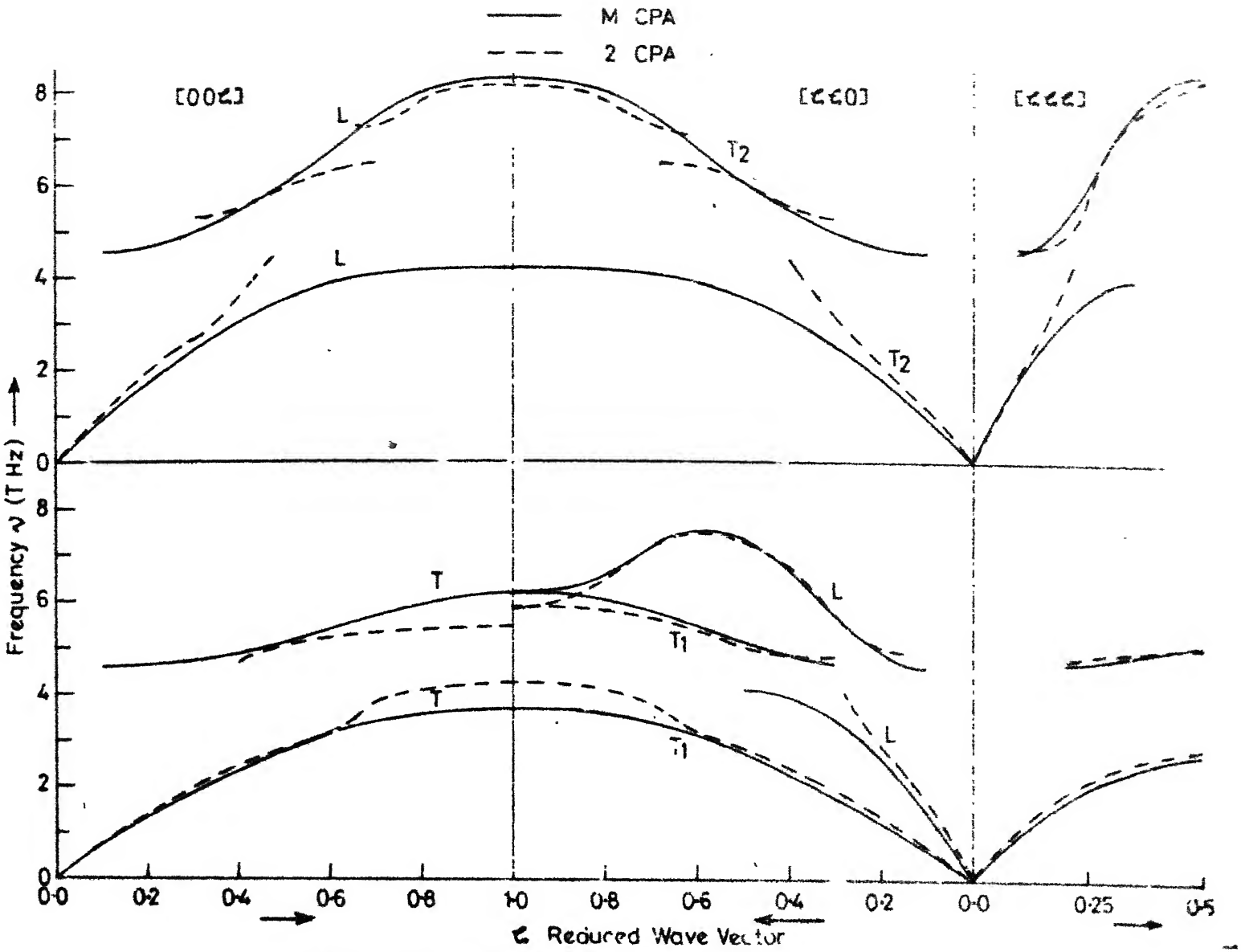

FIG. 3·19 Dispersion Curves for $Ni_{50}Pt_{50}$

the right direction is encouraging. Next we study the 50-50 alloy.

3.5.3 $Ni_{50}Pt_{50}$

We display the dispersion curves along the symmetry directions in Figure 3.19, after MCPA and 2CPA calculations. MCPA results do not show direction or branch dependence. In $[00\zeta]$ L, $[\zeta\zeta 0]$ T_2, $[00\zeta]$ T and $[\zeta\zeta 0]$ T_2 branches resonance occurs at about 4.15 THz in MCPA calculations. It is about 4.4 THz in other directions e.g. $[\zeta\zeta\zeta]$ L, $[\zeta\zeta\zeta]$ T and $[\zeta\zeta 0]$ L. In $[\zeta\zeta\zeta]$ T branch the width is largest compared to other branches. It is similar to the nature observed in $Ni_{55}Pd_{45}$. In 2CPA calculations there are few extra features: the secondary resonance is enhanced in $[00\zeta]$L and $[\zeta\zeta 0]$ T_2 directions, the $[\zeta\zeta\zeta]$ L is more distorted, there is prominent kink in $[\zeta\zeta 0]$ T_1 and $[00\zeta]$ T direction: the branch and direction dependence is easily visible, in $[00\zeta]$ T direction resonance occurs at about 3.95 THz (if we follow the procedure mentioned in the previous section), at ζ = 0.6. The experimental value is 3.5 THz. The primary resonance in $[00\zeta]$ L direction occurs at about 4.9 THz and the secondary one is at about 6.8 THz. Experiment shows only one resonance of large width at about 5.2 THz. Although the experimental interpretation is difficult in this region, because of large width (Tsunoda et al, 1979).

Now we compare the frequency distribution function for MCPA and 2CPA. The nature found in 2CPA is same as in the previous alloy supporting our views. Experimental partial density of states are shown inside the inset. 2CPA results follow the trend

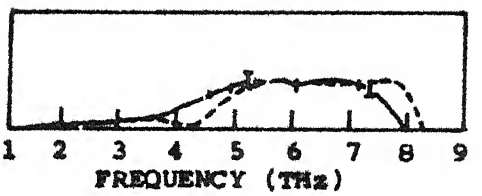

Phonon density of states from experiments by Tsunoda et al. with the partial density of states (broken curve) of Ni in the $Ni_{1-c}Pt_c$ calculated with the MCPA.

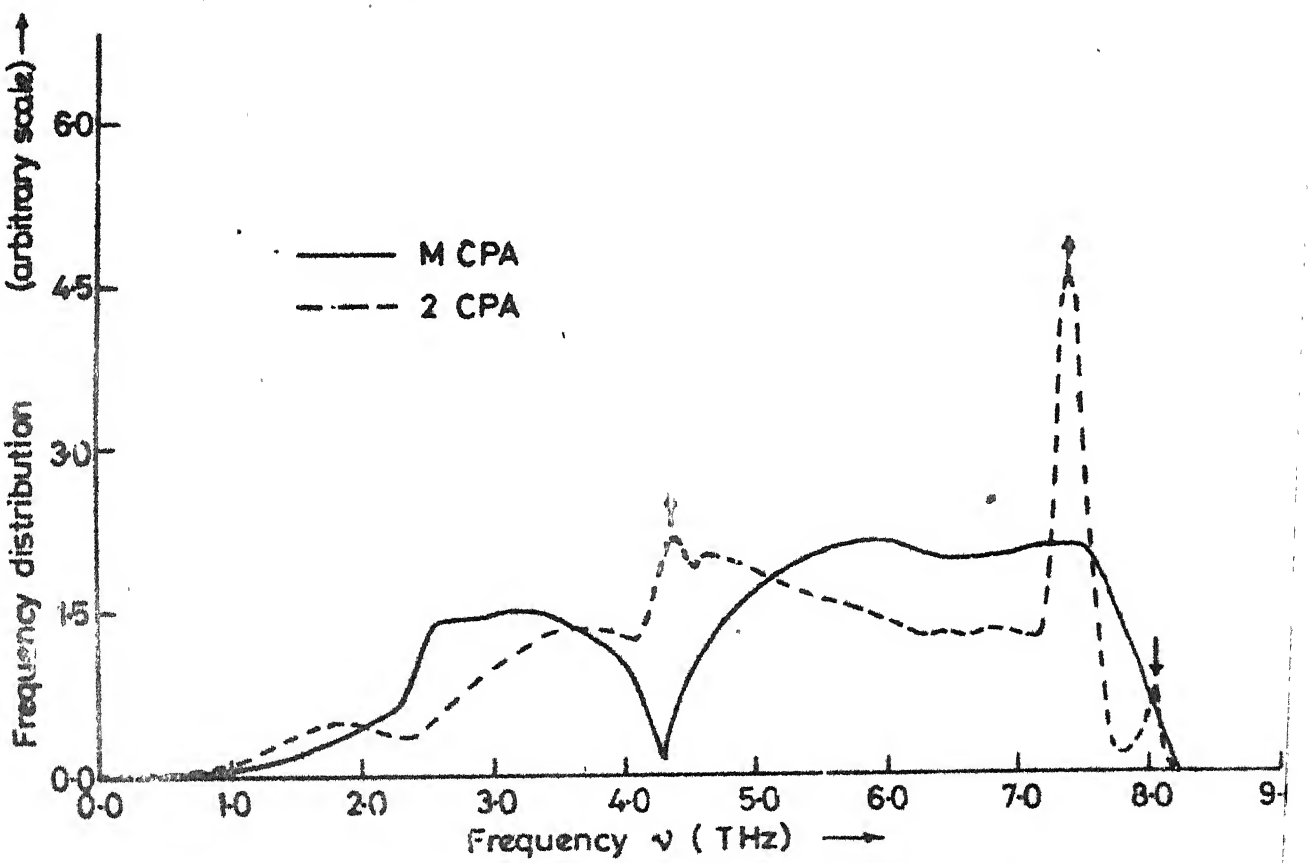

FIG.3·20 Frequency distribution for $Ni_{50}Pt_{50}$ alloy

of experimental observations near the resonance mode and at the band edge. In 2CPA we get one extra small delta function like peak near the band edge. The origin of this peak is not very clear to us. It seems to be that the some frequency of host atom is not affected by the presence of impurity (an off-diagonal disorder effect), or may be due to cluster effects. Again partial density of states will not show these cluster structure of impurities and the rest of the frequency distribution is in excellent agreement with the experiment (inset), far superior to the MCPA calculation.

3.6 Conclusion

In conclusion it must be said that despite the 2CPA being first approximation with off-diagonal disorder, its application to FCC structured transition metal alloys is found to be quite satisfactory qualitatively and quantitatively as well. In all the three systems considered above, most of the observable quantities are better explainable by 2CPA as compared to the existing MCPA predictions. The $\underline{k}$- and w-dependence of spectral functions and width functions is an achievement of the 2CPA. Since nearest neighbours are large in number in FCC lattice and environmental disorder is properly accounted for in 2CPA, the effect of larger clustering is not expected to be important in these systems.

Chapter IV

Concluding Remarks

A self-consistent cluster coherent potential approximation (CCPA) is developed for the study of disordered alloys of materials very different in masses and force constants. This is a significant development over existing MCPA (1CPA). The formulation, being general, is applicable to any kind of elementary excitations. Out of CCPA's, 2CPA is fully developed for the study of vibrational properties of substitutionally disordered binary alloys.

To sum up, the following are the achievements of this work:

(1) A self-consistent CCPA based on augmented space formalism of Mookerjee, has been developed to take into account the effect of large clusters.

(2) The translational invariance condition is properly incorporated which seems to be difficult to include in conventional CPA theories (Mostoller and Kaplan, 1979; Grunewald, 1976).

(3) The analytic properties (Herglozicity) of the Green's functions are maintained in the CCPA theory at all energies, concentrations and degrees of disorder.

(4) Out of CCPA's, 2CPA theory is applied to FCC structured transition metal alloys in the systematic way - with diagonal disorder only; off-diagonal disorder only and with both disorders being predominant.

However, there are a few refinements still essential over the calculations presented here. They are:

(1) The real-space methods for the calculation of different Green's functions ($\underline{G}_{ij}(w^2)$) need further refinements. Since we go down up to 12 steps in recursion method, there are some spurious oscillations near the von-Hove singularities. These oscillations can be avoided by going down more steps in the recursion. This can be facilitated by the use of real space symmetries (Chapter I) which will reduce the working time enormously. Haydock (Solid State Physics, Vol. 35) has shown that the entire basis $|u_i\rangle$ of tight-binding functions is unnecessary, for the recursion method, only those combinations which have the symmetry of the lattice and the starting state $|0\rangle$ contribute. This drastically reduces the "effective" basis and thus CPU time on the computer.

Another approach is to take a finite cluster and use the 'super smooth' programme of the Cambridge group to smoothen out the resulting histograms.

(2) We have considered nearest-neighbour force constant interaction obtained from Born-von Karman models. Instead we can use other near neighbours also for the exact input information. This can also be achieved by recursion and some modifications in our formalism. Such alteration will provide a general formulation for the epplications to other lattices e.g. SC, BCC and diamond.

(3) We can solve the configurationally averaged Green's function (2.46) alternatively. Instead of following the above self-consistent scheme, we can exploit graphical method with recursion directly. On these lines some initial work has been carried out by Hersovici and Fibich (1980a,b), in which they have considered only diagonal disorder. With all disorders we are trying to exploit this scheme.

(4) Though we have concentrated mainly on the determination of spectral functions, width functions, dispersion curves and frequency distributions, it is also possible to extend this formalism for the calculation of vibrational density of states, cluster density of states, etc. used in the calculation of scattering cross-sections, elastic constants and thermal conductivity of alloys with little modifications.

(5) In this theory, we could include Markovian type short-range order (Srivastava, 1982).

(6) The effect of bigger clusters can be included by performing a recursion calculation in the full augmented space.

So far, we have confined ourselves only to crystalline systems with compositional disorder. Amorphous alloys, where there is a departure from crystalinity, but there is an underlying distorted network on which the atom sit (Meek, 1976; Yamamoto et al, 1980) may also be considered by the use of 'recursion' with the tractable size of a cluster. These refinements we leave as possible future extensions of this work.

In addition, as an extra piece of investigation, we have studied the screening density around a static charge in an electron liquid using a dielectric function proposed by Tripathi and Mandal (1977) (See Appendix B). The non-linear behaviour of this function is due to the approximate averaging scheme of double-time retarded Green's function in their Eq. (2.14). This calculation is an important check of the accuracy of their approximation in evaluating the dielectric function.

References

Alben, R., M. Blume, M. Krakauer and L. Schwartz (1975). Phys. Rev. B12 , 4090.

Bishop, A.R. and A. Mookerjee (1974). J. Phys. C7, 2165.

Bosi, P., F. Dupre, F. Menzinger, F. Sacchetti and M.C. Spinelli (1978). Nuovo Cimento 46, 337.

____ (1978). Nuovo Cim. Lett. 21, 436.

Bosi, P., F. Menzinger andF. Sacchetti (1980). J. Phys. F: Metal Phys. 10, 1673.

Butler, W.H. (1973). Phys. Rev. B8, 4499.

Birgeneau, R.J., J. Cordes, G. Dolling and A.D.B. Woods (1964). Phys. Rev. 136A, 1359.

Cunningham, R.M., L.D. Muhlenstein, W.M. Shaw and C.W. Thompson (1970). Phys. Rev. B2, 4864.

Choudhry, V. (1981, Thesis), I.I.T. Kanpur (Unpublished).

Chen, A.B. (1977). Phys. Rev. B16, 3291.

Dederichs, P.H. and R. Zeller (1980). (Point Defects in Metals II, Springer-Verlag, Berlin).

Dutton, D.H., B.N. Brockhouse and A.P. Muller (1972). Can. J. Phys. 50, 2915.

Dean, P. (1961). Proc. Roy Soc. (London) A260, 263.

____ (1972). Rev. Mod. Phys. 44, 127.

Diehl, H.W. and P.L. Leath (1979a). Phys. Rev. B19, 587.

____ (1979b). Phys. Rev. B19, 596.

Diehl, H.W., P.L. Leath and T. Kaplan (1979). Phys. Rev. B19, 5044.

Da es, R.W. and J.S. Langer (1963). Phys. Rev. 131, 163.

Elli t, R.J. and P.L. Leath (1975). Dynamical Properties of Solic II, ed., Horton and Maradudin (North-Holland Publishing Corpo. ion).

Elliott R.J., J.A. Krumhansl and P.L. Leath (1974). Rev. Mod. Physics 46, 465; references there in.

Elliott, R.J. and D.W. Taylor (1967). Proc. Roy. Soc. (London) A296, 161.

Fetter, A.L. and J.D. Walecka (1971). Quantum Theory of Many Particle Systems (McGraw-Hill).

Feldmann, J.L. (1970). Phys. Rev. B1, 448.

Grunewald, G. (1976). J. Phys. F6, 999.

____ (1980). J. Phys. C13, 2103.

Hansen, M. (1958). Constitution of Binary Alloys (McGraw-Hill, New York).

Hove, L. Von (1954). Phys. Rev. 95, 249.

Haydock, R. (1972). Ph.D. Thesis, Univ. of Cambridge.

Haydock, R., V. Heine and M.J. Kelly (1972). J. Phys. C: Solid State Physics 5, 2845.

____ (1975). J. Phys. C8, 2591.

Haydock, R. and A. Mookerjee (1974). J. Phys. C7, 2165.

Haydock, R. (1980). (Solid State Physics, Vol. 35, edited by Ehrenreich et al, Academic Press, New York).

Joshi, S., Private communication.

Kelly, M.J. (1980). (Solid State Physics, Vol. 35, edited by Ehrenreich et al, Academic Press, New York).

____ Private communication.

Kaplan, T. and L.J. Gray (1976). Phys. Rev. B14, 3462.

____ (1977). Phys. Rev. B15, 3260.

____ (1981). Phys. Rev. B24, 1872.

Kaplan, T., L.L. Leath, L.J. Gray and H.W. Diehl (1980). Phys. Rev. B21, 4230.

Kamitakahara, W.A. and B.N. Brockhouse (1974). Phys. Rev. B10, 1200.

Kamitakahara, W.A. and D.W. Taylor (1974). Phys. Rev. B10, 1190.

Kumar, V. and S.K. Joshi (1975). J. Phys. C8, L148.

Kumar, V., A. Mookerjee and V.K. Srivastava (1982). J. Phys. C: Solid State Physics 15, 1939.

Lifshitz, L.M. and G.I. Stepanova (1956). Sov. Phys. JETP 3, 656.

Leibfried, G. and N. Breuer (1978). Points Defects in Metals I (Springer Tracts in Modern Physics, Vol. 81, Springer-Verlag, Berlin, New York).

Mookerjee, A. (1973). Ph.D. Thesis, Univ. of Cambridge.

____ (1973a). J. Phys. C6, L205.

____ (1973b). J. Phys. C6, 1340.

____ (1975a). J. Phys. C8, 29.

____ (1975b). J. Phys. C8, 1524.

____ (1979). (Disordered Systems, Hindustan Publishing House, India).

Myles, C.W. and J.D. Dow (1979). Phys. Rev. B19, 4939.

Maradudin, A.A., E.W. Montroll, G.H. Weiss and I.P. Ipatova, (1971). Theory of Lattice Dynamics in the Harmonic Approximation (Solid State Physics, Suppl. 3, Academic Press, New York and London).

Mostoller, M. and T. Kaplan (1979). Phys. Rev. B19, 3948.

Muller, A.P. and B.N. Brockhouse (1971). Can. J. Phys. 49, 704.

____ (1968). Phy. Rev. Lett. 20, 798.

Meek, P.E. (1976). Phil. Mag. 33, 897.

Payton, D.N. and W.M. Visscher (1967). Phys. Rev. 174, 802.

____ (1968). Phys. Rev. 175, 1201.

Lord Rayleigh (1892). Phil. Mag. Str. (5), 34, 481.

Sacchetti, F. (1978). J. Phys. F: Metal Physics 8, 743.

Sjolander, A. (1964). in Phonons and Phonon Interaction, edited by T.A. Bak (Benjamin, New York).

Svensson, E.C. and W.A. Kamitakahara (1971). Can. J. Phys. 49, 2291.

Soven, P. (1967). Phys. Rev. 156, 809.

Srivastava, V. and S.K. Joshi (1973). J. Phys. F: Metal Phys. 3, L179.

Srivastava, V.K. (1982, Thesis). I.I.T. Kanpur.

Taylor, D.W. (1967). Phys. Rev. 156, 1097.

Tsunoda, Y., N. Kunitomi, N. Wakabayashi, R.M. Nicklow and H.G. Smith (1979). Phys. Rev. 19, 2876.

Tsukada, M. (1972). J. Phys. Soc. (Japan) 36, 1477.

Wilkinson, J.H. (1965). The Algebraic Eigenvalue Problem.

Yamamoto, R., K. Haga, T. Mihara and M. Doyama (1980). J. Phys. F: Metal Physics 10, 1389.

Zubarev, D.N. (1960). Sov. Phys. Uspeki 3, 320.

Appendix A

Recursion Method

The 'recursion' method of Haydock et al. (1972; 1975) is developed for finding density of states as well as other matrix elements of the resolvents and wavefunctions. Its motivation was that since many observable properties of amorphous and disordered solids depend mostly on local structure, it ought to be possible to formulate a theory in which local effects are explicitly separated from bulk averages. It is closely related to Lanczos method (Wilkinson, 1965). The philosophy of this technique is as follows. For a given Hamiltonian matrix $\underline{H}$, in a suitable Hilbert space $\mathcal{H}$, the recursion method generates a unitary transformation such that

$$\underline{U}\,\underline{H}\,\underline{U}^{-1} = \underline{H}_{TD} \tag{A.1}$$

where $\underline{H}_{TD}$ is tridiagonal i.e.

$$[\underline{H}_{TD}]_{mn} = \begin{cases} a_m & n = m \\ b_{m+1} & n = m+1 \\ b_m^+ & n = m-1 \\ 0 & \text{otherwise} \end{cases} \tag{A.2}$$

For this, new basis functions are constructed iteratively so as to guarantee that each new member interact with its preceding and following members. The first function in this new basis is chosen to be the one whose local density is sought. Here, we now, discuss its practical use.

The representation of the Hamiltonian $\underline{H}$ for the vibrational system given by eq. (1.1) is suitable for the use of recursion method. Our interest is in finding the one-phonon spectral density given by (1.46). Rewriting it

$$\rho(w) = -\frac{2w}{\pi} \sum_{\alpha} \text{Im } G^{oo}_{\alpha\alpha} (w^2 + i\delta); \quad (\delta = 0^+)$$

where

$$G^{oo}_{\alpha\alpha} (w^2) = \langle \alpha , o | (w^2 \underline{I} - \underline{D})^{-1} | \alpha , o \rangle \qquad (A.3)$$

with

$$\underline{D} = \underline{M}^{-1/2} \underline{\phi} \underline{M}^{-1/2} ,$$

$\underline{M}$ and $\underline{\phi}$ are the mass-tensor and force constant matrix, respectively. $|\alpha , o\rangle$ is the component of the vibrational state of the atom o. $\rho(w)$ is normalised (in modes per atom) as

$$\int_{o}^{w_{max}} \rho(w)\, dw = 3$$

where w_{max} is the maximum frequency.

For constructing $G^{oo}(w^2)$ as a continued fraction we start with a given element $|u_o\rangle = |\alpha, o\rangle$ and an arbitrary sequence of numbers $\{a_n, b_n\}$. Let us define a sequence of elements $\{|u_n\rangle\}$ by

$$|u_n\rangle = \underline{D} |u_{n-1}\rangle - a_{n-1} |u_{n-1}\rangle - b^2_{n-1} |u_{n-2}\rangle , \quad b_o = 0 \qquad (A.4)$$

The sequence terminates at n if u_{n+1} is the null vector ($b_n = 0$) otherwise we generate an infinite sequence of elements. The numbers $\{a_n, b_n\}$ are real if $\underline{H}(\underline{D})$ is Hermitian. If the sequence of elements $\{|u_n\rangle\}$ is such that $\langle u_n | u_m \rangle = 0$ for $n \neq m$ then equation (A.4) immediately implies

$$a_n = \frac{\langle u_n | \underline{D} | u_n \rangle}{\langle u_n | u_n \rangle} \; ; \quad b_n^2 = \frac{\langle u_{n-1} | \underline{D} | u_n \rangle}{\langle u_{n-1} | u_{n-1} \rangle} = \frac{\langle u_n | u_n \rangle}{\langle u_{n-1} | u_{n-1} \rangle} \tag{A.5}$$

If we take $\{|u_n\rangle\}$ as our basis of representation the Hamiltonian $\underline{D}$ becomes tridigonal with the a_n's down the diagonal and b_n's down the off-diagonal positions.

If $\underline{D}$ is a non-Hermitian matrix (as is often the case with effective Hamiltonian arising out of any coherent potential approximation) then, alternatively we choose an arbitrary set of complex numbers a_n, b_n, c_n as follows

$$b_o |u_1\rangle = (D - a_o) |u_o\rangle \; ; \quad c_o = 0 \tag{A.6}$$

for $n > 0$

$$b_n |u_{n-1}\rangle = (\underline{D} - a_n) |u_n\rangle - c_n |u_{n-1}\rangle$$

Using Equation (A.6), it is easy to see that

$$\begin{aligned} a_n &= \langle u_n | \underline{D} | u_n \rangle \, , \quad c_n = \langle u_{n-1} | \underline{D} | u_n \rangle \\ b_n &= \langle u_n | (\underline{D} - a_n)^+ (D - a_n) | u_n \rangle - |c_n|^2 \; ; \end{aligned} \tag{A.7}$$

if we assume $\langle u_n | u_m \rangle = \delta_{nm}$.

The off-diagonal elements of the Green's operator $G^{11'}_{\alpha\alpha'}(w^2)$ may also be calculated in the same way. For example, if we wish to calculate

$$G^{01}_{\alpha\beta}(w^2) = \langle \alpha, 0 | (w^2 \underline{I} - \underline{D})^{-1} | \beta, 1 \rangle$$

then we must start with

$$|u_o\rangle = \frac{1}{2} |\alpha, 0\rangle + |\beta, 1\rangle$$

which gives

$$\langle u_o | (w^2 \underline{1} - \underline{D})^{-1} | u_o \rangle = \frac{1}{2} [G^{oo}_{\alpha\alpha} + G^{11}_{\beta\beta} + G^{o1}_{\alpha\beta} + G^{1o}_{\beta\alpha}]$$

But $G^{oo}_{\alpha\alpha} = G^{oo}_{\beta\beta}$ and $G^{o1}_{\alpha\beta} = G^{1o}_{\beta\alpha}$, in general, for pure lattices and for configurational Green's functions in case the disorder is homogeneous in space. So

$$G^{o1}_{\alpha\beta}(w^2) = \langle u_o | (w^2 \underline{I} - \underline{D})^{-1} | u_o \rangle - G^{oo}_{\alpha\alpha}(w^2) \qquad (A.8)$$

Here the first term of the right hand side of above equation can be calculated by continued fraction expansion with $|u_o\rangle = \frac{1}{2} |\alpha,0\rangle + |\beta,1\rangle$ and $G^{oo}_{\alpha\alpha}$ is the term which has already been obtained by the same procedure with $|u_o\rangle = |\alpha,0\rangle$. Hence we can calculate $G^{o1}_{\alpha\beta}(w^2)$. Similarly other $G^{11}_{\alpha\alpha}(w^2)$ are also calculated.

The reason why this method is called 'recursion' method now becomes clear. Starting from a Hamiltonian and an element $|u_o\rangle$ with $b_o = 0$ we may generate with the help of equation (A.4), a_o, b_o and thus $|u_1\rangle$. Now we may determine in turn a_1, b_1 and thus $|u_2\rangle$ and so on recursively. As a calculation technique this method is very economical. At each stage we need to store $|u_n\rangle$ and $|u_{n-1}\rangle$ and the coefficients calculated upto that stage. All extraneous information is left out.

Now, let M be the determinant of the matrix $(w^2 \underline{I} - \underline{D}_{TD})$ and M_n ($n = 0, 1, 3, \ldots$) be the determinant of the matrices derived from $(w^2 \underline{I} - \underline{D}_{TD})$ after rows and columns from 0 to n have been eliminated. Then if we wish to obtain $G^{oo}_{\alpha\alpha}(w^2) = M_o/M$, we may use the Cauchy expansion for the determinant M_n and write down a recursion relation for M_n as

$$M_n = (w^2 - a_n)\, M_{n+1} - b_n^2\, M_{n+2} \qquad (A.9)$$

$G^{oo}_{\alpha\alpha}(w^2)$ becomes a continued fraction expansion from the repeated application of equation (A.9)

$$G^{oo} = \frac{M_o}{(w^2 - a_o)\, M_o - b_1^2 M_1} = \frac{1}{(w^2 - a_o) - b_1^2\, M_1/M_o}$$

$$= \cfrac{1}{w^2 - a_o - \cfrac{b_1^2}{w^2 - a_1 - \cfrac{b_2^2}{w^2 - a_2 - \cfrac{b_3^2}{\ddots \cfrac{b_{n-1}^2}{w^2 - a_{n-1}^2 - b_n^2 \left(\frac{M_N}{M_{N-1}}\right)}}}}} \qquad (A.10)$$

By the recursion method we can calculate iteratively (a_n, b_n) from n_o to some N. The effect of all further iterations can be absorbed in $\frac{M_{N+1}}{M_{N+2}}$ if (a_n, b_n^2) converge fast (which, in general, happens). Then $(a_n, b_n^2) = (a_\infty, b_\infty^2)$, $n > N$ will give an analytical expression for the remainder resolvent

$$\frac{M_N}{M_{N+1}} = G_\infty(w^2) = \cfrac{1}{w^2 - a_{N+1} - \cfrac{b_{N+2}^2}{w^2 - a_{N+2} - \cfrac{b_{N+3}^2}{\ddots}}} \qquad (A.11)$$

$$= \frac{1}{w^2 - a_\infty - b_\infty^2\, G_\infty(w^2)}$$

which yields

$$G_{\infty}(w^2) = \frac{1}{2b_{\infty}^2}\left[(w^2 - a_{\infty}) - \sqrt{(w^2 - a_{\infty})^2 - 4b_{\infty}^2}\right] \qquad (A.12)$$

We reject the second solution of the quadratic as the $G_{\infty}(w^2)$ must vanish as $w^2 \to \infty$ in order that the resolvent preserve its analytic character (of the form $(w^2)^{-1}$), there. It is clear that $G_{\infty}(w^2)$ is real for real w^2 outside the range $(a_{\infty} - 2|b_{\infty}|)$ and $(a_{\infty} + 2|b_{\infty}|)$, so that the continued fraction will be real. Inside the same interval $G_{\infty}(w^2)$ has a branch cut and we obtain a band of allowed energies. Since w^2 cannot be negative (a consequence of sum rule), its lower limit is 0, hence $a_{\infty} = 2b_{\infty}$ holds in the phonon density of states calculation by recursion. If we know w_{max} homehow (here we used K-space maximum frequency limit in Born-von Karman model). We can fix exact value of a_{∞}, b_{∞} and hence $G_{\infty}(w^2)$.

Now we can obtain $G^{oo}(w^2)$ from (A.10) and hence phonon density of states

$$(w) = -\frac{2w}{3\pi}\cfrac{1}{w^2 - a_o - \cfrac{b_1^2}{w^2 - a_1 - \cfrac{b_2^2}{w^2 - a_2 - \cfrac{b_3^2}{\ddots}}}} \qquad (A.13)$$

The tridiagonalisation of $\underline{D}$ thus reduces the original system to a fictitious linear chain of atoms with local vibrational displacements with diagonal energies a_n and n-n interactions b_n (Solid State Physics, Vol. 35).

APPENDIX - B

short note

reprinted from

physica
status
solidi (b)

phys. stat. sol. (b) 101, K93 (1980)
Subject classification: 13.4; 22

Department of Physics, Indian Institute of Technology, Kanpur[1)]

Dielectric Function, Static Screening, and Non-Linear Response

By
R. P. SINGH and M. YUSSOUFF[2)]

Tripathy and Mandal /1/ proposed a new dielectric function $\epsilon(\vec{k}, \omega)$ solving the equations of motion of the double-time retarded Green's functions by decoupling the higher order Green's functions $G(\vec{k}, \omega)$ with the conservation of frequency moments up to infinite order. The resulting $G(\vec{k}, \omega)$ satisfies the compressibility sum rule and yields the asymptotic value of G(k) equal to 1/3. Unlike previous theories /2, 3/ here G(k) has a sharp peak around $k = 2k_f$.

The new features of $\epsilon(\vec{k}, \omega)$ given by Tripathy and Mandal arise from the approximations made in evaluating it. These authors proposed a decoupling scheme which amounts to expressing the higher order Green's function in terms of the lower order Green's function along with a frequency and wave-number dependent coefficient $A_{\vec{q}_1, \sigma_1}(\vec{k}, \omega)$ in their equation (2.14). But their evaluation of this coefficient is rather arbitrary because they fall back on the same equation involving the higher order Green's function to evaluate $A_{\vec{q}_1, \sigma_1}(\vec{k}, \omega)$. Then they evaluate the former approximately by trying to retain terms in $A_{\vec{q}_1, \sigma_1}(\vec{k}, \omega)$ that are linear in $v(\vec{k})$. The effect of such an unclear approximation may be expected to show up in the static limit which reflects itself in the screening density around an impurity of unit charge. The following calculation shows that this is the case.

In the linear response theory, the screening density at a distance r from the static impurity of unit charge situated at the origin is given by /4/

$$\frac{\delta\varrho(r)}{k_f^3} = \frac{1}{2\pi^2} \int_0^\infty dk \, \frac{k \sin(kr)}{r} \left(1 - \frac{1}{\epsilon(k, 0)}\right), \tag{1}$$

where r is in units of k_f^{-1} and k in units of k_f. The static dielectric function according to Tripathy and Mandal is given by

$$1 - \frac{1}{\epsilon(k, 0)} = \frac{Q_0(k)}{1 + Q_0(k)[1 - G(k)]}, \tag{2}$$

---

1) Kanpur-208016, India.

2) Present address: Kernforschungsanlage, Jülich, BRD.

where

$$Q_o(k) = \frac{2\alpha r_s}{\pi k^2} F(k) \tag{3a}$$

with

$$F(k) = 1 + \frac{1}{k}\left(1 - \frac{1}{4}k^2\right)\ln\left|\frac{k+2}{k-2}\right| ; \tag{3b}$$

substituting (2) in (1) one gets

$$\frac{\delta\varrho(r)}{k_f^3} = \frac{1}{2\pi^2}\int_0^\infty dk\, \frac{k\sin(kr)}{r}\, \frac{Q_o(k)}{1 + Q_o(k)[1 - G(k)]} . \tag{4}$$

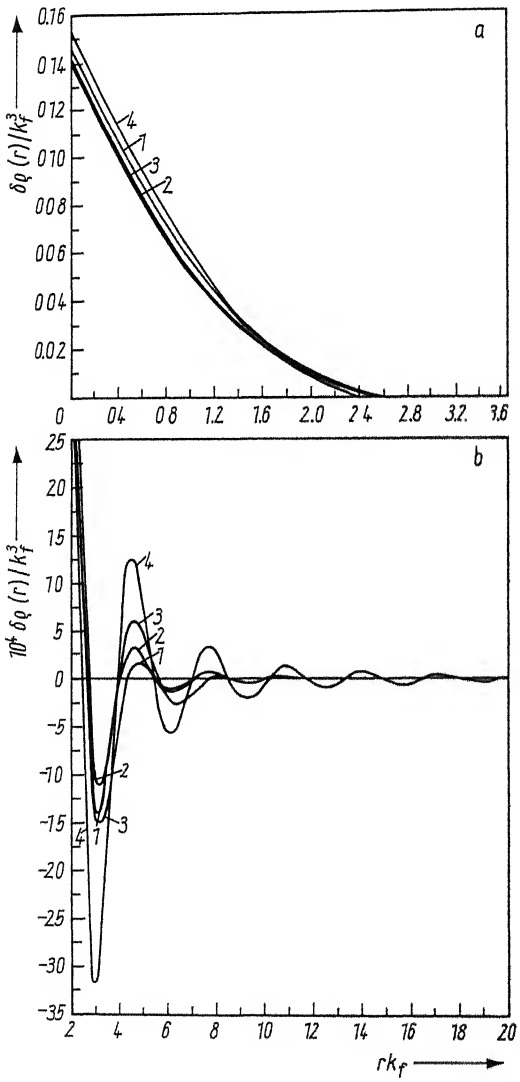

Fig. 1. Screening density $\delta\varrho(r)/k_f^3$ versus rk_f for $r_s = 3$; a) for small values of rk_f and b) for large values of rk_f. (1) Singwi and Tosi /6/, (2) Pathak /5/, (3) Toigo and Woodruff /7/, (4) present results

The numerical values of G(k) given by Tripathy and Mandal are used to evaluate the integral (4) using Simpson's rule. Very good convergence was obtained with the interval 0.01 to the upper limit 100. The results are compared with those of Pathak /5/, Singwi and Tosi /6/, and Toigo and Woodruff /7/ for $r_s = 3$ in Fig. 1.

It is clear that the present results are very different from the earlier ones. The amplitudes of oscillations are larger by almost a factor of two and the decay is slow. But the initial value of $\delta\varrho(r)$ is close to that obtained in earlier work. All these can be explained in terms of the behaviour of G(k) as k varies. Since the asymptotic limit of G(k) is comparable to the Hartree-Fock value the behaviour of

$\delta\varrho(r)$ for small r is close to earlier formulations. Also G(k) of Tripathy and Mandal is similar to that of others in the range of $0 \leqq k \leqq 1$ which governs the decay at large r values. The difference in the range $1 \leqq k \leqq 2$ with a notable feature that a peak exists around $k = 2k_f$ is responsible for the large amplitude oscillations and decay at moderate values of r. Thus the value of G(k) around $= 2k_f$ is debatable and the above calculations might serve as an experimental check of the accuracy of Tripathy and Mandal's approximation.

One of us (R. P. S.) is indebted to CSIR, New Delhi, for a Junior Research Fellowship while we were working on this problem.

References

1/ D.N. TRIPATHY and S.S. MANDAL, Phys. Rev. B 16, 231 (1977).
2/ P. VASHISHTA and K.S. SINGWI, Phys. Rev. B 6, 875 (1972).
3/ F. TOIGO and T.D. WOODRUFF, Phys. Rev. B 2, 3958 (1970).
4/ D. PINES and P. NOZIERES, Theory of Quantum Liquids, Vol. 1, Benjamin, New York 1966.
5/ A.P. PATHAK, Phys. Rev. B 2, 3021 (1970).
6/ K.S. SINGWI and M.P. TOSI, Phys. Rev. 181, 784 (1969).
7/ F. TOIGO and T.O. WOODRUFF, Phys. Rev. B 4, 371 (1971).

(Received September 24, 1979)